UNIVERSITY OF CALIFORNIA

Santa Barbara

The Geomorphic Transition between the Santa Barbara and Ventura Fold Belts near Rincon

Point, California

A Thesis submitted in partial satisfaction of the

requirements for the degree Master of Science

in Earth Science

by

Shelby Marie Fredrickson

Committee in Charge:

Professor Edward A. Keller, Chair

Professor Alexander Simms

Professor Phillip Gans

June 2016

The thesis of Shelby Marie Fredrickson is approved.

_____

Alexander Simms

_____

Phillip Gans

_____

Edward A. Keller, Committee Chair

June 2016

The Geomorphic Transition between the Santa Barbara and Ventura Fold Belts near Rincon

Point, California

ACKNOWLEDGMENTS

The Geomorphic Transition between the Santa Barbara and Ventura Fold Belts near Rincon Point, California

ABSTRACT

The Santa Barbara and Ventura fold belts have very different uplift rates based on marine terrace data: ~1-2 m/ky and ~6-8 m/ky, respectively. The onshore transition between these fold belts occurs at Rincon Creek, near Carpinteria, where the first emergent marine terrace rises from below sea level to nearly 200 m elevation over less than 10 km. A statistical comparison of normalized stream steepness values in weak rocks supports higher uplift rates east of Rincon Creek within the field area. Optically stimulated luminescence dating of the first emergent marine terrace between Carpinteria and Rincon Creek yields ages ranging from ~18-40 ka including error. The most reliable of these ages yield an average age of 32.81 ± 6.06 ka. This age is younger than previous dates of ~45 ka on the Punta Gorda terrace east of Rincon Creek but within the range of ages collected on MIS 3 terraces in Santa Barbara. These ages suggest the Carpinteria Bluffs marine terrace is continuous with the Punta Gorda terrace. Based on the age of 32.81 ± 6.06 ka and a local sea level curve, uplift rates on the Carpinteria Bluffs marine terrace are 1.8 ± 0.6 m/ky near Tar Pit Park and 3.2 ± 1.1 m/ky near the Carpinteria Bluffs Nature Preserve. Because the terrace is tilted toward the west, there is an east-west gradient in uplift rates from ~0 m/ky where the wave-cut platform emerges from below sea level at Carpinteria Beach to ~4-5 m/ky near La Conchita. The age and vertical offset of marine terrace deposits indicate minimum vertical slip rates of 0.06 m/ky and 0.20 m/ky on the Railroad fault and Carpinteria fault, respectively.

Digital topographic analysis indicates Rincon Point is a geomorphic boundary between the subsiding Carpinteria basin and the uplifting Rincon Mountain. This geomorphic boundary may coincide with a proposed tear fault, but it is most likely influenced by the position of the Red Mountain fault, which takes a left turn offshore of Rincon Point. The profile of the Carpinteria Bluffs marine terrace can be interpreted as either vertically offset or kinked across Rincon Creek. The former supports the presence of a tear fault with an east-side-up sense of slip, but the latter discounts the tear fault in favor of uplift by the Red Mountain fault. Alluvial cover, brush, and private property have hindered discovery of convincing tear fault outcrops. A subaqueous delta at Rincon Point may conceal a bedrock ridge that coincides with the trend of the proposed tear fault, but no direct evidence for a structural origin of Rincon Point is available.

TABLE OF CONTENTS

LIST OF FIGURES

LIST OF TABLES

INTRODUCTION

The western end of the Ventura fold belt has experienced uplift rates as high as ~10 m/ky, which are among the highest in the world (Lajoie et al., 1979; Yeats and Rockwell, 1991). GPS surveys across the Ventura basin indicate modern convergence rates of 7-10 m/ky (Huftile and Yeats, 1995). Controversy surrounds the anomalously high uplift rates indicated by marine terrace data on the coast of Ventura east of Rincon Point. Here, Holocene marine terraces have been uplifted 5-10 m on the flank of the Ventura Avenue anticline during discrete slip events on the Ventura fault (Hubbard et al., 2014; Rockwell, 2011). Based on standard scaling relationships, this amount of uplift would require a high magnitude earthquake of M_w 7.7-8.1 (Hubbard et al., 2014; McAuliffe et al., 2015) and a fault rupture longer than ~100 km (Wyss, 1979). However, the Ventura fault is only ~20 km long. Furthermore, slip generally occurs at similar rates along the length of a rupture, except at the ends of the rupture where slip tapers (Cowie and Scholz, 1992a, b). Why then does Ventura experience such anomalously high rates of uplift in spatially heterogeneous patterns? In addition, how can actively subsiding structural basins such as the Carpinteria and Ventura basins exist in close proximity to rapidly uplifting features such as the Ventura Avenue anticline and Rincon Mountain? Perhaps fault segmentation contributes to such heterogeneous patterns. Rincon Point, located just west of the Ventura Avenue anticline, is a natural laboratory for studying this phenomenon.

Gurrola and Kamerling (1996) proposed that a tear fault exists at Rincon Point. A tear fault can segment larger reverse or thrust faults, potentially limiting the rupture zone and magnitude of local earthquakes (Corbett and Johnson, 1982; Gurrola, 2006). The proposed tear fault separates the Carpinteria basin from Rincon Mountain. A geomorphic investigation

1

is appropriate for evaluating this proposal because the Santa Barbara and Ventura fold belts are characterized by young deformation; therefore, topography largely reflects underlying tectonic structures (Gurrola, 2006; Keller and Gurrola, 2000).

The main objective of this project is to characterize the tectonic geomorphology of the transition between the Santa Barbara fold belt and Ventura fold belt near Carpinteria by identifying patterns of uplift with stream profile analysis, calculating rates of uplift using marine terrace chronology, and estimating slip rates on local faults. Interesting geomorphic features are investigated using various techniques, including digital topographic analysis, stream profile analysis, optically stimulated luminescence (OSL) dating of deformed landforms, and the examination of bucket auger core logs. Several tractable questions central to characterizing the pattern of deformation at this geomorphic boundary are explored: 1) what do local streams reveal about patterns of tectonic uplift; 2) what is the age and uplift rate of the Carpinteria Bluffs marine terrace; and 3) what are the slip rates of the Carpinteria and Railroad faults. This work complements decades of research invested in understanding deformation within the Santa Barbara and Ventura fold belts.

BACKGROUND

Geologic Setting

The Santa Barbara and Ventura fold belts are located in the Western Transverse Ranges south of the restraining bend in the San Andreas Fault. North-south shortening and east-west extrusion created by convergence at the Big Bend have produced east-west trending faults and folds (Figure 1) that accommodate crustal shortening (Keller and Gurrola, 2000). The Santa Barbara coastal piedmont experiences high uplift rates of ~1-2 m/ky

(Gurrola et al., 2014; Keller and Gurrola, 2000), and the coast of Ventura experiences uplift rates as high as ~6-8 m/ky near the Ventura Avenue anticline (Lajoie et al., 1982). The coastal geomorphology of the Santa Barbara and Ventura fold belts is primarily influenced by the location of synclines and anticlines. Linear ridges are commonly active anticlines, and low-relief areas such as sloughs and marshes are typically faulted synclines. Sea cliffs are found where anticline limbs meet the coast, and sea cliffs are generally absent where synclines meet the coast (Gurrola et al., 2014; Keller and Gurrola, 2000). The coast is lined with uplifted marine terraces preserved on the margins of active anticlines (Gurrola et al., 2014).

The Ventura fold belt continues to the west as the Santa Barbara fold belt (Keller and Gurrola, 2000). These fold belts are continuous, but they have unique structures and heterogeneous tectonic frameworks. The Ventura basin is an east-west trending basin bounded by the San Cayetano fault and the Red Mountain fault to the north and the Oak Ridge fault to the south (Jackson and Yeats, 1982). The Ventura Avenue anticline, a structurally complex east-west striking linear ridge, is a major topographic feature of the Ventura fold belt which deforms several marine terraces (Lajoie et al., 1982; Rockwell et al., 1988). The Ventura basin is actively deforming at exceptionally high rates and contains a thick sequence of Pleistocene sediments (Yeats and Rockwell, 1991).
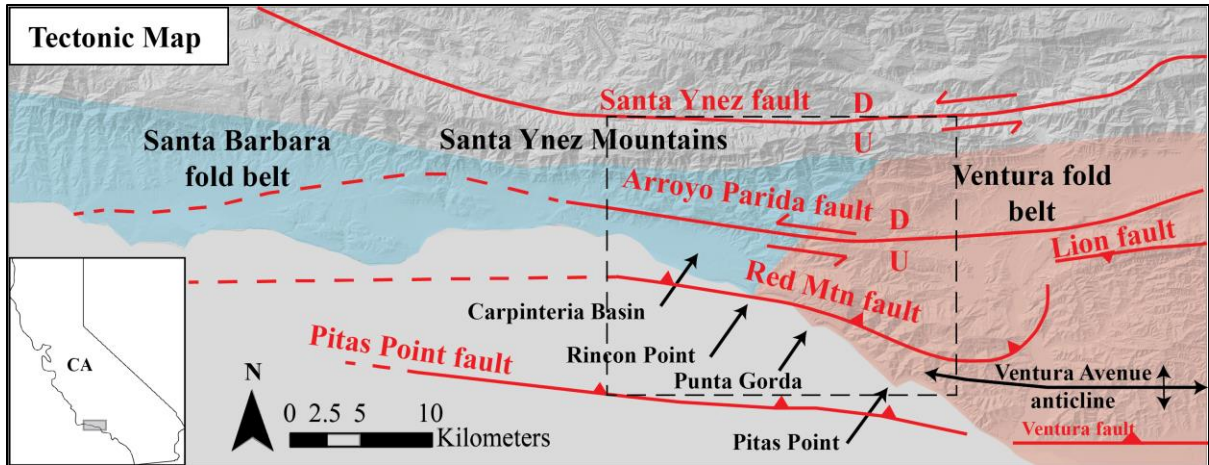
Figure 1: Tectonic Map. The onshore transition from the Santa Barbara fold belt to the Ventura fold belt is mapped at Rincon Creek. Major faults and folds are mapped according to Hubbard et al. (2014) and Gurrola et al. (2014). The dashed box indicates the field area for this study. Background: USGS NED n35w120 1/3 arc-second 2013 DEM available online through the National Map Viewer.

The Santa Ynez anticlinorium forms the northern boundary of the Santa Barbara fold belt and is the primary topographic structure. The Santa Barbara fold belt has several blind reverse faults with active hanging-wall anticlines (Gurrola et al., 1998). Faults and folds are generally oriented east-west or southeast-northwest in the Santa Barbara fold belt. Melosh and Keller (2013) postulate that the east-west striking structures are younger than the southeast-northwest striking structures based on valley width to height ratio (Vf), mountain front sinuosity (Smf), and drainage density (Dd) values. They suggest that faults and folds first strike east-west and are then rotated clockwise to a southeast-northwest orientation. The Western Transverse Ranges have experienced clockwise rotation (Luyendyk, 1991), but the hypothesis that east-west structures are younger than southeast-northwest structures has not been confirmed with absolute age dates. At several points along the coast, lateral cross faults strike northeast and segment larger east-west oriented faults. For example, the segment

boundaries in the More Ranch-Mission Ridge-Arroyo Parida fault coincide with proposed cross faults at Goleta Point, Fernald Point, and Rincon Point (Gurrola and Kamerling, 1996; Keller and Gurrola, 2000).

Between the Santa Barbara and Ventura fold belts is the Carpinteria Basin syncline (Figure 1). This north-verging syncline stretches from Rincon Mountain to Sand Point on the west side of Carpinteria (Jackson and Yeats, 1982). Due to downwarping in this basin, the first emergent marine terrace disappears below sea level. Jackson and Yeats (1982) found that the dip of the south limb of the syncline decreases where the greatest displacement on the Rincon Creek fault occurs. As a result, Jackson and Yeats (1982) suggest that the shape of the Carpinteria Basin syncline and the greater Carpinteria Basin is influenced by slip on the Rincon Creek fault. Carpinteria Basin is actively subsiding at a rate of 1.2±0.4 m/ky (Simms et al., 2016).

Previous Work

Marine Terraces

Emergent marine terraces, also known as marine strandlines, have been studied since the late 1890's (Lajoie et al., 1991). Bradley and Griggs (1976) studied the gradients of offshore wave-cut platforms of Ben Lomond terraces near Santa Cruz, California, and calculated Late Tertiary uplift rates. They concluded that platforms must have been eroded during times with high eustatic sea level because of tectonic uplift. William Bull (1985) developed a method to date successive terraces within a flight of terraces, given the age of one terrace, the elevations of the terraces, and a local sea-level curve. The pitfall of this method is its dependence on the assumption that uplift rate is constant. Recent studies utilize

multiple techniques to carefully date each marine terrace. For example, Gurrola et al. (2014) performed extensive dating of uplifted marine terraces in Santa Barbara County using uranium-series dating of terrace corals, optically stimulated luminescence of terrace sands, ^{14}C dating of shells and charcoal, and marine isotopic signatures of mollusks. Gurrola et al. (2014) dated the first emergent marine terrace (MIS 3 and 5) at several locations between the University of California, Santa Barbara (UCSB)-Isla Vista terrace (~45 ka) in Goleta and the Summerland terrace (~105 ka) near Carpinteria.

Chronology of marine terraces in the Santa Barbara fold belt allows for calculations of local surface uplift. Keller and Gurrola (2000) use the UCSB, Ellwood, More Mesa, La Mesa, Montecito, and Summerland terraces (~45 ka-~125 ka) to calculate a surface uplift rate of ~1-2 m/ky for Santa Barbara County. The first emergent marine terrace increases in age from west to east, indicating decreasing uplift rates from west to east within Santa Barbara County (Gurrola et al., 2014).

Putnam (1942) recognized the difficulty of correlating terraces near Ventura, California. Marine terraces near Rincon Mountain slope westward toward Carpinteria and are offset extensively by several faults. Putnam (1942) describes nine marine terraces uplifted at different elevations on Rincon Mountain. One of these terraces, the "200-ft" terrace, is described as disappearing below sea level at Carpinteria. This terrace is also known as the Carpinteria Bluffs marine terrace. Lajoie et al. (1982) dated and mapped three uplifted marine terraces in the Ventura area: the Ventura terrace (85-105 ka), the Punta Gorda terrace (40-60 ka), and the Sea Cliff terrace (1.8-5.8 ka) described by Putnam (1942). The Punta Gorda terrace is discontinuous but has been correlated from Carpinteria to Pitas Point using amino acid racemization of fossilized shells, the cool-water aspect of mollusks (Lajoie et al.,

1979; Lajoie et al., 1982) and geomorphic data (Lajoie et al., 1982). Other dates on the Punta

Gorda terrace include: U-series on mollusk shells (Kaufman et al., 1971); amino acid

racemization of mollusk shells (Lajoie et al., 1979; Wehmiller et al., 1978); and oxygen

isotope signatures from shells (Trecker, 1999), which correlate the Punta Gorda terrace with

the Carpinteria Bluffs marine terrace across the Red Mountain fault. Lajoie et al. (1982)

dated the Punta Gorda terrace using uranium-series methods; although, it is unclear which

remnants of this terrace were actually dated. Therefore, chronology of the Carpinteria Bluffs

marine terrace needs development in order to determine whether the Carpinteria Bluffs

marine terrace is continuous across Rincon Creek as previous studies have implied (Lajoie et

al., 1982; Putnam, 1942).

Rock Strength

Duvall et al. (2004) took over 1000 Schmidt Hammer rock strength measurements in

the Santa Barbara fold belt. They classify the Pico Formation (Tp), Sisquoc Shale (Tsq),

Monterey Formation (Tm), Rincon Shale (Tr), Vaqueros Sandstone (Tvq), and Sespe

Formation (Tsp) as "less resistant" with a mean rebound value of 23.4 ± 4.1 overall, and the

Gaviota Sandstone (Tgss), Sacate Sandstone (Tsash), and Matilija Sandstone (Tma) as

"resistant" with a mean rebound value of 43.8 ± 6.1 overall. The mean rebound value was

42.1 ± 1.3 for Tma and 30.8 ± 1.6 for Monterey Shale depending on location. Keller et al.

(2015) took rock strength measurements with a Schmidt Hammer within Rattlesnake Creek

located on the south side of the Santa Ynez Mountains, west of the field area for this study.

The Cozy Dell Shale was too weak to measure, but was apparently armored with large Tma

boulders in the creek, allowing the creek to maintain a steeper gradient (Keller et al., 2015).

Sespe Formation had a mean rebound value of 17.3, Tcw had a mean value of 32.9, and Tma was most resistant with a mean value of 44.8. These lithologies had statistically different rock strengths within 5% confidence. Based on the rock strength measurements of Duvall et al. (2004) and Keller et al. (2015), the most resistant rocks in this study area belong to the Coldwater Sandstone (Tcw) and Matilija Sandstone (Tma), and all other rocks in the field area for this study are considered weak in comparison.

Fault and Fold Growth

Fault ruptures nucleate at a point and then propagate uniformly away from this point in two directions, accommodating more slip at the center of the fault and less at the ends of the fault (Cowie and Scholz, 1992a, b). With successive earthquakes, the surface area and length of the fault increase as displacement accumulates (Cowie and Scholz, 1992a, b). The presence of barriers, however, may restrict a fault to one propagation direction or impede lateral propagation altogether (Manighetti et al., 2001). In areas experiencing crustal shortening, reverse and thrust faults commonly have hanging-wall anticlines that grow in response to slip along a fault (Suppe and Medwedeff, 1990). Consequently, folds can propagate in one or two directions, producing sutured folds or en echelon patterns (Burbank et al., 1996; Keller et al., 2013).

Keller et al. (1999) describe several geomorphic indicators that demonstrate lateral fold propagation. Drainage density, wind gap elevation, topographic profile relief, age of deformed material, and rotation and inclination of the fold forelimb all decrease in the direction of fold propagation (Jackson et al., 2002; Keller et al., 1999). Jackson et al. (1996) estimate fold growth rates using the elevation of wind gaps (uplifted, abandoned channels),

propagation distance, and the number of earthquakes needed to produce the observed amount of uplift.

Drainage Rearrangement

Drainage patterns are influenced by multiple factors including stream power, erosion rate, and aggradation rate (Burbank et al., 1996). In active fold belts, these factors must contend with the growth rate and geometry of folds as well as the changes in substrate resistance they present (Burbank et al., 1996; Schumm, 1986). Laterally propagating folds interfere with stream networks, challenging existing streams to incise through newly created topography or to modify their flow paths. Lateral fold propagation often leads to the incision of water gaps across the fold. Water gaps become wind gaps when streams that once traversed the fold are diverted around the nose of the growing fold (Figure 2). Some streams are able to maintain their original flow paths despite active deformation and fold growth. These are called antecedent streams. Some folds may terminate growth at tear faults, such as Wheeler Ridge in California (Keller et al., 1998; Mueller and Talling, 1997). Antecedent streams may take advantage of these tear faults to traverse the anticline because the fault gouge is easier to erode (Medwedeff, 1992).

Drainages can also be rearranged by stream capture, which occurs when one stream breaches a drainage divide and steals another stream's drainage area. This often produces streams with anomalous bends, oddly-shaped drainage areas, and knickpoints (reaches of unusual profile steepness) due to the sudden increase in discharge (Prince et al., 2011).
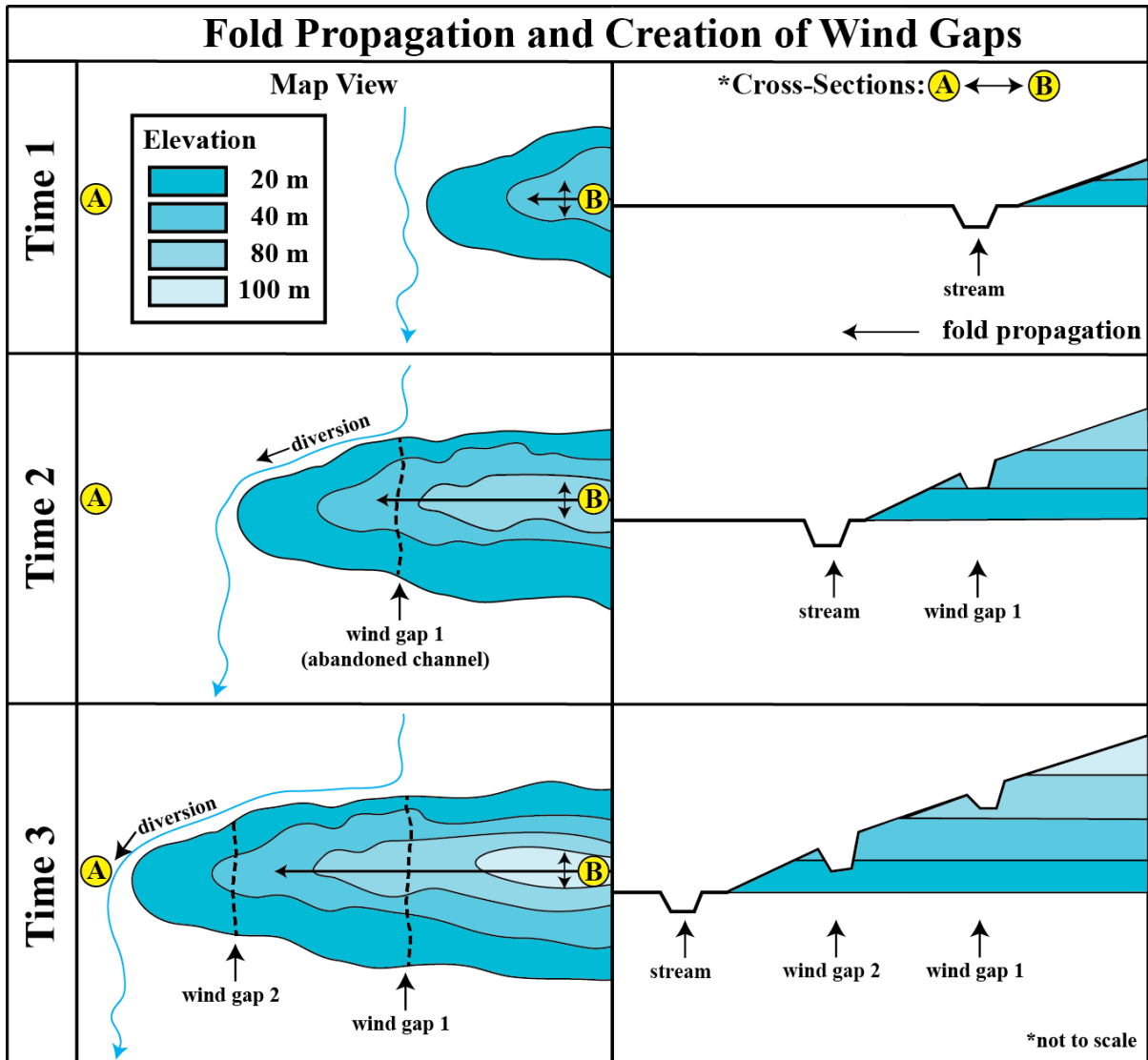
Figure 2: Wind Gap Model. This conceptual diagram illustrates the evolution of wind gaps due to stream diversion by laterally propagating folds. This process could explain the series of wind gaps on the Rincon Creek anticline within the study area.

Rincon Creek Anticline

The Rincon Creek anticline is an asymmetric fault-bend fold (Webber, 1999) associated with the Rincon Creek fault, a south-dipping blind reverse fault (Jackson and Yeats, 1982). The Rincon Creek anticline tapers westward and has three wind gaps, which suggest that it has propagated laterally to the west. Webber (1999) determined a minimum lateral propagation rate of 3.2-55 m/yr using the length of the anticline (2.5 km) and age limits of 790 ka (folded Casitas Formation) and 45 ka (marine terrace). Webber (1999) assumed that the base of the Rincon Creek anticline backlimb coincides with the shoreline angle of a ~45 ka marine terrace.

Hartleb (2000) describes a "refolded fold hypothesis" explaining the pattern of dipping strata in the backlimb of the Rincon Creek anticline. Bedding attitudes from the backlimb of the Rincon Creek anticline collected by Dibblee (1987) present the only concrete evidence for two folding events in the study area. First, the Casitas Formation was folded as part of the Carpinteria syncline (Jackson and Yeats, 1982) hundreds of thousands of years ago. The southern limb of the Carpinteria syncline was more recently refolded into the Rincon Creek anticline. The uncharacteristic pattern of dips in the backlimb of the Rincon Creek anticline reflects this refolding hypothesis, given that dips would be much steeper had the strata been horizontal before formation of the Rincon Creek anticline.

Study Area

The project area is located near the Santa Barbara and Ventura county border on the coast of California at Rincon Point (Figure 1). The study area sits on the east edge of the Carpinteria Basin syncline, where topographic relief starts to increase (Figure 3) and the first

emergent marine terrace reappears. This area is bounded to the north by the Santa Ynez

Mountains, to the west by Toro Creek, and to the east by San Juan Creek. East of Rincon

Point, the first emergent marine terrace, dated at ~45 ka, rises up to ~200 m above present

mean sea level (Gurrola et al., 2010). The first emergent terrace has not yet been numerically

dated to the west of Rincon Point. Relevant geomorphic features within the study area

include: the Rincon Creek anticline, Shepard Mesa, Carpinteria Bluffs marine terrace, incised

meanders, an uplifted paleochannel, and a sag pond (Figure 4).
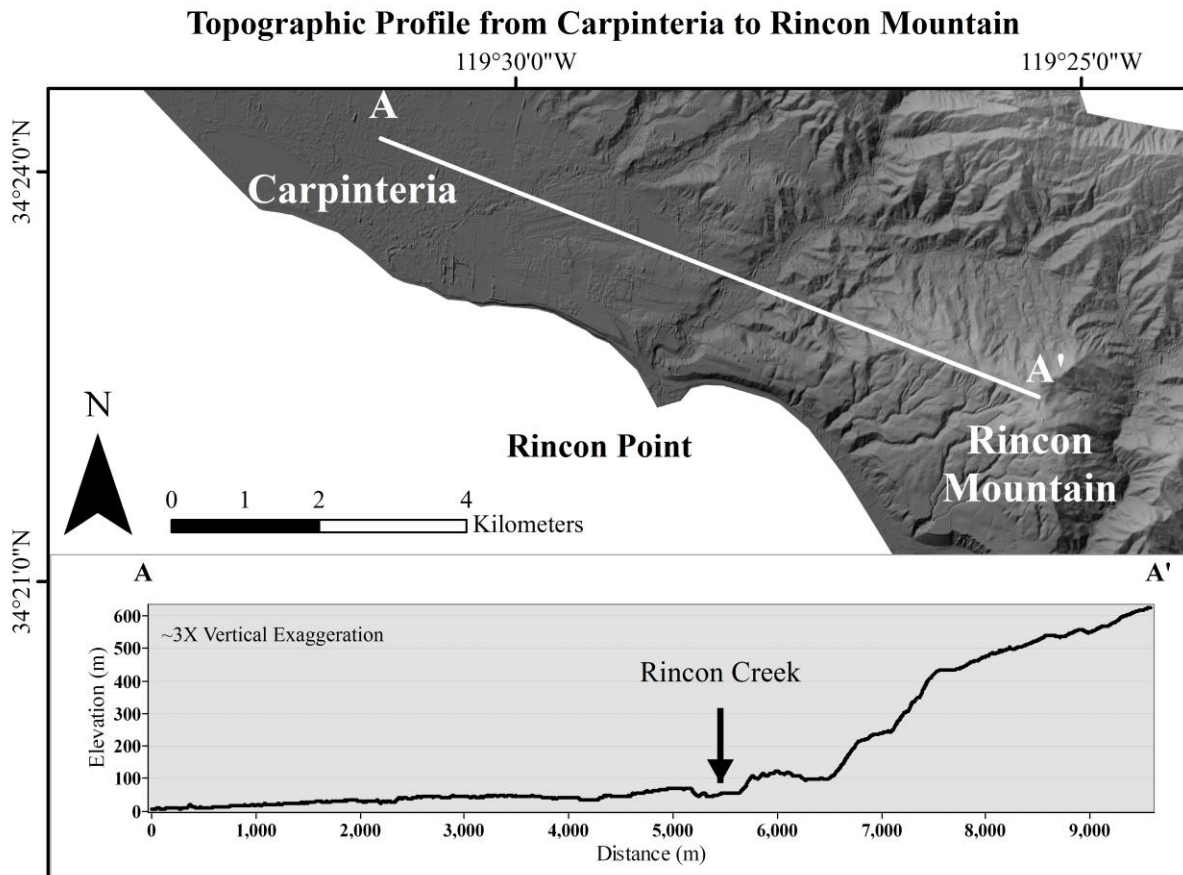
Figure 3: Topographic profile from Carpinteria to Rincon Mountain showing the dramatic rise in elevation east of Rincon Creek. Elevations were extracted from a 3-m IfSAR DEM accessed on NOAA's Data Access Viewer (DOC/NOAA/NOS/OCM, 2004).
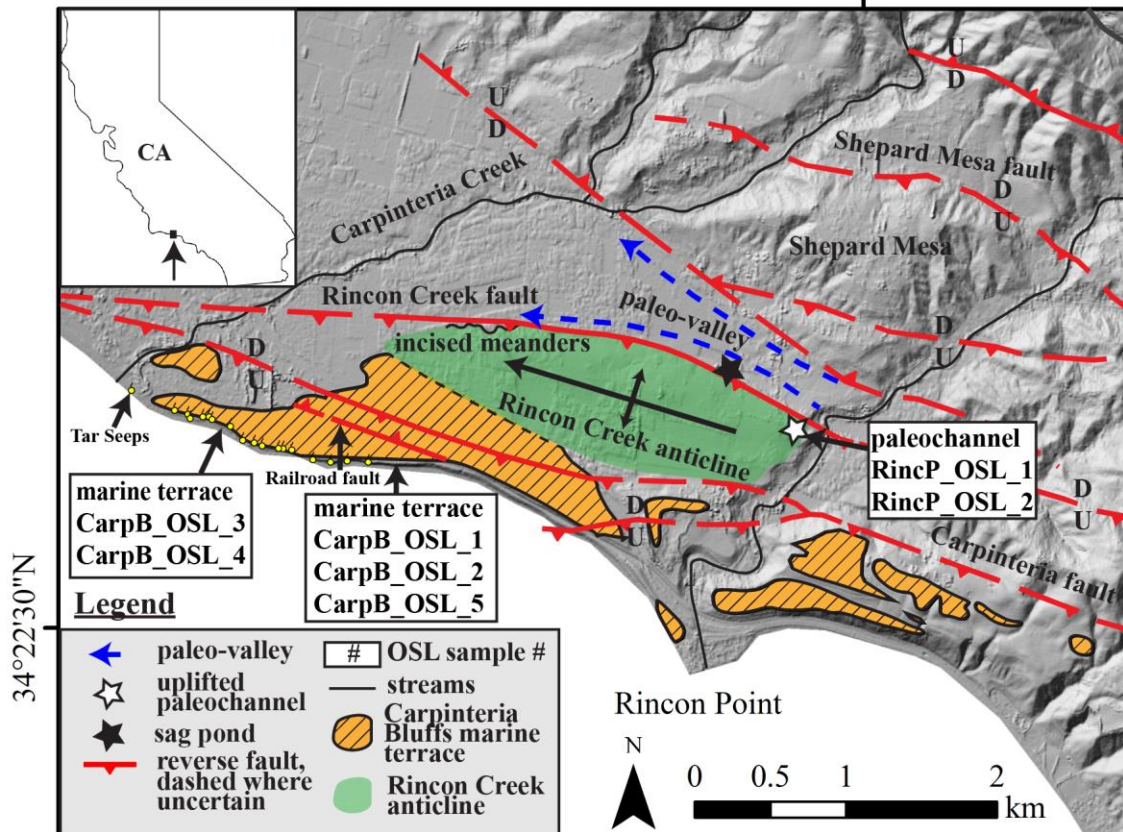
Figure 4: Geomorphic map of Rincon Point and the Carpinteria Bluffs marine terrace. Recent geologic mapping in the study area by Minor et al. (2009) and Minor and Brandt (2015) are detailed and agree with field observations noted in this study. Marine terrace deposits (striped) and faults are mapped after Minor and Brandt (2015). The Rincon Creek anticline in green is a hanging-wall anticline associated with the Rincon Creek fault. Fault locations are indicated with solid red lines where known and dashed lines where approximate. Dashed blue arrows represent the paleovalley thought to have been occupied by Rincon Creek before it was captured by a headward eroding stream. The white star indicates an uplifted paleochannel exposure in a landslide scar from which samples were taken for OSL dating. The black star indicates the sag pond, Lake Jocelyn. OSL sample locations are indicated in boxes. Tar seeps are indicated with yellow circles and mapped as in Minor and Brandt (2015). Background: 3-m IfSAR DEM available through NOAA Data Access Viewer (DOC/NOAA/NOS/OCM, 2004). Coordinate system: NAD1983 UTM Zone 11N; Projection: Transverse Mercator; Datum: North American 1983; Units: Meter.

METHODS

Digital Topographic Analysis

High resolution digital elevation models (DEMs) were used to explore prominent geomorphic features including the Carpinteria Bluffs marine terrace, the Rincon Creek anticline, and the Carpinteria fault scarp (Figure 4). For features over 1 km inland, a first surface return 3-m IfSAR DEM from 2002/2003 data was used (DOC/NOAA/NOS/OCM, 2004). A hydro-flattened bare-earth 1-m LiDAR DEM from the 2009-2011 CA Coastal Conservancy Coastal LiDAR Project was used for coastal features (DOC/NOAA/NOS/OCM, 2012). Both DEMs are available with Data Access Viewer hosted by the National Oceanic and Atmospheric Association (NOAA) Office for Coastal Management (OCM). Dibblee's (1986, 1987, 1988) geologic maps of Carpinteria, White Ledge Peak, and Ventura and Pitas Point quadrangles, Minor et al.'s (2009) geologic map, and Minor and Brandt's (2015) geologic map were also consulted. Geologic mapping is beyond the scope of this project. Digital topographic analysis is a convenient way to study the surface expression of faults and folds, especially in developed areas with private property. Topographic profiles were extracted directly from these DEMs to examine the relief of the Carpinteria fault scarp, the elevation of the Carpinteria Bluffs marine terrace, and the morphology of the Rincon Creek anticline. Digital topographic analysis was followed by visits to the field area for ground-truthing.

Measuring the Elevation of the Carpinteria Bluffs Wave-cut Platform

Elevations of the Carpinteria Bluffs marine terrace wave-cut platform were collected with a TruPulse 200 Laser Rangefinder from sea cliffs and railroad cuts. The rangefinder was

14

used to measure vertical distance, and measurements were adjusted for eye height as well as the elevation from which the measurement was taken. Each measurement has an error of ±30 cm. Measurements begin at Carpinteria State Beach and end at Rincon Creek. The wave-cut platform is distinguished by a planar, beveled bedrock surface, often covered with a layer of cobbles bearing pholad borings.

Chronology: Optically Stimulated Luminescence (OSL)

Concept

OSL provides a way to date the last time minerals were exposed to sunlight (Aitken, 1998). Natural background ionizing radiation in sediment displaces electrons, which are trapped in the crystal lattices of quartz and feldspar (Huntley et al., 1985). Exposure to sunlight upon erosion, transportation, and subsequent depositional events resets the dose of the sediment, causing trapped electrons to escape their crystal lattices and release photons of light, called luminescence, which can be measured (Huntley et al., 1985). Age is determined by dividing the amount of stored radiation (equivalent dose) by the rate at which the radiation is absorbed (dose rate). OSL dating is the best geochronometer for dating the Carpinteria Bluffs marine terrace: 1) OSL spans the appropriate timescale (up to 200 kya), 2) sandy sediment for dating is abundant, and 3) others have had success dating similar marine terrace sands nearby (Gurrola et al., 2014).

Sampling

Sampling techniques follow those of the Utah State University (USU) Luminescence Lab (Rittenour, 2015). See Nelson et al. (2015) for a complete luminescence sampling guide.

Units were sampled at a minimum of 1 m depth from the surface. Bioturbated and otherwise disturbed sediments were avoided as conditions allowed. Fine-grained sandy sediments with primary sedimentary structures (laminations, rippled laminations, alternating light and dark laminae) were preferentially sampled, as these were most likely exposed to sunlight before deposition and least likely reset by bioturbation (Rittenour, 2015). Samples were collected with a ~20-cm (8-in) long, ~4-cm (1.5-in) diameter stainless steel electrical conduit, which is impervious to light. A dose rate sample was collected from a ~15 cm radius around the sample tube, and water content sample was collected and stored in an airtight container.

Seven samples were collected, five from the Carpinteria Bluffs marine terrace and two from the Rincon Creek paleochannel exposed in the Rincon Creek anticline. Samples CarpB_OSL_1 and CarpB_OSL_2 were collected with the supervision of USU professor Dr. Joel Pederson. The expected age of the Carpinteria Bluffs marine terrace is between ~45 and ~105 ka because the first emergent marine terrace has been dated at ~45 ka to the east at Rincon Mountain (Wehmiller et al., 1977) and at ~105 ka to the west at Summerland (Gurrola et al., 2014).

Processing

OSL samples were processed at the USU Luminescence Lab under the supervision of Dr. Tammy Rittenour. Sample preparation included sieving, removing carbonates and organics, and isolating quartz for analysis. Luminescence was measured with a Risø TL/OSL Model DA-20 reader. The USU Luminescence Lab uses the single-aliquot regenerative-dose (SAR) method (Murray and Wintle, 2000, 2003; Wintle and Murray, 2006) for determining OSL age of quartz sand. Blue-green light was used to stimulate and measure natural

luminescence from quartz grains. Dosing was performed in the lab to build a dose-response curve in order to determine how efficiently a sample accumulates radiation. The intercept of the natural dose with the dose-response curve gives the equivalent dose (D_E) that the sample absorbed during the last burial event. This process was repeated for multiple aliquots for each sample. The age of the sample was calculated by dividing D_E by the dose rate, D_R (Nelson et al., 2015). In this study, D_E for each sample was calculated using the Central Age Model (CAM) of Galbraith and Roberts (2012). See Appendix for detailed description of OSL procedures.

$$\text{Age (ka)} = \frac{D_E(Gy)}{D_R(Gy\ ka^{-1})} \quad \text{(Eq. 1)}$$

D_E=equivalent dose

D_R=dose rate

Slip Rates

The age of the Carpinteria Bluffs marine terrace and several bucket auger logs from Chevron Oil Co. (Keller, pers. comm., 2015) are used to calculate a vertical slip rate for the Carpinteria fault. The stratigraphy of the bucket auger logs was measured with accuracy to 0.03 m (0.1 ft). A topographic map with 0.76-m (2.5-ft) contour intervals from Hoover and Associates (1989), which predates grading for development, was used to construct a geologic cross-section that compiles boring data. Unit contacts were extrapolated between borings to measure offset of the Carpinteria Bluffs marine terrace across the Carpinteria fault. Slip rate was calculated by dividing the amount of terrace offset by the age of the terrace.

$$R_{vs} = \frac{t_{offset}}{\Delta t} \qquad (Eq.\ 2)$$

R_{vs} = vertical slip rate

t_{offset} = vertical offset of marine terrace

Δt = age of the marine terrace

The slip rate of the railroad fault was calculated by observing terrace offset exposed in the railroad cut in the Carpinteria Bluffs. These faults may have a lateral component of slip, but only vertical slip rates are calculated here. Slip rates reported are assumed to be constant, and therefore, minimum rates.

Calculating Uplift Rate of the Carpinteria Bluffs Marine Terrace

To estimate the uplift rate of the Carpinteria Bluffs marine terrace, relative sea level was subtracted from the elevation of the shoreline angle and divided by the age of the terrace. The local sea level curve from Simms et al. (2015) defines sea level at the time the terrace was formed.

$$R_u = \frac{(E-SL)}{\Delta t} \qquad (Eq.\ 3)$$

R_u = uplift rate of the terrace

E = shoreline angle elevation

Δt = age of the marine terrace

SL = local relative sea level (at the above age) measured in distance above (+)

or below (-) modern sea level

modified from Keller and Pinter (2002)

Error in uplift rate was calculated as in Simms et al. (2015):

$$\varepsilon_R = \left[\varepsilon_E^2 + \varepsilon_P^2 + \varepsilon_T^2 \times (E\text{-}P)^2 / T^2 \right]^{0.5} / T \qquad \text{(Eq. 4)}$$

ε_R = uncertainty in tectonic uplift rate estimate

ε_E = uncertainty in marine terrace elevation (E)

ε_P = uncertainty in predicted sea level (P) in the same location at time T

ε_T = uncertainty in marine terrace age (T)

Generally, uplift rates of marine terraces are calculated using the elevation of the shoreline angle. The shoreline angle of the Carpinteria Bluffs marine terrace is approximately coincident with the backlimb of the Rincon Creek anticline. This is based on the mapped extent of the terrace by Minor and Brandt (2015). The elevation of the shoreline angle was determined by correcting platform elevations measured at OSL sites. The correction amount was calculated using distance from the OSL site to the shoreline angle location and the gradient of the wave-cut platform. OSL samples 1, 2, and 5 are located about 0.5 km from the approximated shoreline angle and samples 3 and 4 are located about 0.8 km from the approximated shoreline angle. The average lowest platform gradient (0.010 or 10 m/km) from a study of central California wave-cut platforms by Bradley and Griggs (1976) was used. The modern slope of the marine terrace is not appropriate to use here because it has been folded and tilted. Wave-cut platform elevation measured at OSL samples sites was corrected by adding 5 m elevation at Carpinteria Bluffs Nature Preserve (samples 1, 2, 5) and 8 m at Tar Pit Park (samples 3 and 4). Error for terrace elevation (ε_E) takes both the elevation measurement and shoreline angle correction into consideration.

Calculating Propagation Rate of the Rincon Creek Anticline

Lateral propagation rate was estimated by dividing the length of the anticline by the anticline age, that is, the time that marks the initiation of lateral propagation. This age is estimated by OSL dating of sediments at the base of an uplifted paleochannel on the forelimb of the Rincon Creek anticline. This paleochannel marks the past flow path of Rincon Creek. The presence of three wind gaps on the Rincon Creek anticline suggests that Rincon Creek was diverted around the nose of the westward-propagating anticline several times before being captured by a small, headward-eroding stream. The wind gaps are located at decreasing elevations to the west, which is convincing evidence for westward lateral propagation. Assuming the fluvial sediments in the paleochannel were bleached before being buried, the OSL age of the sediments at the base of the paleochannel should reflect the minimum age of the uplift event that caused this stream to become abandoned. Naturally, this age underestimates the age of folding. A stream is diverted when uplift outpaces the stream's ability to incise. Therefore, it is reasonable to assume that some uplift and even propagation occurred before Rincon Creek was diverted. Nevertheless, the OSL ages provided here represent the best available estimate of the anticline age.

Stream Profile Analysis

Stream Steepness

Eleven drainage basins, including Rincon Creek, were analyzed for normalized stream steepness (k_{sn}) values (Figure 5). If uplift rate decreases significantly to the west of Rincon Creek, stream steepness should also decrease. K_{sn} values describe the steepness of a

stream at a given point in its profile according to that river's concavity and upstream

drainage area. More specifically, k_{sn} can be described by the following equation:

$$k_{sn}=k_s*A_{cent}^{(\theta_{ref}-\theta)} \quad \text{(Eq. 5)}$$

k_s = steepness index

θ = concavity index

θ_{ref} = reference concavity

A_{cent} = midpoint value of upstream drainage area of the stream segment being analyzed

(Wobus et al., 2006)

K$_{sn}$ values are always positive and typically range from about 1-1000. In this study,

k_{sn} values are calculated directly from a 3-m IfSAR DEM (DOC/NOAA/NOS/OCM, 2004)

using ArcGIS, Matlab, and a free stream profiler tool available online at

www.geomorphtools.org. The stream profiler tool was initiated by Noah Snyder and Kelin

Whipple and refined by others including Daniel Sheehan, Eric Kirby, Joel Johnson, Ben

Crosby, Cam Wobus, and Will Ouimet. The k_{sn} values reported are determined from linear

regressions of slope-area plots. Regression boundaries were chosen manually based on the

character of the longitudinal profiles and the slope-area data for each stream. Uppermost,

debris-flow dominated channel reaches were avoided. The lowermost 0.25-0.5 km of stream

length were excluded due to human intervention such as culverts. Streams with prominent

knickpoints required multiple regressions. Regressions begin at the lip of the knickpoint and

continue to lip of the following knickpoint, if present. Slope-area data was used to distinguish

between debris flow-dominated and fluvial-dominated channel processes. Slope-area plots

were also useful for identifying changes in stream steepness along the channel profile. Basins

8-11 in this study were also included in the k_{sn} analysis of Duvall et al. (2004) for the

purpose of examining controls on bedrock channel profiles. The same reference concavity of

0.4 is used to corroborate and compare with existing k_{sn} values. Longitudinal profiles with

regression results for each stream are included in the appendix. See Whipple et al. (2007) for

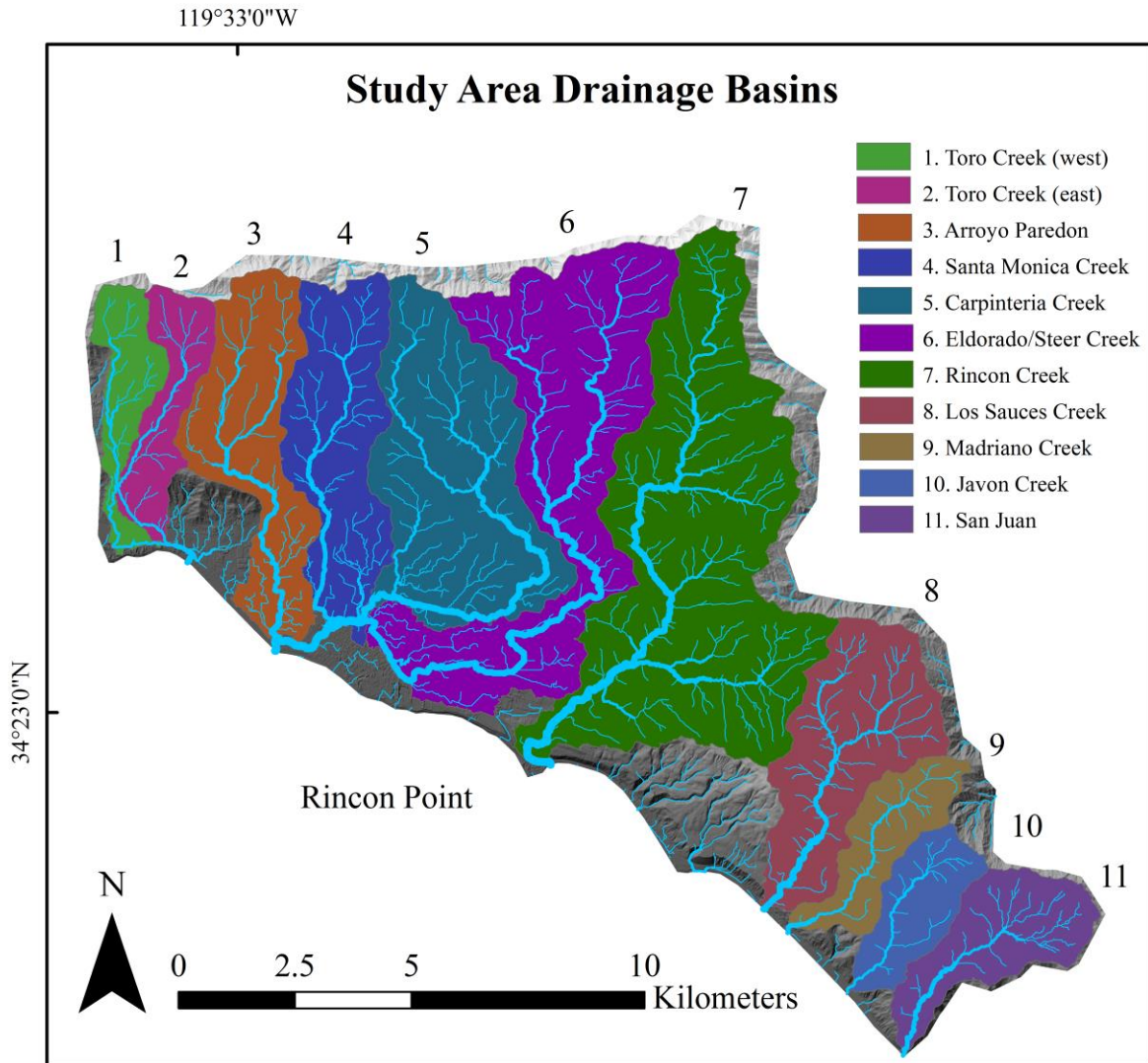detailed instructions on DEM preparation and stream steepness analysis.

Figure 5: Drainage basin map for the study area. Eleven basins are analyzed in this study. Basins west of and including Rincon Creek belong to the Carpinteria group and basins to the east of Rincon Creek belong to the Ventura group for comparison. 3-m DEM in background (DOC/NOAA/NOS/OCM, 2004).

Knickpoints

Knickpoint data was provided by Alexander Neely and a custom algorithm which uses TopoToolbox Matlab codes (Schwanghart and Scherler, 2014) and a 3-m DEM (DOC/NOAA/NOS/OCM, 2004) to automatically select knickpoints from the stream profiles generated during the aforementioned DEM preparation. Knickpoints are identified as inflections in chi plots, plots of elevation versus the integral quantity χ (Perron and Royden, 2013). Knickpoints consist of an upstream lip (convex up) and a downstream base (concave up), and the magnitude of a knickpoint is here defined as the change in elevation from lip to base. Small knickpoints in close proximity are lumped together, and knickpoints below a threshold magnitude of 10 m are omitted.

The presence and pattern of knickpoints can be very telling about the amount and duration of tectonic uplift, experienced as base level (sea level) fall in stream networks. Knickpoints may be stationary or transient. Lithologic knickpoints are stationary and generally situated on resistant beds or lithologic contacts. Since geologic units are well-mapped, lithologic knickpoints should occur in predictable locations in multiple stream profiles. Pulses of tectonic uplift, such as during seismic events, may generate transient knickpoints that propagate through the stream network (Cook et al., 2013). These transient knickpoints steepen the profile of the stream at a propagation rate proportional to upstream drainage area (Loget and Van Den Driessche, 2009). Migratory knickpoints, if present, are expected to occur at similar elevations throughout a given drainage basin (Whipple and Tucker, 1999).

RESULTS

Tear Fault

A tear fault is here defined as a fault that crosses and segments one or more major faults, especially thrust faults, at a high angle. The tear fault at Rincon Point proposed by Gurrola and Kamerling (1996) strikes north-east and follows the linear, downstream portion of Rincon Creek (Figure 6). This tear fault might partition slip by impeding westward-propagating ruptures along intersected faults (e.g. Red Mountain fault, Carpinteria fault, Rincon Creek fault). This phenomenon may explain the juxtaposition of Rincon Mountain with Carpinteria basin; however, other structures also affect the geomorphology of Rincon Point. The tear fault may continue north as a dashed right-lateral fault mapped by Minor and Brandt (2015) which apparently offsets the Sespe Formation and Coldwater Formation. The right-lateral sense of offset may be explained by east-side-up slip on the proposed tear fault, followed by erosion. There are no geomorphic indications that the tear fault continues north of the Arroyo Parida fault. The tear fault is probably not seismogenic but seismically passive, accomodating slip generated by other, active faults (Rockwell, pers. comm., 2016). Nevertheless, a tear fault can significantly affect patterns of tectonic uplift. Digital topographic anlaysis provides several pieces of observational evidence supporting the presence of a tear fault at Rincon Creek:

1) the dramatic increase in elevation of the first emergent marine terrace across Rincon Creek from west to east,

2) the unusual linearity of lower Rincon Creek,

3) the possible left-lateral offset of Tertiary and Quaternary units mapped by Minor and Brandt (2015) including: Casitas Formation (Qca), Monterey Formation (Tm), Santa Barbara Formation (Qsb),

4) and the eastern termination of the Rincon Creek anticline at Rincon Creek suggests it might be structurally pinned by the tear fault.

Shepard Mesa Fault

Minor and Brandt (2015) map an approximated, north-side-up reverse fault at the base of the south side of Shepard Mesa (Figure 4). This fault is not visible at the surface, and Shepard Mesa is not folded; however, the base of the southern flank of the Mesa is linear, supporting a tectonic origin. Alternatively, one could argue that the southern flank of the mesa has been carved by fluvial erosion. The southern end of the Mesa is punctuated by a broad paleovalley, which was occupied by Rincon Creek before it was captured by a headward-eroding stream. Because the aforementioned linear front extends beyond the paleovalley, a tectonic origin for Shepard Mesa is more likely than an erosional origin.
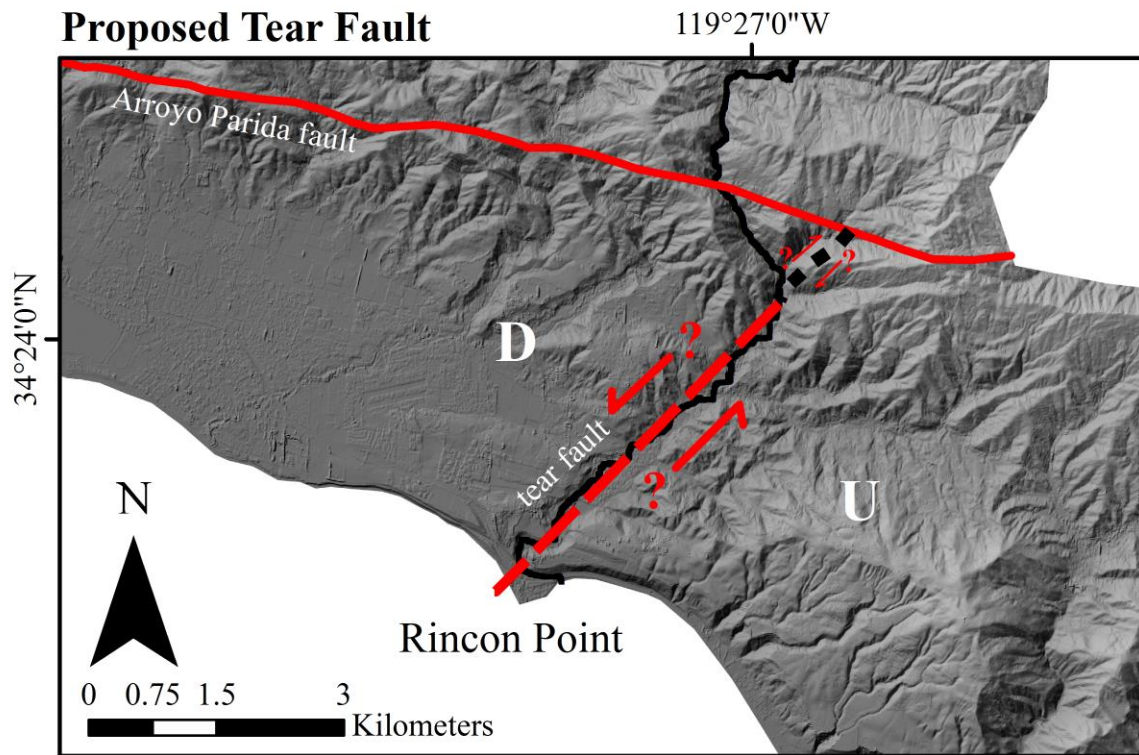
Figure 6: Proposed tear fault. The red dashed line represents the tear fault and follows the downstream, linear reach of Rincon Creek, shown in black. Sense of slip on the tear fault is unknown, but may include an east-side-up dip slip component and possibly a left lateral slip component. The tear fault separates the actively subsiding Carpinteria Basin to the west and the uplifting Rincon Mountain to the east. The tear fault lines up with a small, dashed right-lateral strike-slip fault (shown in black) as mapped by Minor and Brandt (2015). This small strike-slip fault terminates at the Arroyo Parida fault as mapped. 3-m DEM in background (DOC/NOAA/NOS/OCM, 2004).

Carpinteria Bluffs Marine Terrace

Tar Seeps and Marine Terrace Shoreface Deposits

Naturally occurring tar seeps blanket the sea cliffs of Carpinteria. Tar appears on the beach precisely where the first emergent marine terrace is visible above sea level at the east end of Carpinteria State Beach. Minor and Brandt (2015) map the tar seeps from Carpinteria State Beach to just west of the Railroad Fault (Figure 4). OSL ages on sediments collected above the wave-cut platform near Tar Pit Park give a maximum age for onshore tar pits. Fresh tar oozes out of the cliffs from above the Monterey Formation, a relatively impermeable unit of white, indurated shale that dominates the base of the sea cliff along Santa Barbara and Carpinteria (Figure 7). Some tar squeezes through fractures within the Monterey Formation. The top surface of the Monterey Formation was beveled by wave action before the platform was elevated to its current position. A permeable, 1-3 m thick sandy unit directly overlying the uplifted wave-cut platform contains tar, abundant cross-bedding, and rock fragments bearing pholad shells and borings (Figure 8). These features indicate deposition in a shoreface environment.

Alternatively, one might argue that the wave-cut platform described is actually a fluvial pediment surface and the pholad-bearing cobbles were carried inland by tsunamis. This interpretation is unfounded considering the following: 1) no tsunami deposits have been identified in Santa Barbara or Ventura, 2) cross-bedded sands do not fit the description of tsunami deposits, 3) transgressive ravinement surfaces (wave-cut platforms) are characterized by gravel lag as shown in Figure 8, and 4) the wave-cut surface can be traced across the Santa Barbara channel. Furthermore, Rockwell et al. (1992) describe marine terrace deposits between Point Conception and Gaviota in the Western Transverse Ranges as well-sorted,

massive to cross-bedded sand with local rounded pebbles to boulders bearing pholad

(Pholadidae) borings, marine molluscan fauna, and tar blebs. This is an apt description of

marine terrace deposits at Tar Pit Park. Gurrola et al. (2014) also note that marine terrace

fossils are often preserved in basal conglomerates on wave-cut platforms in Santa Barbara. In

contrast, Goff et al. (2012), in a review of paleotsunami research, describe tsunami deposits

as normally-graded, inversely-graded, or massive, depending on width of the source region

and wave duration.

Figure 7: Photo of the Carpinteria tar seeps at Tar Pit Park. Notice the tar seeping out of the
sea cliff directly above the Monterey Formation at the uplifted wave-cut platform. Cross-
bedding in the overlying sandy unit can be seen on the left side of the photograph.

Figure 8: Top: Tar-inundated sandy unit overlying the wave-cut platform and Monterey Formation on Carpinteria State beach. This unit exhibits cross-bedding and intermittent pebbly layers, here including a rock fragment with pholad borings. Bottom: modern pholad shells in their borings from Carpinteria State beach.

Elevation of the Carpinteria Bluffs Marine Terrace

At Carpinteria, the first emergent marine terrace has been uplifting slowly above sea level. The pace of subsidence within the Carpinteria Basin, ~1.2±0.4 m/ky (Simms et al., 2016), is nearly equivalent to the rate of tectonic uplift in the Santa Barbara fold belt (~1-2 m/ky). As a result, the first emergent terrace disappears below sea level where Carpinteria beach reaches farthest inland. At Loon Point, the wave-cut platform is carved into Casitas Formation. The Loon Point fault hanging wall anticline folds the platform. The platform has eroded the top of the anticline, but appears again on the backlimb of the anticline before it disappears below sea level. The wave-cut platform remains below sea level at Carpinteria Slough and for most of Carpinteria State Beach, appearing above sea level again at Tar Pit Park in Carpinteria. From here eastward, the platform is carved into the white shale of the Monterey Formation, making it easy to identify from overlying marine terrace deposits. The Carpinteria Bluffs marine terrace slopes westward and continues relatively uninterrupted to Rincon Creek. Several faults warp the wave-cut platform, which rises steadily to about 75 m of elevation at Rincon Creek (Figure 9). Though laser rangefinder measurements were only collected on the west side of Rincon Creek, the terrace continues on the east side of Rincon Creek as a collection of stepped fragments with a steeper westward slope. The terrace disappears across the Rincon Mountain megaslide and reappears near Punta Gorda where it is offset by the Red Mountain fault (Gurrola et al., 2010).

Careful topographic analysis of the Carpinteria Bluffs marine terrace with a 1-m LiDAR DEM (DOC/NOAA/NOS/OCM, 2012) reveals a kink in the terrace profile across Rincon Creek (Figure 10 and 11). Here the terrace slope is much steeper compared to the slope of the terrace just west at the Carpinteris Bluffs Nature Preserve. This change in tilt

could be explained by slip on the Red Mountain fault, which takes a left turn offshore just east of Rincon Point (Figure 1). This suggests that there is no vertical offset of marine terrace deposits across Rincon Creek and no tear fault at Rincon Point. Alternatively, if one continues the slope of the terrace from west to east across Rincon Creek, one can find a range of vertical offsets. Three topographic profiles, roughly parallel to the coastline, transect marine terrace deposits mapped by Minor and Brandt (2015) and Gurrola et al. (2014). Each topographic profile transects a different "step" (Figure 10) in the marine terrace on the east side of Rincon Creek in order to capture all offset possibilities (Figure 11). One of the steps can be explained by an east-west trending dashed fault (Minor and Brandt, 2015) which separates Profiles B and C. The step between Profiles A and B is mapped as a paleoshoreline and does not correspond with any proposed faults. To calculate offset, the westward slope of the Carpinteria Bluffs marine terrace on the west side of Rincon Creek was projected to the east side. The difference in elevation between this projection and the actual elevation of marine terrace deposits was calculated to give a conservative estimate of vertical offset. The southernmost profile, Profile A, is most conservative and yields a vertical offset of ~15 m. Profile B suggests an offset of ~38 m and Profile C an offset of ~45 m. The observed vertical offset may be explained by the presence of a fault at Rincon Creek with some east-side-up dip-slip component. The terrace kink due to uplift on the Red Mountain fault is favored as the simpler explanation for the morphology of the terrace.
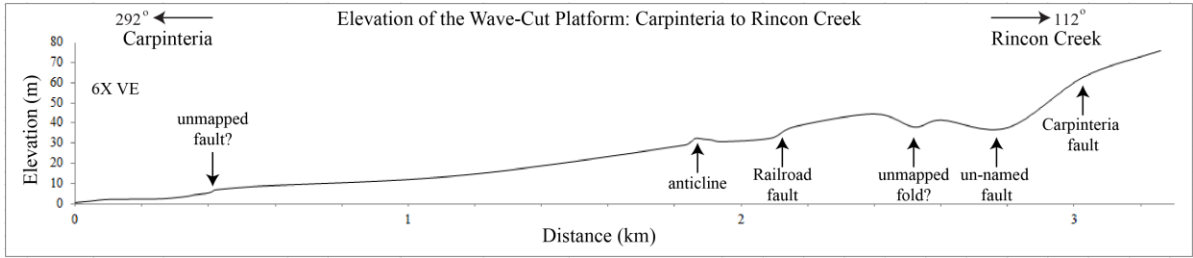
Figure 9: Carpinteria Bluffs marine terrace wave-cut platform elevations measured with a laser rangefinder. Elevations begin at Carpinteria Beach and end at Rincon Creek. View is looking northeast. Marine terrace deposits and other deposits overlying the wave-cut platform are not shown. Local faults and folds (Minor and Brandt, 2015; Minor et al., 2009) warp the wave-cut platform surface.
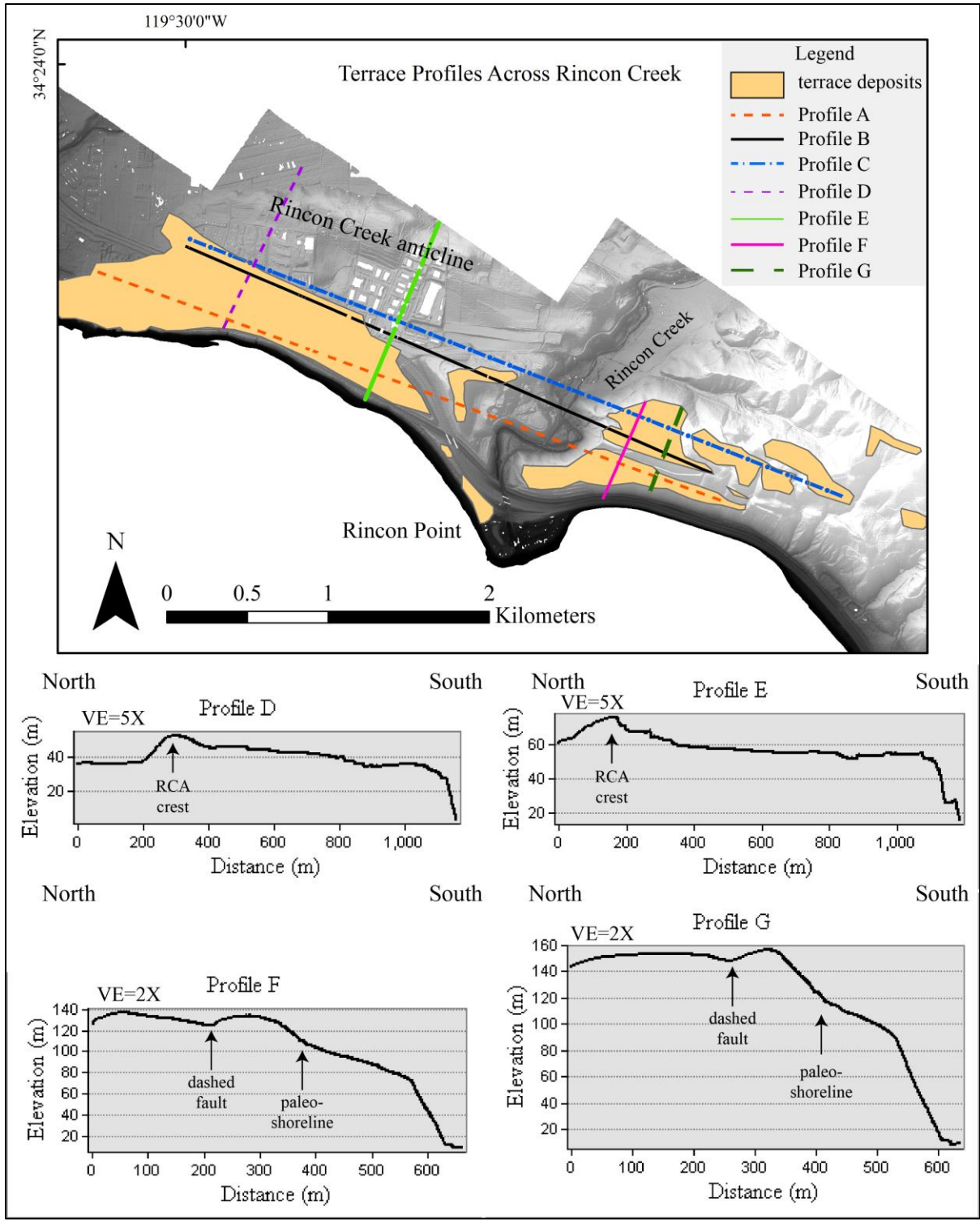
Figure 10: Map of topographic profiles across Rincon Creek. Profiles 1 and 2 show that terraces are stepped to the east of Rincon Creek. Profiles A, B, and C (Figure 11) capture all offset possibilities across Rincon Creek. The dashed fault (not shown here) is mapped by Minor and Brandt (2015). Background: 1-m LiDAR DEM (DOC/NOAA/NOS/OCM, 2012).
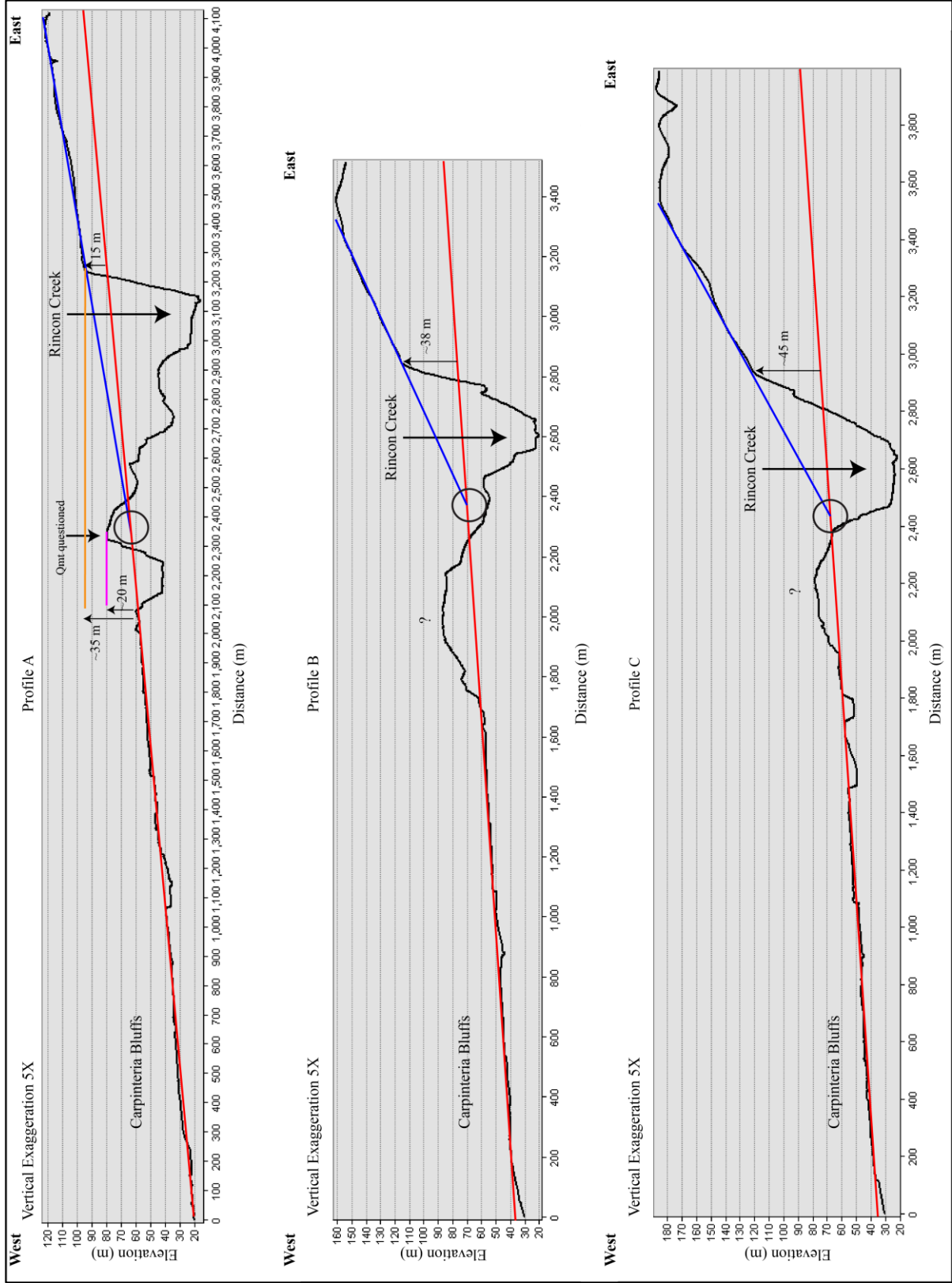
34

Figure 11: Profiles across marine terrace deposits shown in Figure 10 with possible vertical offsets of 15 m, 38 m, and 45 m depending on elevations of different terrace remnants. Vertical offsets depend on the assumption that the westward tilt of the terrace is consistent. Based on the mapped extent of terrace deposits, this scenario is unlikely. Gradient of the terrace west of Rincon Creek is shown in red and the gradient of the terrace east of Rincon Creek is shown in blue. The terrace gradients are extended across Rincon Creek; the point of intersection is circled. This defines a "kink" in the terrace profile that may be due to uplift or folding associated with the Red Mountain fault. The section labeled with a question mark or "Qmt questioned" appears to have been uplifted between two strands of the Carpinteria fault, which might explain why it does not match the profile of the rest of the terrace.
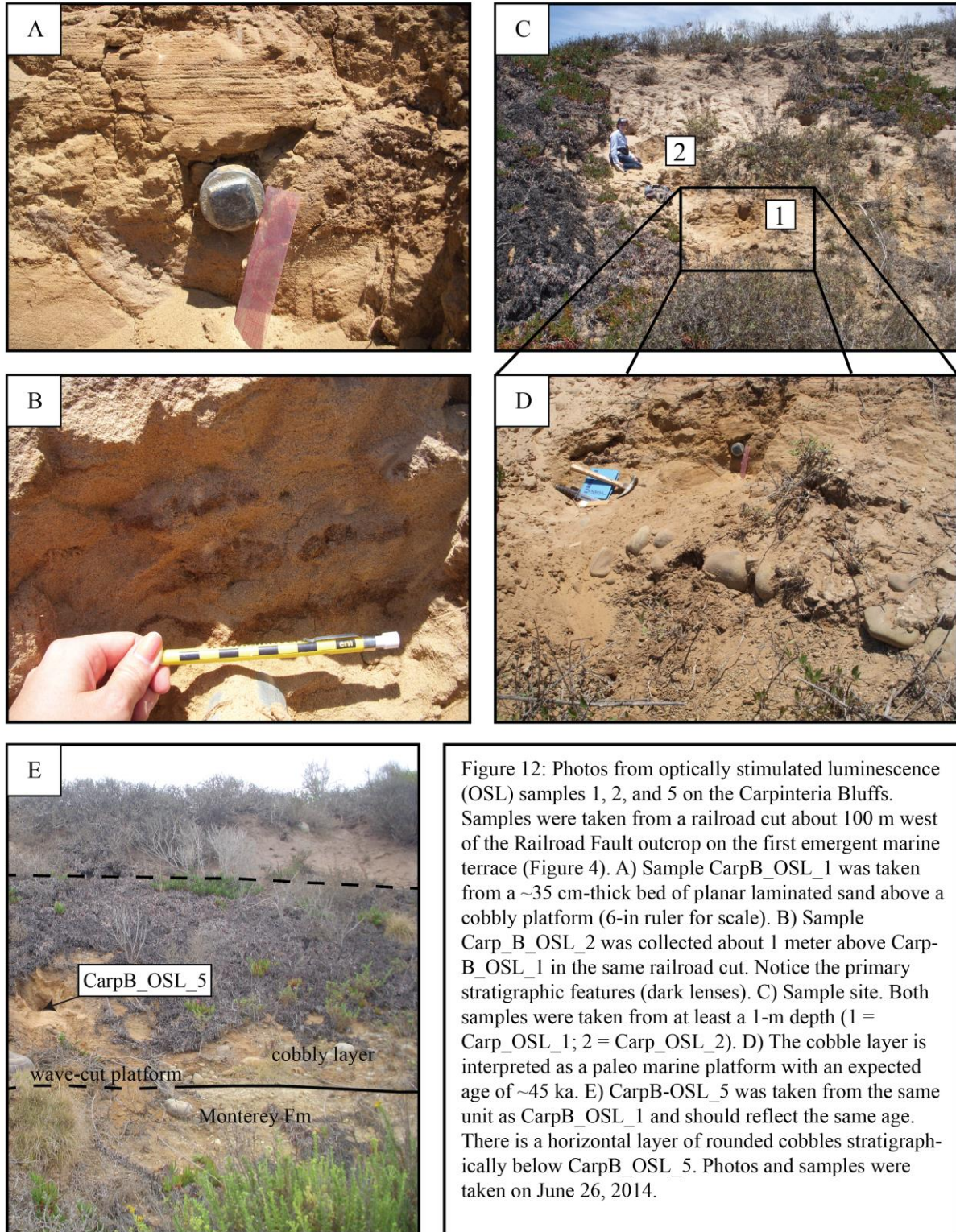
Chronology of the Carpinteria Bluffs Marine Terrace

Preliminary OSL dates yield an average age of 28.44 ± 7.36 ka for the Carpinteria Bluffs marine terrace (Table 1). Samples 1, 2, and 5 (Figure 12) were collected in close proximity near the eastern edge of the Carpinteria Bluffs Nature Preserve and have an average age of 25.53 ± 7.36 ka. Samples 3 and 4 (Figure 13) were collected in close proximity to Tar Pit Park and have an average age of 32.81 ± 6.06 ka. This age serves as a maximum age for the onshore tar pits at Tar Pit Park. These preliminary ages place the Carpinteria Bluffs marine terrace in marine isotope stage (MIS) 3 between 60 and 25 ka B.P. (Siddall et al., 2008). These dates are younger than the Punta Gorda terrace, dated at ~45 ka; however samples 3 and 4 from this study fall within the range of dates collected from MIS 3 Santa Barbara and Ventura terraces. Samples descriptions are provided in Table 2.

Table 1: Optically Stimulated Luminescence Ages									
Sample #	Sample Name	USU #	[1]Location	Depth (m)	[2]Number of aliquots	Dose rate (Gy/ka)	[3]$D_E \pm 2\sigma$ (Gy)	[4]OD (%)	OSL age $\pm 2\sigma$ (ka)
1	CarpB_OSL_1	USU-2021	CB Preserve	4.0	14 (29)	3.48 ± 0.15	96.77 ± 23.71	38.4 ± 9.8	**27.79 ± 7.36**
2	CarpB_OSL_2	USU-2022	CB Preserve	2.8	19 (42)	3.14 ± 0.14	79.32 ± 20.82	51.3 ± 10.1	**25.27 ± 7.09**
3	CarpB_OSL_3	USU-2023	Tar Pit Park	4.5	18 (32)	3.52 ± 0.15	110.17 ± 18.19	30.6 ± 6.4	**31.31 ± 6.06**
4	CarpB_OSL_4	USU-2024	Tar Pit Park	4.5	17 (35)	3.53 ± 0.15	121.19 ± 15.60	22.8 ± 5.2	**34.31 ± 5.61**
5	CarpB_OSL_5	USU-2027	CB Preserve	4.5	17 (31)	3.59 ± 0.15	84.42 ± 16.79	34.9 ± 8.0	**23.54 ± 5.25**
Mean Age of the Carpinteria Bluffs Marine Terrace									**28.44 ± 7.36**
6	RincP_OSL_1	USU-2025	Rincon Creek	14.0	24 (35)	2.91 ± 0.13	112.07 ± 12.43	21.5 ± 4.6	**38.58 ± 5.72**
7	RincP_OSL_2	USU-2026	Rincon Creek	16.0	22 (36)	3.00 ± 0.13	119.57 ± 13.96	21.0 ± 5.1	**39.80 ± 6.07**
Effective Paleochannel Age									**39.80 ± 6.07**

[1]There are three sample sites: the east edge of the CB Preserve (Carpinteria Bluffs Nature Preserve), the west side of Tar Pit Park, and the base of the uplifted paleochannel of Rincon Creek exposed in a landslide scar on the Rincon Creek anticline.

[2]Age analysis using the single-aliquot regenerative-dose procedure of Murray and Wintle (2000) on 1-2 mm small-aliquots of quartz sand. Number of aliquots used in age calculation and number of aliquots analyzed in parentheses.

[3]Equivalent dose (DE) calculated using the Central Age Model (CAM) of Galbraith and Roberts (2012).

[4]Overdispersion (OD) represents variance in DE data beyond measurement uncertainties, OD >20% may indicate significant scatter due to depositional or post-depositional processes.

OSL Samples: Carpinteria Bluffs Nature Preserve

Figure 12: Photos from optically stimulated luminescence (OSL) samples 1, 2, and 5 on the Carpinteria Bluffs. Samples were taken from a railroad cut about 100 m west of the Railroad Fault outcrop on the first emergent marine terrace (Figure 4). A) Sample CarpB_OSL_1 was taken from a ~35 cm-thick bed of planar laminated sand above a cobbly platform (6-in ruler for scale). B) Sample Carp_B_OSL_2 was collected about 1 meter above CarpB_OSL_1 in the same railroad cut. Notice the primary stratigraphic features (dark lenses). C) Sample site. Both samples were taken from at least a 1-m depth (1 = Carp_OSL_1; 2 = Carp_OSL_2). D) The cobble layer is interpreted as a paleo marine platform with an expected age of ~45 ka. E) CarpB-OSL_5 was taken from the same unit as CarpB_OSL_1 and should reflect the same age. There is a horizontal layer of rounded cobbles stratigraphically below CarpB_OSL_5. Photos and samples were taken on June 26, 2014.
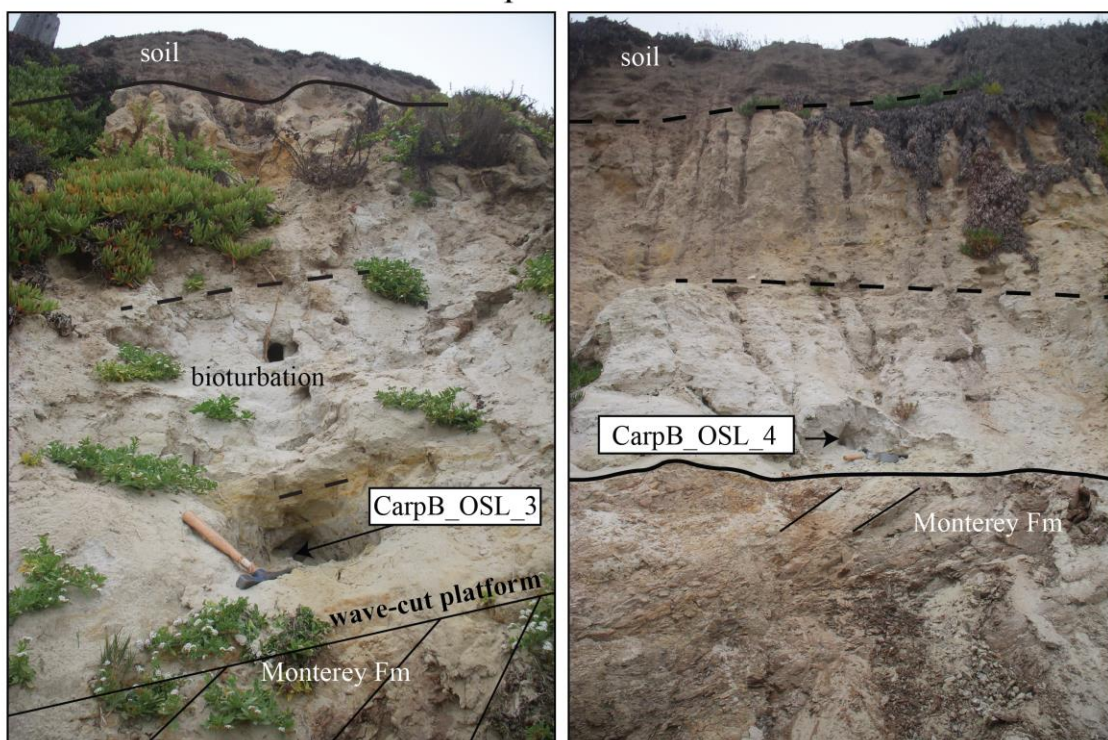
Figure 13: Photos of OSL samples 3-4 near Tar Pit Park. CarpB_OSL_3 and 4 were sampled from 30 cm above the wave-cut platform and ~22 m apart (Figure 4). These samples are located 0.3 m stratigraphically above the wave-cut platform. No cobbles were identified below samples CarpB_OSL_3 and 4. Sediment from this site is quartz-rich, light gray in color, and contains abundant shell fragments.

Table 2: OSL Sample Descriptions

Sample #	Sample Name	[1]Location	Elevation (m)	[2]Grain Size	Munsell Color (dry)		Distance above Platform (m)	Notes
1	CarpB_OSL_1	CB Preserve	32.0	fL-mU	10YR 5/8	yellowish brown	0.5	planar laminations, plant rooting, oxidation
2	CarpB_OSL_2	CB Preserve	33.0	fL-mL	10YR 6/4	light yellowish brown	1.5	ripple laminations, plant rooting
3	CarpB_OSL_3	Tar Pit Park	7.0	fU-mL	2.5Y 7/2	light gray	0.3	laminations, bioturbation, plant rooting, shells, charcoal
4	CarpB_OSL_4	Tar Pit Park	7.0	fL-mL	2.5Y 7/1	light gray	0.3	alternating black and white laminae, plant rooting, shells, charcoal
5	CarpB_OSL_5	CB Preserve	32.0	fU-mU	10YR 6/4	light yellowish brown	1.0	laminations, plant rooting, slightly damp when sampled
6	RincP_OSL_1	Rincon Creek	55.0	mU-cL	5YR 4/4	reddish-brown	N/A	laminations?, black roots?, above carbonaceous horizon
7	RincP_OSL_2	Rincon Creek	53.0	mU-cL	7.5YR 4/3	brown	N/A	laminations?, roots?, bioturbation

[1]There are three sample sites: the east edge of the CB Preserve (Carpinteria Bluffs Nature Preserve), the west side of Tar Pit Park, and the base of the uplifted paleochannel of Rincon Creek exposed in a landslide scar on the Rincon Creek anticline.

[2]Grain Size:

fL = 125-177μ
fU = 177-250μ
mL = 250-350μ
mU = 350-500μ
cL = 500-710μ

Uplift Rate of the Carpinteria Bluffs Marine Terrace

Uplift rates were calculated for each OSL sample based on unique age and wave-cut platform elevation (Table 3). For comparison, uplift rates were also calculated using the adjusted terrace age at 45 ± 10 ka. Samples 1, 2, and 5 yield an average uplift rate of 3.2 ± 1.1 m/ky and a rate of 1.8 ± 0.5 m/ky for an age of 45 ka. Samples 3 and 4 yield an average uplift rate of 1.8 ± 0.6 m/ky and a rate of 1.3 ± 0.4 m/ky for an age of 45 ka. Because the terrace is tilted toward the west, there is an east-west gradient in uplift rates: essentially ~0 m/ky where the wave-cut platform emerges from below sea level at Carpinteria Beach, ~1-2 m/ky near Tar Pit Park, ~2-3 m/ky at the Carpinteria Bluffs Nature Preserve, and ~4-5 m/ky near La Conchita. The total average uplift rate of the Carpinteria Bluffs marine terrace is 2.6 ± 1.1 m/ky based on OSL results and 1.6 ± 0.5 m/ky based on the adjusted terrace age of 45 ka. The uplift rates calculated for OSL ages and adjusted terrace age are within error of one another. Furthermore, the average uplift rate for samples 3 and 4 is very close to the average uplift rate calculated using a terrace age of 45 ka. These uplift rates are consistent with previous work in the Santa Barbara area.

Table 3: Carpinteria Bluffs Marine Terrace Uplift Rates

Uplift Equation: uplift rate=(platform elevation-sea level)/terrace age

Uplift Rates for Each OSL Sample

Sample #	Sample Name	terrace age (ka)	[1]elevation (m)	[2]SA correction	[3]sea level (m)	uplift rate (m/ky)	uplift rate (m/ky) for terrace age of 45±10 ka
1	CarpB_OSL_1	27.79 ± 7.36	28 ± 10	5	-47 ± 10	2.9 ± 0.9	1.8 ± 0.5
2	CarpB_OSL_2	25.27 ± 7.09	30.25 ± 10	5	-47 ± 10	3.3 ± 1.1	1.8 ± 0.5
5	CarpB_OSL_5	23.54 ± 5.25	27.5 ± 10	5	-47 ± 10	3.4 ± 1.0	1.8 ± 0.5
3	CarpB_OSL_3	31.31 ± 6.06	2.5 ± 10	8	-47 ± 10	1.8 ± 0.6	1.3 ± 0.4
4	CarpB_OSL_4	34.31 ± 5.61	2.5 ± 10	8	-47 ± 10	1.7 ± 0.5	1.3 ± 0.4

Average Uplift Rates

average (1,2,5)		25.53 ± 7.36				3.2 ± 1.1	1.8 ± 0.5
average (3,4)		32.81 ± 6.06				1.8 ± 0.6	1.3 ± 0.4
Total average		28.44 ± 7.36				2.6 ± 1.1	1.6 ± 0.5

[1]Elevation of wave-cut platform of the Carpinteria Bluffs marine terrace at the OSL sampling site (sea cliff or railroad cut very near the sea cliff). Error includes both the error from measuring elevation and the error associated with the SA correction.

[2]Difference between the platform elevation and the estimated shoreline angle (SA) elevation. Samples 1, 2, and 5 are located about 0.5 km from the approximated shoreline angle position and samples 3 and 4 are located about 0.8 km from the approximated shoreline angle position. Slope used to calculate correction is an average of lowest platform gradients (0.010 or 10 m/km) from the Bradley and Griggs (1976) study of central California wave-cut platforms.

[3]sea level at 49.5 ka MIS 3 highstand according to Simms et al. (2015)

Slip Rates on the Carpinteria and Railroad Faults

Slip rates were calculated using the average OSL age of the most reliable samples (CarpB_OSL_3 and CarpB_OSL_4) at 32.81 ± 6.06 ka and the adjusted age (45 ka) of the Carpinteria Bluffs marine terrace for comparison (Table 4). The Railroad fault vertically offsets the wave-cut platform by 2.1 m in a railroad cut on the Carpinteria Bluffs (Figure 14). Based on OSL ages, the minimum vertical displacement rate of the Railroad fault is 0.06 m/ky and 0.05 m/ky based on the adjusted terrace age. Bucket auger borings in the hanging wall and footwall of the Carpinteria fault and a splay reveal 4.6 m of vertical offset of the marine terrace deposits (Figure 15). This amount of offset yields a minimum vertical displacement rate of 0.14 m/ky or 0.10 m/ky based on adjusted terrace age. Just west of the bucket auger borings along Highway 101, there is a fold scarp with 6.5 m vertical relief

(Figure 16). This scarp is discontinuous across the Carpinteria Bluffs marine terrace due to

development and leveling practices. Nevertheless, the scarp is still preserved in some areas.

With 6.5 m of vertical offset, the minium vertical slip rates of the Carpinteria fault are 0.20

m/ky or 0.14 m/ky based on adjusted terrace age. Due to a lack of laterally offset features and

limited fault exposure, lateral slip rates were not calculated.

Table 4: Vertical Slip Rates					
	slip rate=vertical offset/terrace age				
Fault	Vertical Offset (m)	[1]Terrace Age (ka)	[2]Adjusted Age (ka)	[3]Vertical Slip Rate (m/ky)	[4]Adjusted Slip Rate (m/ky)
Railroad fault	2.1	32.81	45	0.06	0.05
Carpinteria fault					
based on borings	4.6	32.81	45	0.14	0.10
based on morphology	6.5	32.81	45	0.20	0.14

[1]Average of the two most reliable OSL dates, Samples 3 and 4 in this study.
[2]Approximated age of the Punta Gorda terrace based on previous dates.
[3]Based on terrace age.
[4]Based on adjusted age.
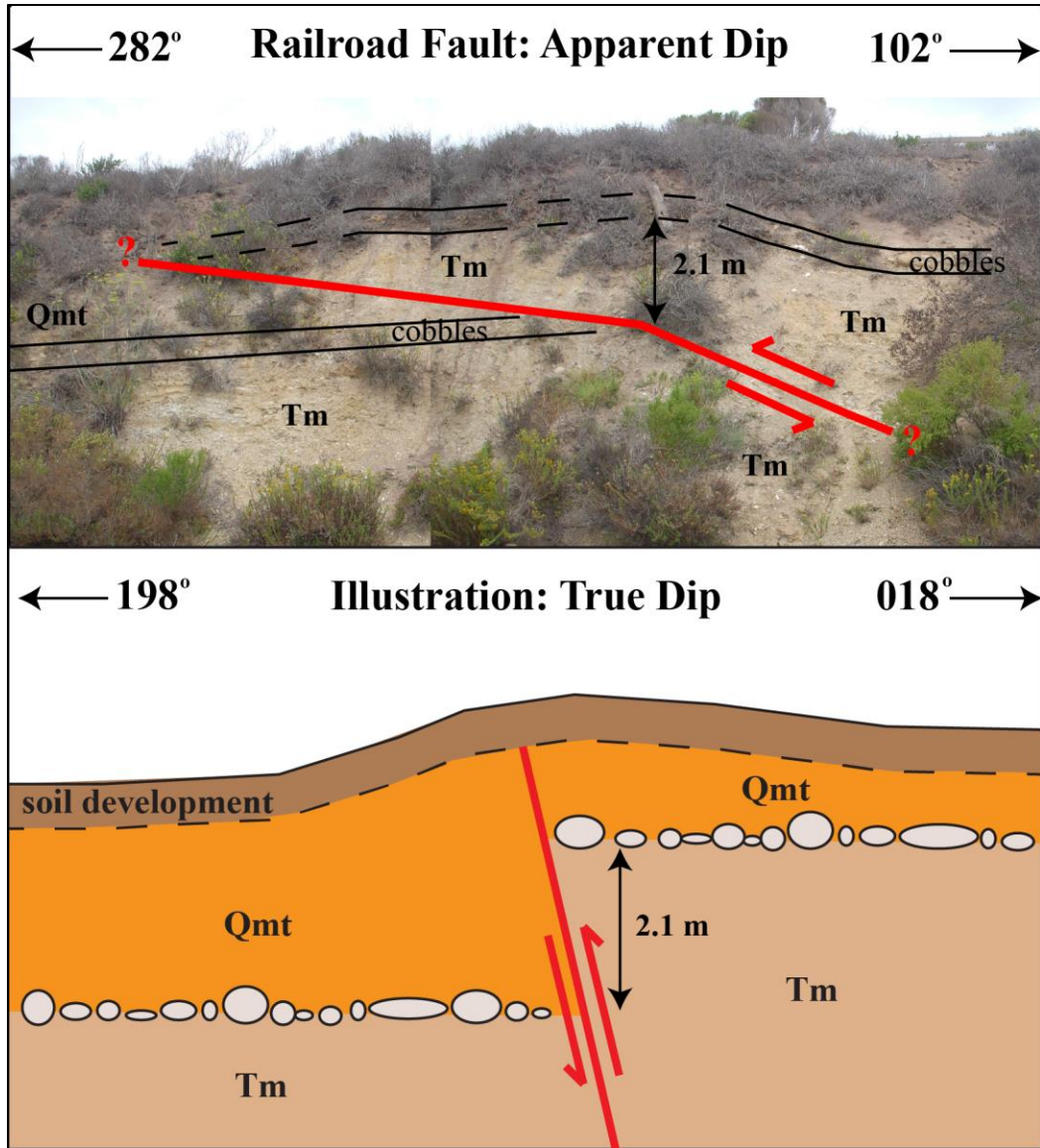
Figure 14: Railroad fault outcrop in the railroad corridor on the Carpinteria Bluffs. This thrust fault has an apparent dip of ~25 degrees to the northeast in the top photo. The true dip of the Railroad fault is about 77 degrees, shown in the illustration. The wave-cut platform has been vertically offset by the Railroad fault by 2.1 m.
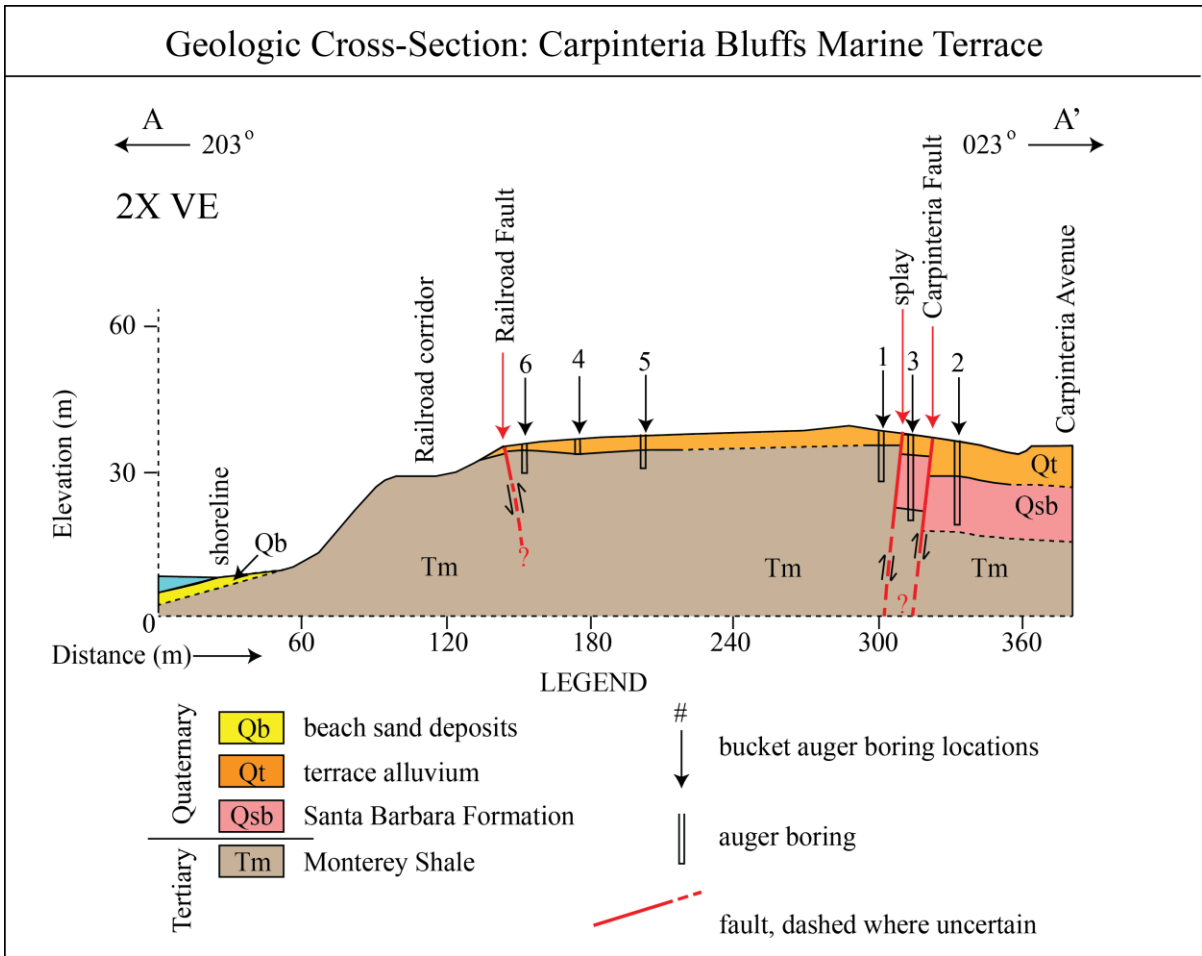
Figure 15: Geologic Cross Section of the Carpinteria Bluffs Marine Terrace. Auger boring logs are from Chevron Oil Co. (Keller, pers. comm., 2015) and topography was derived from Hoover and Associates (1989). Designed after Figure A-2 in Metcalf (1990).
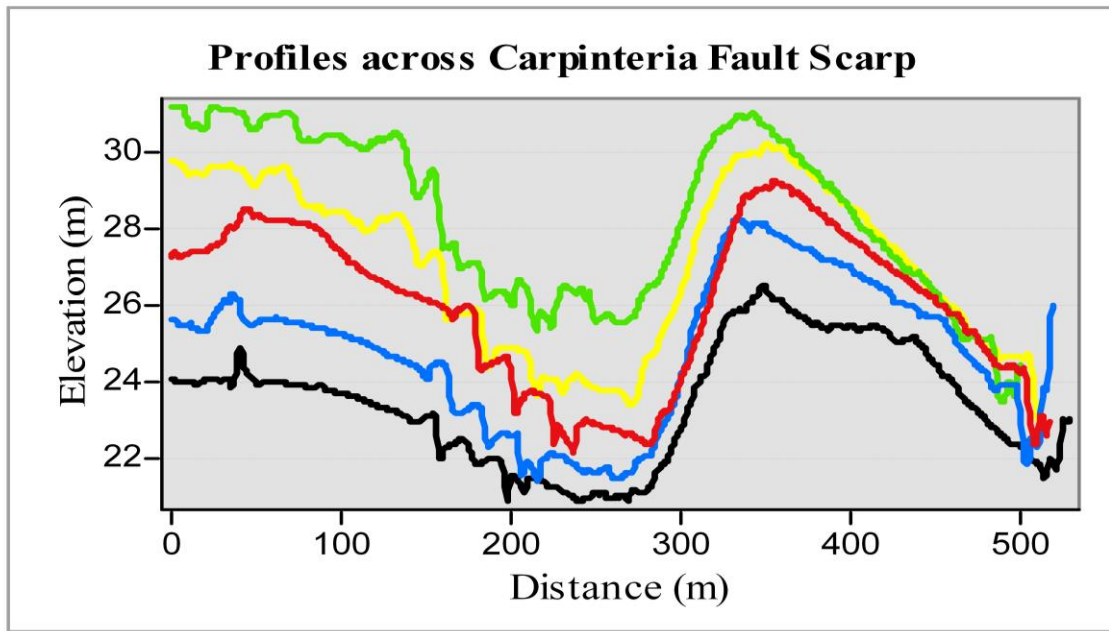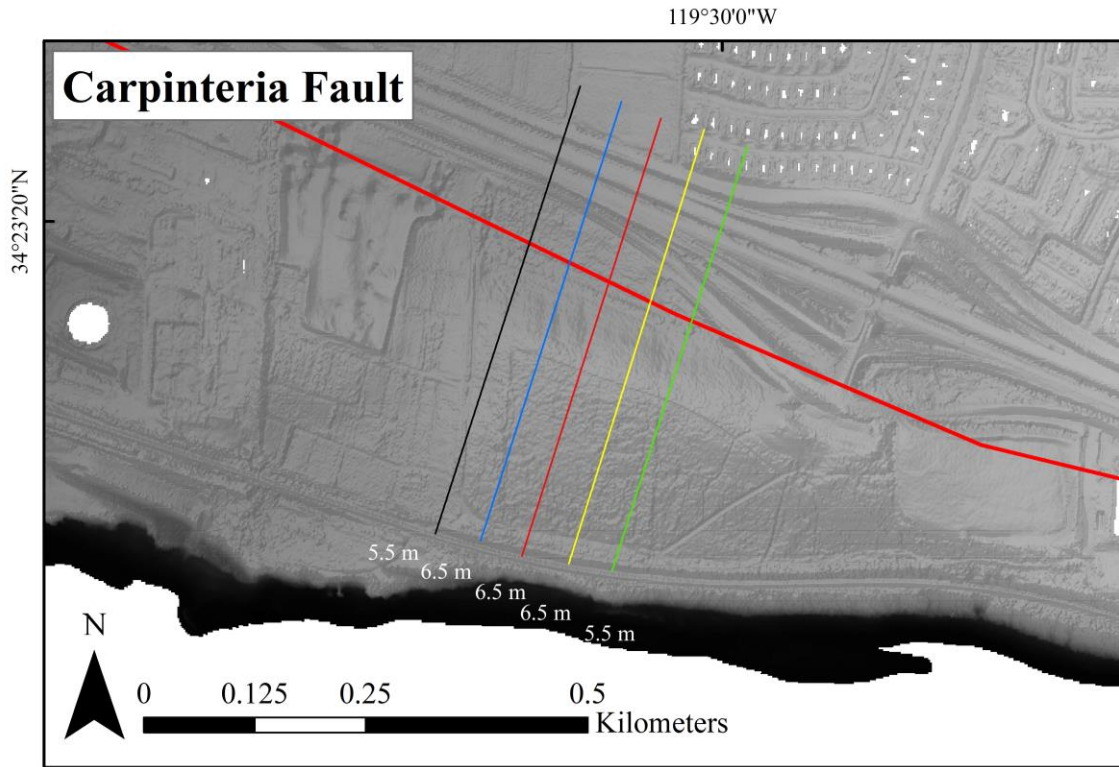
Figure 16: Topographic profiles across the fold scarp associated with the Carpinteria fault. Elevations were extracted from a 1-m LiDAR DEM (DOC/NOAA/NOS/OCM, 2012). Carpinteria fault is mapped according to Minor and Brandt (2015). Though little of the scarp remains due to construction and leveling practices, the scarp is visible here and exhibits a maximum relief of 6.5 m. This topographic relief serves as a minimum estimate for vertical offset of the Carpinteria Bluffs marine terrace.
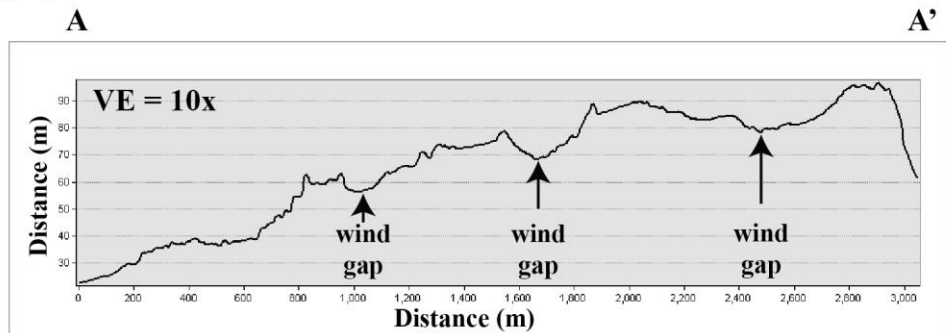
Rincon Creek Anticline

A prominent feature recognized in this study but absent from the Minor and Brant (2015) map is the Rincon Creek anticline. In areas experiencing crustal shortening, reverse and thrust faults commonly have hanging-wall anticlines that grow in response to slip along a fault (Suppe and Medwedeff, 1990). Geomorphic evidence suggests that the Rincon Creek anticline is a westward-propagating hanging-wall anticline controlled by the Rincon Creek fault (Hartleb, 2000; Webber, 1999). The strongest geomorphic evidence that this feature is a laterally-propagating fold is the succession of wind gaps preserved on the axis of the anticline (Figure 17). These wind gaps are identified by topography only (Hartleb, 2000); no channelized gravels or fluvial deposits have been discovered on the anticline. The wind gaps are suggestive of westward propagation because they decrease in elevation westward along the profile of the anticline (Keller et al., 1999). Lateral fold propagation often leads to the incision of water gaps across the fold. Water gaps become wind gaps when streams that once traversed the fold are diverted around the nose of the growing fold, such as during an earthquake. Furthermore, fold growth may cause these diverted streams to decrease in gradient and develop meanders (Jackson et al., 1996). After fold propagation, the stream experiences uplift and incises, leaving entrenched meanders on the flank of the fold. This may explain the incised meanders (Figure 18) on the forelimb of the Rincon Creek anticline, revealed by 1-m LiDAR data (DOC/NOAA/NOS/OCM, 2012).

Rincon Creek is responsible for the winds gaps and incised meanders on the Rincon Creek anticline. As the Rincon Creek anticline grew in response to earthquake events on the Rincon Creek fault, Rincon Creek was diverted westward along the forelimb (north flank) of the anticline. This diversion is evidenced by a broad paleovalley north of the anticline, an

uplifted paleochannel, and incised meanders at the propagating tip of the fold. Later, Rincon

Creek was captured, bringing it to its current position at the east end of the Rincon Creek

anticline. A possible mechanism for this capture could have been facilitated by an earthquake

event that caused slip on the proposed tear fault, creating an opportunity for a pre-existing

stream at Rincon Point to erode headward and capture Rincon Creek. This scenario could

explain the linearity of the lower Rincon Creek. The capture event might have delivered

gravel and boulder-rich material to the ocean, depositing a coarse fan at Rincon Point. This

fan is visible in the United States Geological Survey's Seismic Investigations Map 3261

(Johnson et al., 2013). Bathymetry from sheet 1 displays detailed surface morphology of the

shoal offshore of Rincon Point. Sheet 6 contains digital still photographs (Cochrane et al.,

2007) of the surface of the fan, showing sub-rounded cobbles and boulders. The shoal is a

lobe-shaped depositional feature with channel-like features, described in Johnson et al.

(2013) as subaqueous delta deposits.
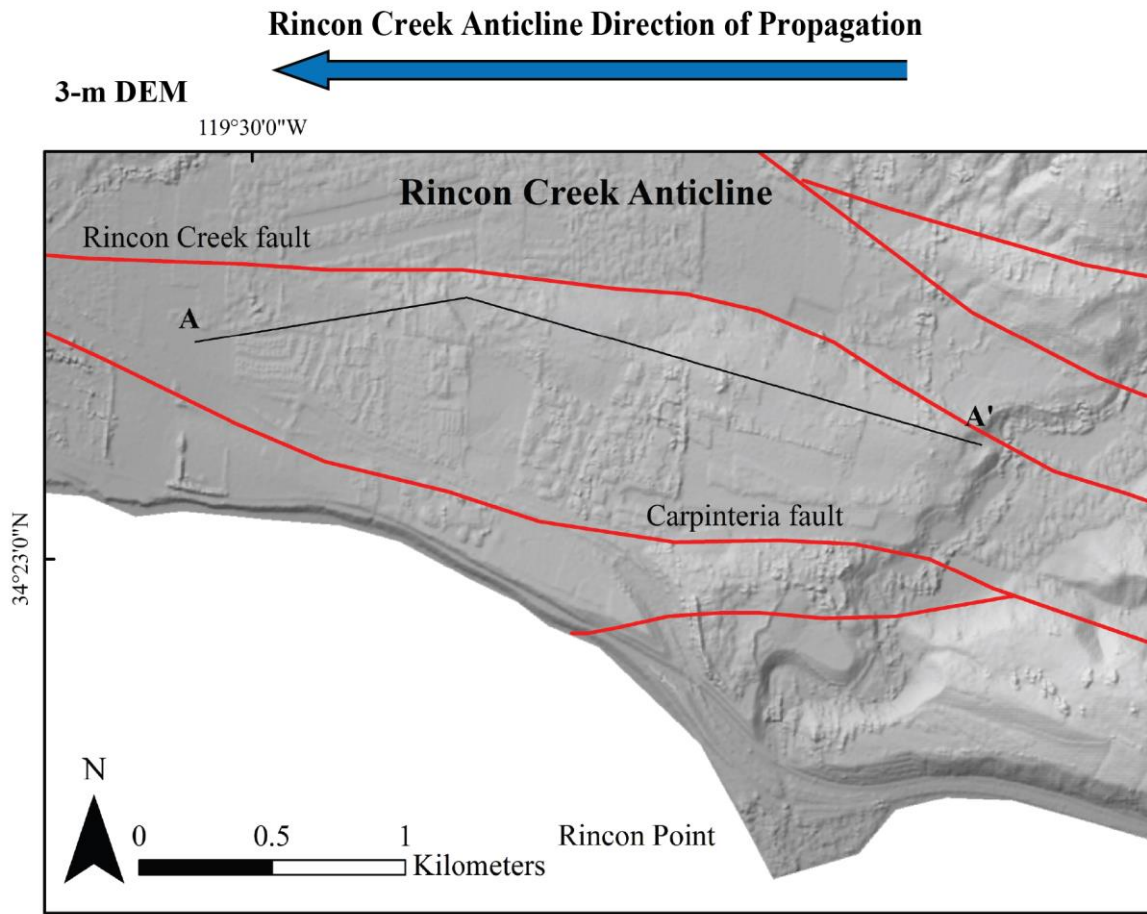
Figure 17: Rincon Creek anticline propagation diagram. Rincon Creek anticline has propagated westward, exhibiting decreasing topographic relief and wind gap elevation to the west. Designed after Figure 1 in Keller et al. (1999). Topographic profile along the axis of the Rincon Creek anticline was extracted from a 3-m IfSAR DEM (DOC/NOAA/NOS/OCM, 2004).
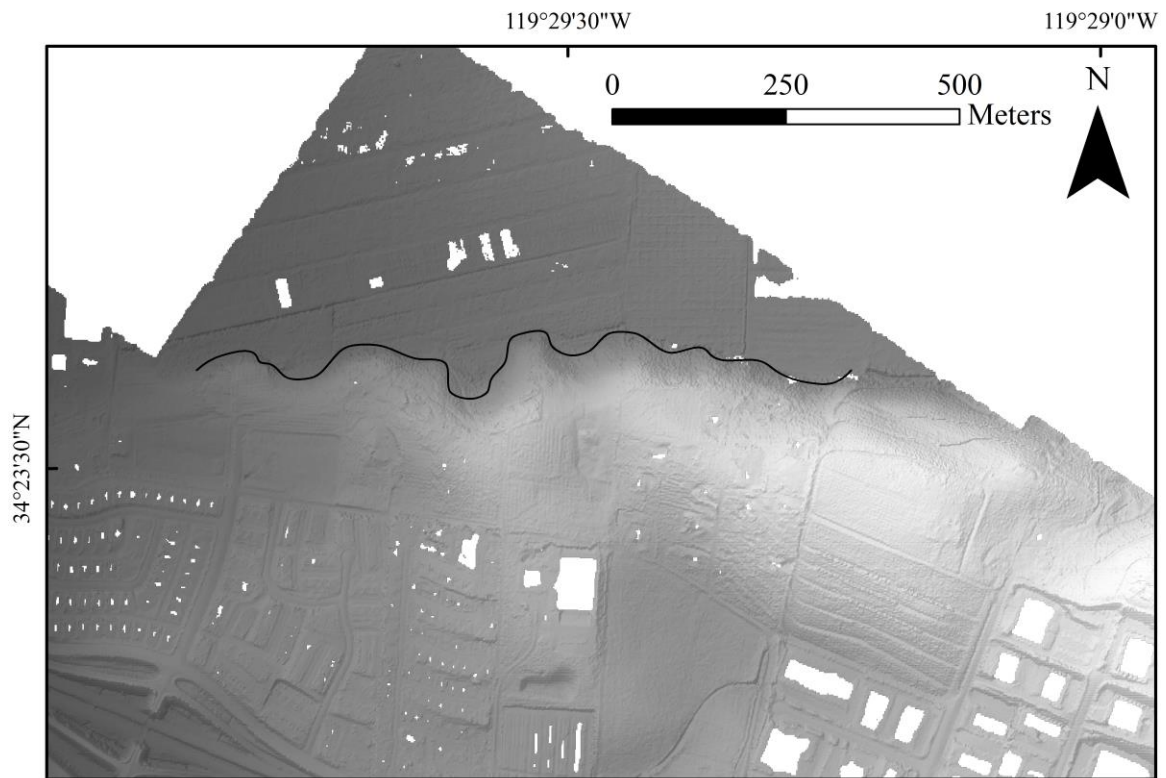
Figure 18: Rincon Creek anticline meander scars. Meander scars are outlined in black on the forelimb of the Rincon Creek anticline. These meander scars were discovered with a 1-m LiDAR DEM (DOC/NOAA/NOS/OCM, 2012).

Chonology of the Rincon Creek Anticline Paleochannel

OSL sample 6 is 38.58 ± 5.72 ka and OSL sample 7 is 39.80 ± 6.07 ka. Sample 7 is

located ~2 m stratigraphically below sample 6 (Figure 19). The age of sample 7 serves as an

approximate age for the initiation of folding and propagation of the Rincon Creek anticline.
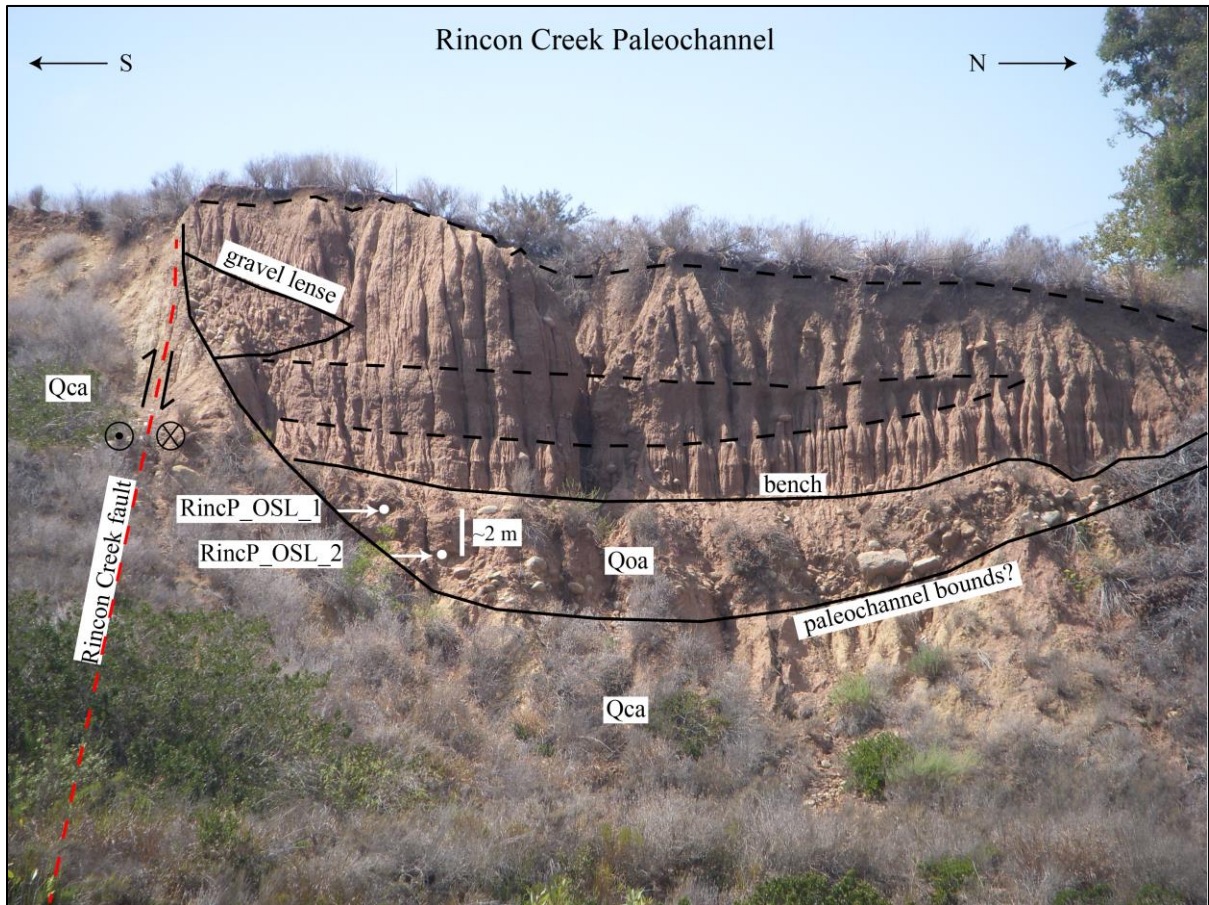

Figure 19: Rincon Creek paleochannel looking west from Highway 150 at the Santa Barbara-Ventura county line. OSL samples RincP_OSL_1 and RincP_OSL_2 are outlined and labeled. The Rincon Creek fault is visible here, according to mapping by Minor and Brandt (2015). Stratigraphically above the OSL samples are what appear to be several well-indurated and organic-rich buried soils.

Uplift Rate of the Rincon Creek Anticline

Two methods were used to estimate the uplift rate of the Rincon Creek anticline. First, the vertical offset of the Casitas Formation (16 m) by the Rincon Creek fault (visible on the eastern side of the anticline in a landslide scar) was divided by the minimum age of the paleochannel at 39.80 ± 6.07 ka (OSL sample RincP_OSL_2). This yields an uplift rate of 0.4 m/ky. Second, the elevation difference between the base of the paleochannel and the Carpinteria Bluffs marine terrace (~45 m) was used to estimate uplift rate of the Rincon Creek anticline. This yields a much higher rate of 1.1 m/ky. This estimate relies on the assumption that the paleochannel once occupied an elevation similar to that of the marine terrace and was subsequently uplifted by the Rincon Creek fault to its present elevation. These estimates are reasonable considering that Jackson and Yeats (1982) calculated a separation rate of 0.74-0.95 m/ky on the Rincon Creek fault.

Lateral Propagation Rate of the Rincon Creek Anticline

Using the minimum anticline age (39.80 ± 6.07 ka) and its length (2.5 km), lateral propagation rate for the Rincon Creek anticline is estimated at 62.8 m/ky. One can also use wind gap placement to estimate propagation rate. The elevation and spacing of wind gaps with an estimated anticline uplift rate of 1.1 m/ky yields an average propagation rate of 62.2 m/ky. These estimates agree well with one another, but they probably overestimate the true propagation rate since the age used here is a minimum. According to the wind gap method, lateral propagation rates decrease to the west, in the direction of propagation. This might imply that propagation rates have slowed over time. These results are highly speculative. It would be best to date material in the wind gaps to calculate a lateral propagation rate.

Stream Profile Analysis

Stream Steepness (k_{sn}) and Concavity

High k_{sn} values are concentrated near faults and correlate with erosionally-resistant lithologies (Figure 20). Contoured k_{sn} values highlight areas with low k_{sn}, particularly Carpinteria Basin and the headwaters of Los Sauces Creek (Figure 21). Streams are divided into two groups for analysis: Carpinteria streams versus Ventura streams. Carpinteria streams include stream numbers 1-8, which have beds that transition from strong lithologies to weak lithologies from the hinterland to the foreland. Ventura streams include stream numbers 9-14, which have beds of low rock strength. These groups of streams are separated by the proposed tear fault along the linear, downstream reach of Rincon Creek. The Carpinteria streams have an averaged regressed k_{sn} value of 36.9±1.2 and a mean concavity of 0.58±0.13 (Table 5). Ventura streams have an average regressed k_{sn} value of 26.0±2.3 and a mean concavity of 0.75±1.8. The mean k_{sn} calculated for Ventura streams is statistically indistinguishable from the Duvall et al. (2004) mean k_{sn} calculated for the same streams. Tributaries that feed into Rincon Creek from the east and from the west have similar stream steepness and concavity values (Table 6). Western tributaries have mean k_{sn} and concavity values of 30.8±1.4 and 0.45±0.14, respectively, and eastern tributaries have mean k_{sn} and concavity values of 29.7±2.3 and 0.49±0.11, respectively.
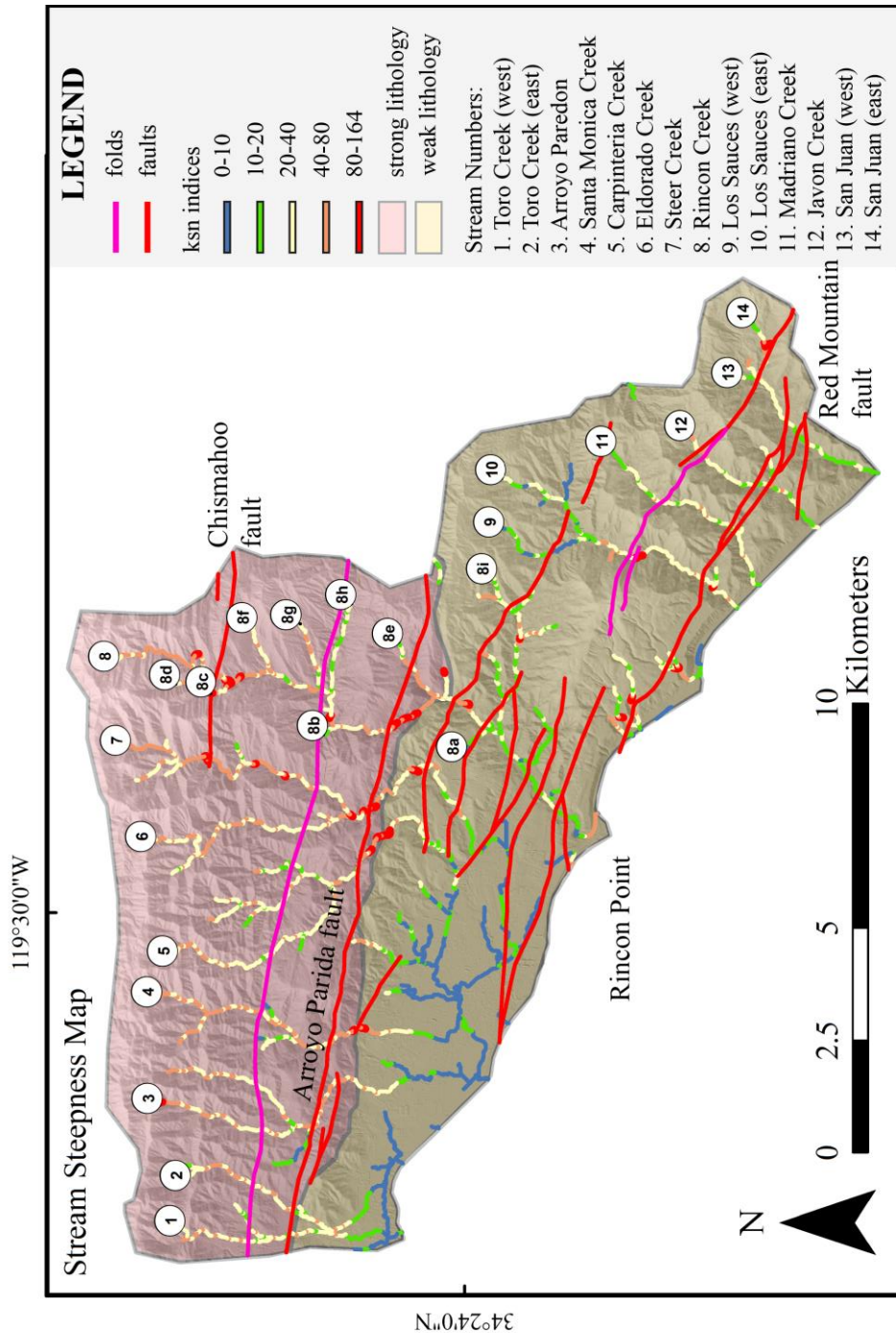
Figure 20: Stream Steepness Map. Normalized stream steepness values (k_{sn}) range from 0-164, with the lowest values concentrated in Carpinteria where streams leave bedrock and become alluvial in nature. Streams 9-4 belong to the Ventura group (uniform rock strength), and all other streams belong to the Carpinteria group (non-uniform rock strength). Faults are mapped according to Minor and Brandt (2015), Minor et al. (2009), and Dibblee (1986, 1987, 1988).
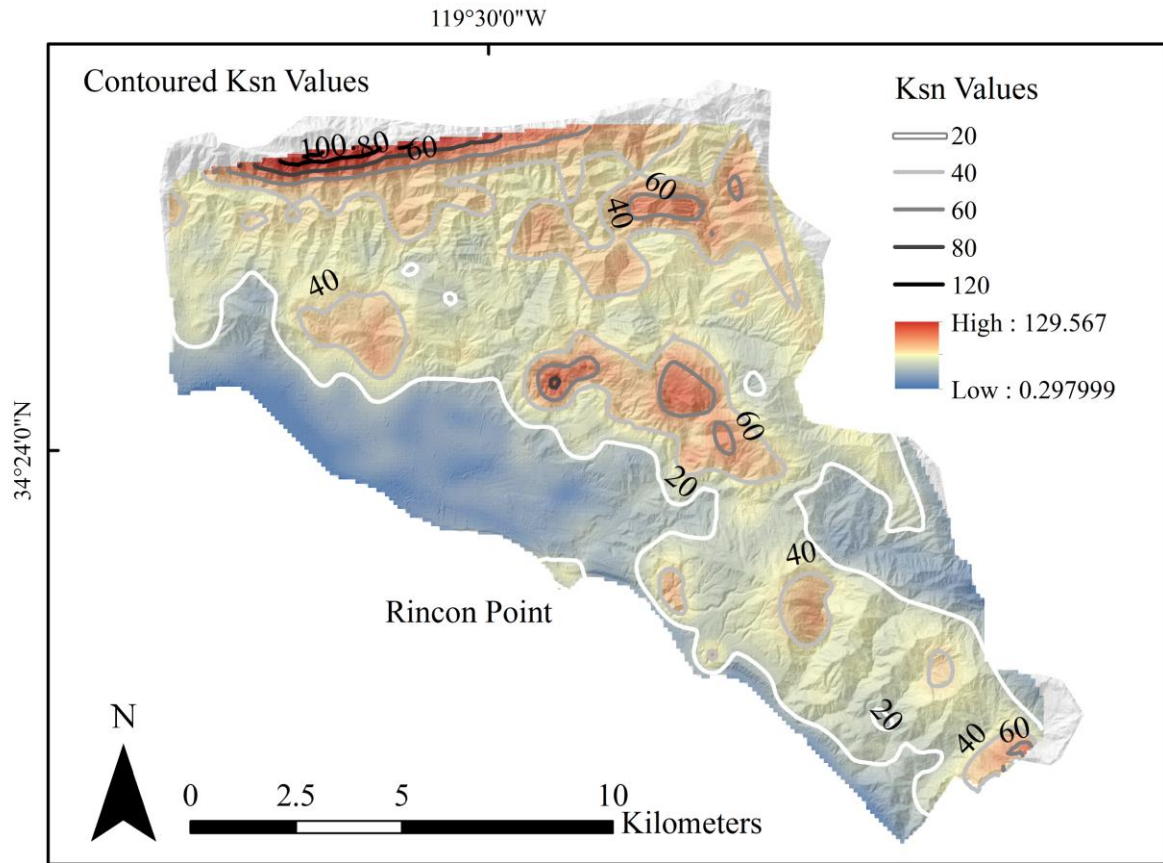
Figure 21: Interpolated and contoured stream steepness values across Rincon Creek. The high values in red at the top left side of the figure correspond with resistant lithologies (Matilija Sandstone) near the crest of the Santa Ynez Mountains. High k_{sn} indices also correspond with the Arroyo Parida fault, Chismahoo Fault, and Red Mountain fault. The large blue area coincides with Carpinteria Basin, an actively subsiding tectonic basin, and the smaller blue area north of Rincon Mountain likely represents a recent stream capture event or relic topography.

Table 5. Stream Channel Data

Channel Name	Channel Length (km)	Drainage Area (km^2)	Stream Number	Channel Concavity	*regressed k_{sn}
Carpinteria: Nonuniform Rock Strength					
Toro Creek (west)	8.0	5	1	0.54±0.12	30.8±0.8
Toro Creek (east)	7.1	5	2	0.51±0.09	33.2±0.4
Arroyo Paredon	10.2	21	3	0.60±0.07	37.3±0.4
Santa Monica Creek	10.9	13	4	0.53±0.05	45.1±0.5
Carpinteria Creek	17.2	13	5	0.64±0.05	34.3±0.8
**Eldorado Creek	20.8	27	6	0.57±0.09	33.8±0.9
**Steer Creek	21.6	27	7	0.76±0.13	36.5±1.2
Rincon Creek	17.1	38	8	0.52±0.06	44.3±0.7
***Mean**	**14.1**	**17.5**		**0.58±0.13**	**36.9±1.2**
Ventura: Uniform Rock Strength					
**Los Sauces Creek (west)	7.3	14	9	1.10±0.32	12.7±1.1
				0.89±1.80	29.7±2.3
**Los Sauces Creek (east)	7.6	14	10	0.91±1.90	10.6±3.5
				1.10±0.35	16.4±1.7
				1.10±1.80	29.7±1.2
Madriano Creek	5.6	6	11	0.34±0.30	5.9±0.7
				0.38±0.22	25.8±0.3
Javon Creek	4.3	5	12	0.75±0.15	24.7±0.9
**San Juan (west)	4.8	8	13	0.46±0.09	21.5±0.4
**San Juan (east)	5.8	8	14	0.60±0.12	22.0±0.1
				0.90±0.10	24.7±1.1
***Mean**	**5.9**	**8.3**		**0.75±1.8**	**26.0±2.3**
ref concavity= 0.4					

*Some streams require multiple regressions. Mean ksn and concavity reflect the most downstream regression of each stream because these are more reflective of erosion/uplift rates. Upstream regressions have lower ksn values and likely reflect relic topography or stream capture.

** Drainage areas are representative of the whole basin, not individual streams.

Table 6. Tributaries of Rincon Creek

Channel Name	Channel Length, km	Stream Number	Channel Concavity	*regressed k_{sn}
Rincon Creek Western Tributaries				
un-named	5.8	8a	0.34±0.14	14.6±0.5
un-named	9.9	8b	0.34±0.08	31.9±1.4
un-named	13.9	8c	0.64±0.10	36.3±0.9
un-named	14.7	8d	0.46±0.06	40.5±0.7
Mean	**11.1**		**0.45±0.14**	**30.8±1.4**
Rincon Creek Eastern Tributaries				
Casitas Creek	9.0	8e	0.50±0.19	18.9±1.0
			0.71±0.09	35.2±2.3
Sulphur Creek	8.4	8f	0.46±0.10	34.6±0.8
un-named	13.5	8g	0.44±0.11	32.0±1.1
un-named	12.5	8h	0.31±0.08	27.4±1.0
Catharina Creek	12.8	8i	0.54±0.09	19.3±0.5
Mean	**11.2**		**0.49±0.11**	**29.7±2.3**
ref concavity= 0.4				

*Some streams require two regressions due to a large knickpoint.

It is best to compare k_{sn} values only within rocks of similar strength because streams tend to be steeper in stronger rocks (Figure 22). Therefore, k_{sn} regressions for the downstream sections of the Carpinteria streams which flow though similar rocks as Ventura streams are calculated for comparison with the Ventura streams. This comparison includes the following lithologies, which are described as having lower rock strength compared to other lithologies in the study area: Sespe Formation, Pico Formation, Sisquoc Formation, Rincon Shale, Monterey Shale, Santa Barbara Formation, Quaternary gravels (Qog) or Quaternary older alluvium (Qoa), and various younger Quaternary alluvium deposits. The mean k_{sn} values for these sections of the Carpinteria streams is 16.4±4.5 and the mean concavity is 1.9±1.4 (Table 7).

In addition to profile regressions, the mean k_{sn} values for distinct lithologies were also calculated within each stream to emphasize how k_{sn} differs with lithology (Table 8). The Matilija Sandstone (Tma) and Coldwater Sandstone (Tcw) units have relatively high associated k_{sn} values. Tma and Tcw also have greater rock strength and resistance to erosion than other units in the field area. The average k_{sn} value for Ventura streams is 27.0 ± 7, which is very close to that calculated by stream profile regressions.

Stream steepness is likely influenced by stream orientation. Tributaries that run roughly east-west (perpendicular to the direction of local convergence) have lower k_{sn} values than streams that run north-south, transverse to the Santa Ynez Mountains. Streams 8h, 8i, and a tributary of stream 3 run parallel to adjacent anticlines and take advantage of faults and synclines.

K_{sn} results did not vary widely based on small (0.3-0.5 km) changes in regression bounds; however, concavity calculations were sensitive to placement of regressions bounds.

For short stream reaches, some concavity values were greater than 1 and had large errors (Figure 23). High concavities may be due to fixed knickpoints, especially at tributary junctions and resistant beds, which artificially steepen the stream profile. High concavities are not unusual for this area, because concavities greater than 1.0 are also reported by Duvall et al. (2004) for some streams south of the Santa Ynez Mountains. Concavity data reported here is not considered in tectonic interpretations.
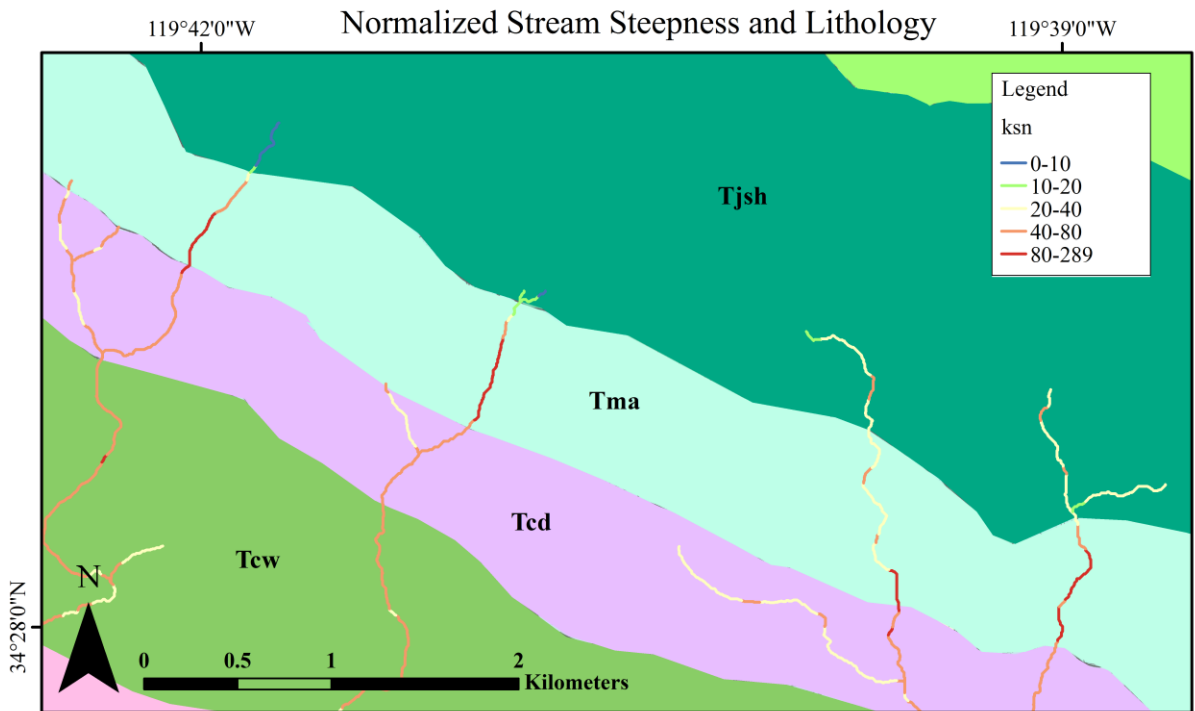

Figure 22: Example of high k_{sn} values corresponding with resistant lithologies. Sections of Mission Creek, Rattlesnake Canyon, and Montecito Creek (just west of the study area). Stream steepness increases consistently across Tma, a resistant sandstone unit. Geology from Dibblee (1987). Tjsh= Juncal Formation; Tma= Matilija Sandstone; Tcd= Cozy Dell Shale; Tcw= Coldwater Sandstone.

Table 7: Stream Channel Data for Carpinteria Stream Sections in Uniform Rock Strength			
Channel Name	**Stream Number**	**Channel Concavity**	**regressed k_{sn}**
Toro Creek (west)	1	2.8±1.40	15.9±2.7
Toro Creek (east)	2	2.0±0.89	25.2±2.6
Arroyo Paredon	3	1.3±0.60	12.9±4.3
Santa Monica Creek	4	1.6±0.82	14.6±4.5
Carpinteria Creek	5	1.5±0.52	11.3±1.4
Eldorado Creek/Steer Creek	6/7	2.4±0.82	13.7±1.7
Rincon Creek	8	1.7±0.79	21.4±1.8
Mean		**1.9±1.40**	**16.4±4.5**
ref concavity= 0.4			

| Table 8: K_{sn} Statistics for Specific Lithologies													
		Carpinteria Streams								Ventura Streams			
	Stream Number	1	2	3	4	5	6	7	8	9 and 10	11	12	13 and 14
Geologic Units	**K_{sn} Statistics**												
Tma	Count:			8.00	6.00								
	Minimum:			41.41	45.64								
	Maximum:			130.69	56.01								
	Sum:			597.61	306.31								
	Mean:			**74.70**	**51.05**								
	Standard Deviation:			27.24	3.08								
Tcd	Count:	11.00	13.00	12.00	17.00	12.00	15.00	26.00	25.00				
	Minimum:	22.11	15.98	28.72	36.19	33.05	22.15	28.10	28.10				
	Maximum:	59.01	32.21	47.84	53.89	46.31	46.46	55.61	66.10				
	Sum:	409.06	330.56	470.43	742.39	478.24	543.11	1142.07	1124.62				
	Mean:	**37.19**	**25.43**	**39.20**	**43.67**	**39.85**	**36.21**	**43.93**	**44.98**				
	Standard Deviation:	12.18	4.63	4.90	5.93	4.25	7.59	6.84	8.37				
Tcw	Count:	20.00	25.00	70.00	39.00	12.00	62.00	59.00	86.00				
	Minimum:	29.38	14.37	24.30	31.28	33.05	23.66	28.95	33.80				
	Maximum:	64.89	53.56	69.56	85.21	46.31	164.10	164.10	124.35				
	Sum:	800.40	917.25	2941.08	1987.53	478.24	3313.03	3612.35	5123.66				
	Mean:	**40.02**	**36.69**	**42.02**	**50.96**	**39.85**	**53.44**	**61.23**	**59.58**				
	Standard Deviation:	8.99	11.86	8.73	12.33	4.25	23.97	22.68	20.90				
Tsp	Count:	69.00	66.00	35.00	65.00	117.00	107.00	125.00	93.00	112.00			
	Minimum:	12.02	18.06	19.82	22.25	17.91	20.87	20.87	16.76	5.79			
	Maximum:	52.06	53.92	44.54	82.89	126.27	102.64	109.99	108.01	38.41			
	Sum:	2053.63	2261.75	1189.62	3052.33	4012.72	4272.33	5413.23	3674.04	1754.04			
	Mean:	**29.76**	**34.27**	**33.99**	**46.96**	**34.30**	**39.93**	**43.31**	**39.51**	**15.66**			
	Standard Deviation:	9.29	8.26	6.15	14.77	18.65	15.81	18.81	16.91	7.78			
Qoa/Qca	Count:					46.00	54.00	54.00	55.00				
	Minimum:					9.93	11.18	11.18	12.24				
	Maximum:					40.08	66.59	66.59	28.20				
	Sum:					958.21	1343.40	1343.40	1010.69				
	Mean:					**20.83**	**24.88**	**24.88**	**18.38**				
	Standard Deviation:					8.01	12.43	12.43	3.89				
all other weak rocks	Count:								38.00	88.00	109.00	79.00	79.00
	Minimum:								8.59	11.19	10.87	13.47	12.14
	Maximum:								39.41	117.94	46.45	53.13	45.22
	Sum:								685.06	2982.13	2808.18	2119.09	1697.76
	Mean:	**<20**	**<20**	**<20**	**<20**	**<20**	**<20**	**<20**	**18.03**	**33.89**	**25.76**	**26.82**	**21.49**
	Standard Deviation:								7.68	19.35	8.12	10.38	6.20
Tma= Matilija Sandstone													
Tcd= Cozy Dell Shale													
Tcw= Coldwater Sandstone													
Tsp= Sespe Formation													
Qca=Casitas Formation													
Qoa=Quaternary Older Alluvium													
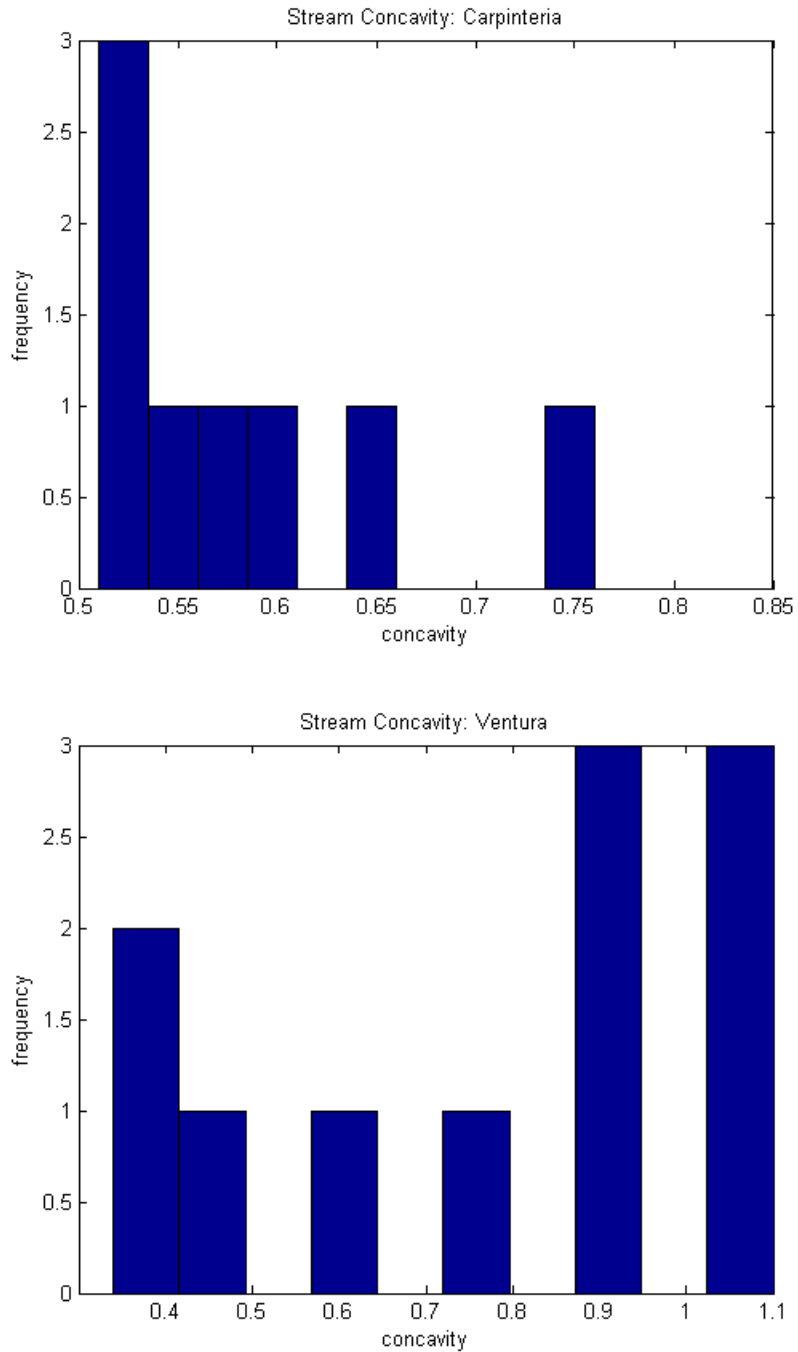
Figure 23: Stream Concavity Histograms. Stream concavities calculated for the Carpinteria and Ventura streams in this study are based on stream profile regressions. Carpinteria streams include Rincon Creek and all streams west of Rincon Creek in the study area. Ventura streams are located east of Rincon Creek in the study area. Note the anomalous concavity values (>1) on the right hand side of the Ventura histogram. A few of the concavities reported for the Ventura streams have high errors and were very sensitive to the regression bounds chosen.

Drainage Rearrangement

Knickpoints corresponding with large increases in drainage area are present in several of the Carpinteria streams in the field area. These knickpoints correspond with tributary junctions which result from stream capture events. As slip occurs on the Arroyo Parida fault (reverse and left-lateral slip), ridges are formed and translated across the landscape, causing drainage rearrangement. These shutter ridges force streams to migrate laterally until they are "pushed" into adjacent streams. This process appears to have occurred several times, as evidenced by streams that fork just north of the Arroyo Parida fault. Streams 3, 5, 6, and 7 fit this description. In the future, streams 1 and 2 may also converge north of the Arroyo Parida fault. Another observation supporting a history of drainage rearrangement by shutter ridges is the 90° bend in Rincon Creek north of the Arroyo Parida fault (Figure 6). This bend is probably caused by westward translation or growth of Laguna Ridge, possibly followed by drainage capture.

Kolmogorov-Smirnov Tests

I performed a Kolmogorov-Smirnov (K-S) two-sample test on my regressed k_{sn} data for each stream in the field area using the built-in Matlab function "kstest2" (Table 9). Three different comparisons were performed. First, Carpinteria streams were compared to Ventura streams. The test returned h=1, a p-value of 0.002647, and a ks statistic of 1. This test rejected the null hypothesis that k_{sn} values from Carpinteria and Ventura streams belong to the same continuous distribution at the 5% significance level. Therefore, the Carpinteria streams have statistically higher k_{sn} values than the Ventura streams within the study area.

A second K-S test compared the k_{sn} data from the Carpinteria and Ventura streams, limiting analysis to similar, weak lithologies. The test resturned h=1, a p-value of 0.018584, and a ks statistic of 0.85714. Therefore, in similar rocks, Ventura streams are steeper than the Carpinteria streams in the field area.

A third K-S test compared k_{sn} values of the east and west tributaries of Rincon Creek. The test returned h=1, a p value of 0.47717, and a test statistic of 0.5. Therefore, k_{sn} values of Rincon Creek tributaries are statistically indistinguishable.

Table 9: Kolmogorov-Smirnov Two-Sample Test Results		
Comparing Carpinteria Streams to Ventura Streams:		
h	1	Reject null hypothesis
p	0.002647	
ks statistic	1	Overall, the Carpinteria streams are steeper
Comparing Carpinteria Stream Sections in Similar Weak Lithologies to Ventura Streams:		
h	1	Reject null hypothesis
p	0.018584	
ks statistic	0.85714	In similar rocks, Ventura streams are steeper
Comparing East and West Tributaries of Rincon Creek:		
h	0	Accept null hypothesis
p	0.47717	
ks statistic	0.5	Tributaries of Rincon Creek have similar steepness
These values were calculated using the built-in "kstest2" Matlab function. Significance level=5%		

Knickpoints

The knickpoint algorithm identified 143 knickpoints with a minimum magnitude of 10 m (Figure 24). Number of knickpoints per stream generally increases eastward for the Carpinteria streams. This is likely related to drainage area since more tributaries provide more opportunities to host knickpoints. According to geologic mapping by Dibblee (1986, 1987, 1988), Minor et al. (2009), and Minor and Brandt (2015), identified knickpoints coincide with distinct geologic features including: lithologic contacts, erosionally-resistant beds within a unit, faults, folds, and landslides. Out of these knickpoints, 46.9 % fall on a lithologic contact or erosionally-resistant bed, 22.3 % occur on a mapped fault or fold, 16.8 % occur on landslides, 7.7 % coincide with a fault and lithologic contact, and 6.3 % fail to coincide with any of these geologic features. Knickpoints that do not correspond with any of the aforementioned geologic features are interpreted as transient. Most of the transient knickpoints are found at the head of Los Sauces Creek at similar elevations.

Seismic Reflection Data

CHIRP seismic reflection data with decimeter-scale resolution was collected offshore of Rincon Point by Ucarkus et al. (2014). The reflection data reveals predominantly onlapping sediments above an irregular bedrock surface. An east-west oriented bedrock ridge with 2-3 m of vertical relief is interpreted to be a structural feature associated with the Red Mountain fault (Driscoll, pers. comm., 2016). Based on CHIRP data and bathymetry, Ucarkus et al. (2014) map this feature as an east-west trending fold that takes a left turn offshore of Rincon Point. Unfortunately, seismic data does not capture the left turn of this bedrock ridge. Additionally, subaqueous delta deposits shown in Johnson et al. (2013)

obscure the surface expression of this bedrock ridge. Thus, it is not certain whether Rincon

Point is structural in origin.
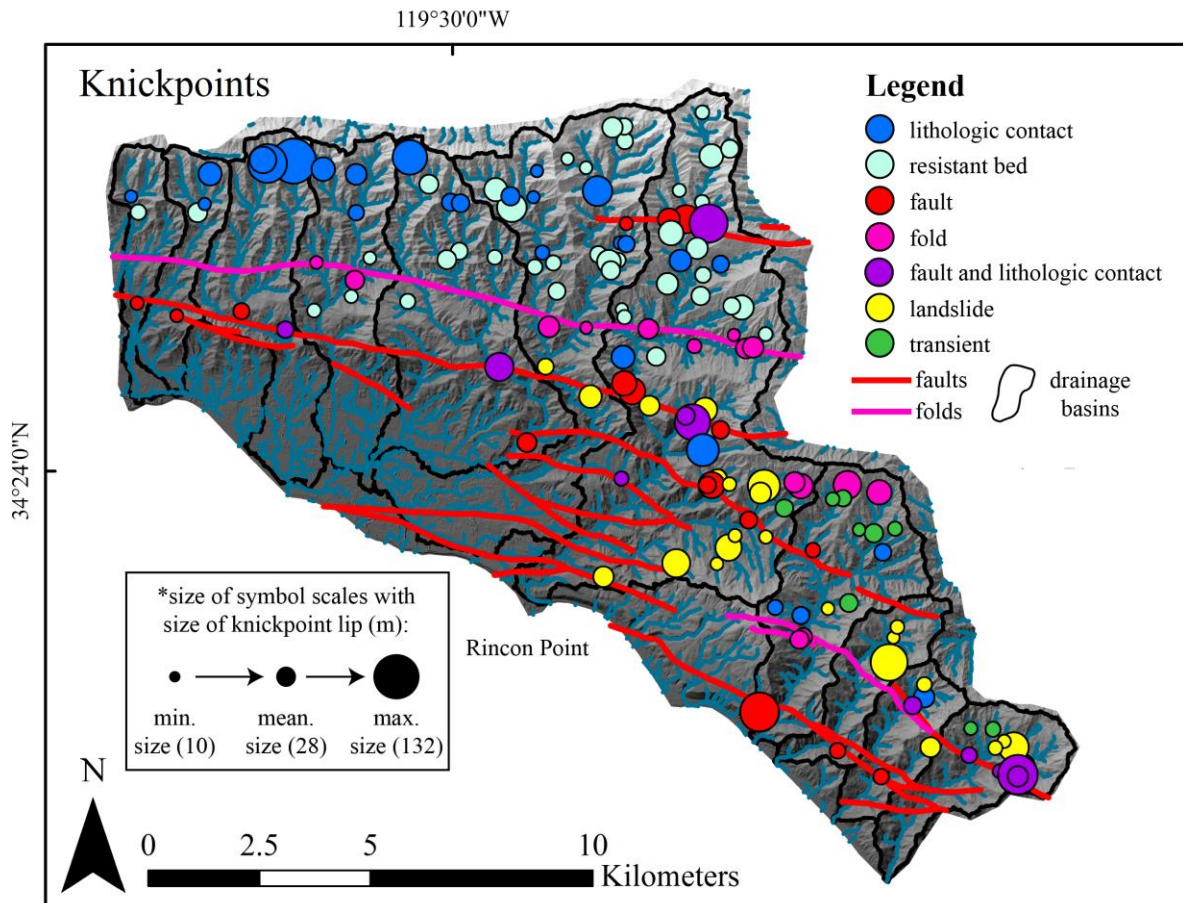
Figure 24: Location of knickpoint lips extracted from stream profiles with a custom algorithm (Neely, pers. comm., 2015). The relative knickpoint magnitude is reflected by the size of the symbol. Note that the color of the symbol indicates a possible explanation for the knickpoint. Green knickpoints do not coincide with any of the listed features and may represent transient knickpoints. Faults are from Minor et al. (2009), Minor and Brandt (2015), and Dibblee (1988).

DISCUSSION

Age of the Carpinteria Bluffs Marine Terrace

The Carpinteria Bluffs marine terrace OSL dates are younger than previous dates on the Punta Gorda terrace. Thus, there are two possible conclusions: 1) the terrace is approximately 30 ka and coincides with a late MIS 3 highstand as shown on the Muhs et al. (2012) relative sea level curve numerically predicted for San Nicholas Island, or 2) the terrace is approximately 45 ka and coincides with an earlier MIS 3 highstand as shown on the Simms et al. (2015) sea level model for Palos Verdes Hills, California. If the actual age of the Carpinteria Bluffs marine terrace is ~30 ka, one should expect to see the ~45 ka Punta Gorda terrace and the ~30 ka terrace on both sides of Rincon Creek. However, no evidence for a second terrace exists. Therefore, it is unlikely that the Carpinteria Bluffs marine terrace is ~30 ka as the OSL dates suggest. Instead, this terrace is interpreted as continuous with the ~45 ka Punta Gorda terrace.

Marine terrace dates less than 45 ka are not unusual for the Santa Barbara coast. Gurrola et al. (2014) dated several marine terraces slightly less than 40 ka at Ellwood Mesa and More Mesa using radiocarbon and OSL techniques. These terraces are close in age to the Carpinteria Bluffs samples 3-4 in this study. OSL samples 3 and 4 are convincing beach deposits because they are quartz-dominated sands with abundant shell fragments. These samples were collected near Tar Pit Park at low elevations, and they are the oldest of the five terrace samples. OSL dates 1, 2, and 5 probably underestimate the age of the Carpinteria Bluffs marine terrace. In general, OSL dates serve as a minimum age for the wave-cut platform because they are determined from sediment located stratigraphically above the wave-cut platform. It is possible that thousands of years of missing time exist between the

wave-cut bedrock surface and the overlying sediments preserved in the stratigraphic record. This effect might be greater if the overlying deposits are not marine in origin. Samples 1, 2, and 5 might be younger than samples 3 and 4 because they were sampled from a greater distance above the wave-cut platform or because they are terrestrial in origin and may not represent the first depositional event after creation of the platform. OSL samples 1, 2, and 5 do not contain shells and have a higher percentage of fine-grained material than the other samples. To confirm that the Carpinteria Bluffs terrace is indeed closer to ~45 ka than ~30 ka, it may be valuable to obtain radiocarbon dates.

Stream Steepness

Contrary to what emergent marine terraces reveal about uplift rate, k_{sn} values are significantly higher to the west of Rincon Point. This is likely a direct result of lithological strength. K_{sn} and lithological resistance to erosion are strongly correlated. If there really is a distinct increase in uplift rate immediately east of Rincon Point, the stream signal is overpowered and even reversed by differences in rock strength. To avoid the influence of lithologic strength, k_{sn} values were compared within lithologies of similar rock strength. In this comparison, Ventura streams had higher k_{sn} values. The validity of this method is questioned because k_{sn} studies are generally restricted to bedrock channels and the downstream portions of the Carpinteria streams are alluvial in nature. Alluvial channels are fundamentally different from bedrock channels, so it may not be appropriate to compare the downstream reaches of Carpinteria streams to the bedrock Ventura streams. Despite these complications, k_{sn} indices still operate as a reconnaissance tool for investigating patterns of uplift in that even in this study, higher k_{sn} values correspond with fault zones.

Tributaries from either side of Rincon Creek have similar regressed k_{sn} values, suggesting that there is no change in uplift rate across the upper reaches of Rincon Creek. Rather, changes in uplift rate are restricted to the lower part of Rincon Creek which coincides with the eastern edge of the Carpinteria Basin. The shape of the Rincon Creek drainage basin is asymmetric, having a higher drainage area on the eastern side, likely due to higher uplift rates and stream capture events.

Knickpoints

Lithology, especially rock strength, has the greatest influence on the presence and pattern of knickpoints in this study, as 46.9% of the knickpoints correspond with lithologic contacts or erosionally-resistant beds. Tectonic activity also controls knickpoint location, as 22.3% of knickpoints fall on faults or folds. An additional 7.7% of knickpoints coincide with both contacts and faults since the faults often juxtapose one unit against another. Other knickpoint sources, such as landslides, have a relatively small effect on knickpoint location. Only a very small percentage of knickpoints are identified as transient in this study. Many of the knickpoints that now correspond with geologic features may actually be temporarily fixed, but this is difficult to confirm. For instance, Los Sauces Creek, Madriano Creek, and Javon Creek all have knickpoints in their lower reaches that line up with the Red Mountain fault and its syncline. If these were transient knickpoints generated by an earthquake on the Red Mountain fault, one would expect them to have migrated upstream at a rate proportional to their drainage areas. Instead, the knickpoints are perfectly aligned with the fault. Although these knickpoints appear to be stationary, they may simply be temporarily fixed.

Transient knickpoints are arguably the most interesting type of knickpoint because they may hold a record of base level fall due to tectonic uplift. However, a variety of events can generate similar patterns of transient knickpoints, including sea level fall, fault rupture, stream capture, changes in bedrock uplift rate, changes in climate, and even incision rate change at tributary junctions (Crosby and Whipple, 2006). In this study, it is not obvious whether knickpoints at similar elevations in a drainage basin represent a change in uplift rate. Los Sauces Creek knickpoints may be the exception. The downstream portion of Los Sauces Creek is much steeper than the upstream, separated by what are considered here to be two transient knickpoints. Thus, Los Sauces Creek is divided into three segments for steepness analysis. Stream segments become progressively steeper downstream (Figure 25). The two gentler upstream reaches of the stream were likely captured by the headward-eroding Los Sauces Creek and have not adjusted to the new flow direction. Alternatively, these transient knickpoints may record increased uplift rates over time. In this case, gentle upstream segments represent relic topography that has not yet adjusted to local uplift rates.
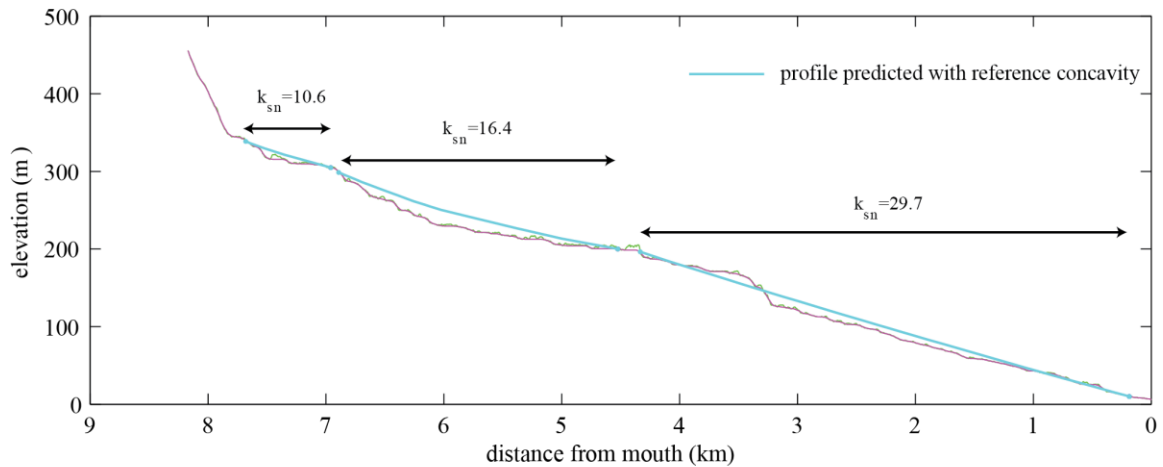
Figure 25: Stream 10: Los Sauces Creek (east). Three k_{sn} regessions were required due to the presence of two knickpoints which separate stream reaches with differing steepness. Regressed k_{sn} values are shown above the stream reach (black arrows) they represent. The stream gets progressively steeper downstream, suggesting that the upstream, gentle segments are out of equilibrium with the rate of uplift. See appendix for complete stream profile regression figures.

Tear Fault

Locating a tear fault at Rincon Point has proved very difficult and the evidence

presented here is inconclusive. Stream profile analysis and topographic relief suggest higher

uplift rates immediately east of Rincon Creek versus immediately west of Rincon Creek

within the field area. This difference could be facilitated by a tear fault, but it could also be

explained by the position of the Red Mountain fault, which comes onshore just east of

Rincon Point and offsets a MIS 3 marine terrace. The Carpinteria Bluffs marine terrace

profile has been interpreted in two ways: 1) the terrace is kinked across Rincon Creek where

it is uplifted by the Red Mountain fault; 2) the terrace exhibits a vertical displacement of

~17-45 m across Rincon Creek assuming that the tilt of the terrace remains consistent. Minor

and Brandt (2015) mapped several paleoshorelines on the east side of Rincon Creek,

implying multiple terraces. One possible explanation for the absence of these paleoshorelines to the west of Rincon Creek is the presence of a tear fault. Alternatively, the terrace fragments could belong to one terrace that was faulted and differentially uplifted by faults that do not continue onshore to the west. Even if dates were collected on each of these terrace fragments, the age resolution may not be fine enough to determine whether the terraces were formed simultaneously. To conclude, much of the evidence for a tear fault may actually be attributed to seismic activity on the Red Mountain fault and smaller, related east-west trending faults. Convincing outcrops of the fault plane are necessary to support the argument of a tear fault at Rincon Point.

FUTURE WORK

The tear fault, once claimed to be visible in the western parking lot roadcut of Rincon Point Park, is now covered in slopewash. Thus, convincing outcrops of the tear fault are lacking. Future research might include excavating the tear fault outcrop, trenching, or using geophysical techniques to locate the fault. Field mapping is needed to confirm that the right lateral fault mapped by Minor and Brandt (2015) is actually displaying apparent as opposed to true lateral offset, though surface outcrops may not be sufficient to answer this question.

Radiocarbon dating should also be used to confirm the OSL ages on the Carpinteria Bluffs marine terrace are not ~30 ka but closer to ~40-45 ka. Otherwise, the accepted age range of the Punta Gorda terrace should be adjusted. Finally, exposure dating could be used as a way to define uplift rates, especially toward the hinterland, where uplift rates determined by marine terraces in the foreland may not be appropriate.

CONCLUSIONS

Some key findings from this study include:

1) OSL ages on the Carpinteria Bluffs marine terrace sediments range from ~18-40 ka considering error. Dates on shoreface deposits near Tar Pit Park are dated at 31.31 ± 6.06 ka and 34.31 ± 5.61 ka. These dates represent a minimum age for the Carpinteria Bluffs terrace and suggest that this terrace is continuous with the Punta Gorda terrace (~45 ka) to the east. OSL dating has proved reliable in dating marine sediments within the Santa Barbara-Ventura fold belt, but caution should be exercised when dating terrestrial sediments.

   a. Using OSL dates from Tar Pit Park, the uplift rate of the Carpinteria Bluffs marine terrace is 1.8 ± 0.6 m/ky. Based on OSL ages from the Carpinteria Bluffs Nature Preserve, the uplift rate just west of Rincon Creek is 3.2 ± 1.1 m/ky. Because the OSL rates reflect minimum ages for the Carpinteria Bluffs marine terrace, these rates are relatively high, but still within error of rates calculated using a terrace age of 45 ka. The terrace is tilted to the west, indicating a gradational change in uplift rate from ~ 0 m/ky near Carpinteria beach to ~ 5 m/ky at Rincon Mountain.

   b. Based on a terrace age of 32.81 ± 6.06 ka, minimum vertical slip rates on the Railroad fault and Carpinteria fault are 0.06 m/ky and 0.20 /ky, respectively.

2) Stream profile analysis suggests an increase in uplift rate across the lower reach of Rincon Creek, at the edge of the Carpinteria Basin.

   a. Stream steepness data suggest that Ventura streams are significantly steeper than Carpinteria streams in similar lithologies.

b. Knickpoints within the field area are dominantly fixed and controlled by substrate strength or geologic structures; however at least two transient knickpoints exist within the Los Sauces Creek, suggesting increased uplift rates over time or multiple stream capture events due to headward erosion.

3) The lowermost reach of Rincon Creek is a geomorphic boundary that is most likely influenced by the position of the Red Mountain fault rather than a tear fault.

   a. There is a small chance that the lowermost, linear reach of Rincon Creek coincides with a tear fault. The asymmetry of the Rincon Creek anticline suggests that it is structurally pinned at Rincon Creek. However, convincing outcrops of the tear fault are lacking and other gemorphic evidence does not exclusively describe a tear fault.

   b. Geomorphic mapping suggests that the Carpinteria Bluffs marine terrace is either kinked by slip on the Red Mountain fault or vertically offset across Rincon Creek by a tear fault. The former explanation is favored.

   c. Seismic reflection data offshore of Rincon Creek is suggestive of a structural origin for Rincon Point, but is considered inconclusive because of the position of the seismic line and the presence of a subaqueous fan.

REFERENCES

Aitken, M. J., 1998, Introduction to Optical Dating: The Dating of Quaternary Sediments by the Use of Photon-stimulated Luminescence, Clarendon Press.

Bradley, W. C., and Griggs, G. B., 1976, Form, genesis, and deformation of central California wave-cut platforms: GSA Bulletin, v. 87, no. 3, p. 433-449.

Bull, W. B., Correlation of flights of global marine terraces, *in* Proceedings Binghamton Geomorphology Symposium, Binghamton, New York, 1985, Allen and Unwin, p. 129-152.

Burbank, D., Meigs, A., and Brozović, N., 1996, Interactions of growing folds and coeval depositional systems: Basin Research, v. 8, no. 3, p. 199-223.

Cochrane, G. R., Golden, N. E., Dartnell, P., Schroeder, D. M., and Finlayson, D. P., 2007, Seafloor Mapping and Benthic Habitat GIS for Southern California, Volume III. U.S. Geological Survey Open-File Report 2007-1271. .

Cook, K. L., Turowski, J. M., and Hovius, N., 2013, A demonstration of the importance of bedload transport for fluvial bedrock erosion and knickpoint propagation: Earth Surface Processes and Landforms, v. 38, no. 7, p. 683-695.

Corbett, E. J., and Johnson, C. E., 1982, The Santa Barbara, California, earthquake of 13 August 1978: Bulletin of the Seismological Society of America, v. 72, no. 6A, p. 2201-2226.

Cowie, P. A., and Scholz, C. H., 1992a, Displacement-length scaling relationship for faults: data synthesis and discussion: Journal of Structural Geology, v. 14, no. 10, p. 1149-1156.

-, 1992b, Physical explanation for the displacement-length relationship of faults using a post-yield fracture mechanics model: Journal of Structural Geology, v. 14, no. 10, p. 1133-1148.

Crosby, B. T., and Whipple, K. X., 2006, Knickpoint initiation and distribution within fluvial networks: 236 waterfalls in the Waipaoa River, North Island, New Zealand: Geomorphology, v. 82, no. 1, p. 16-38.

Dibblee, T. W., 1986, Geologic Map of the Carpinteria Quadrangle, Santa Barbara County, California: Dibblee Geological Foundation, scale 1:24,000.

-, 1987, Geologic Map of the White Ledge Peak Quadrangle, Santa Barbara and Ventura Counties, California: Dibblee Geological Foundation, scale 1:24,000.

-, 1988, Geologic Map of the Ventura and Pitas Point Quadrangles, Ventura County, California: Dibblee Geological Foundation, scale 1:24,000.

DOC/NOAA/NOS/OCM, 2004, 2002/2003 IfSAR data for Southern California: Digital Elevation Model (NAVD88), produced by Department of Commerce (DOC), National Oceanic and Atmospheric Administration (NOAA), National Ocean Service (NOS), Office for Coastal Management (OCM): Charleston, SC, NOAA.

-, 2012, 2009 - 2011 CA Coastal Conservancy Coastal LiDAR Project: Hydro-flattened Bare Earth DEM, produced by Department of Commerce (DOC), National Oceanic and Atmospheric Administration (NOAA), National Ocean Service (NOS), Office for Coastal Management (OCM): Charleston, SC, NOAA.

Duvall, A., Kirby, E., and Burbank, D., 2004, Tectonic and lithologic controls on bedrock channel profiles and processes in coastal California: Journal of Geophysical Research: Earth Surface, v. 109, no. F03002, p. 1-18.

Galbraith, R. F., and Roberts, R. G., 2012, Statistical aspects of equivalent dose and error calculation and display in OSL dating: An overview and some recommendations: Quaternary Geochronology, v. 11, p. 1-27.

Goff, J., Chagué-Goff, C., Nichol, S., Jaffe, B., and Dominey-Howes, D., 2012, Progress in palaeotsunami research: Sedimentary Geology, v. 243–244, p. 70-88.

Gurrola, L. D., 2006, Active Tectonics and Earthquake Hazards of the Santa Barbara Fold Belt, California [Ph.D. in Geology: University of California, Santa Barbara, 224 p.

Gurrola, L. D., DeVecchio, D. E., and Keller, E. A., 2010, Rincon Mountain megaslide: La Conchita, Ventura County, California: Geomorphology, v. 114, p. 311-318.

Gurrola, L. D., and Kamerling, M., 1996, Role of cross faults as tears in thrust ramps in the Ventura and Santa Barbara fold belts, California, Abstracts for the Southern California Earthquake Center Annual Meeting, p. 49.

Gurrola, L. D., Keller, E. A., Chen, J. H., Owen, L. A., and Spencer, J. Q., 2014, Tectonic geomorphology of marine terraces: Santa Barbara fold belt, California: Geological Society of America Bulletin, v. 126, no. 1-2, p. 219-233.

Gurrola, L. D., Keller, E. A., Trecker, M. A., Hartleb, R., and Dibblee Jr., T. W., 1998, Active folding and buried reverse faulting of the Santa Barbara Fold Belt, California: Geological Society of America Field Trip Guide Book Number 11.

Hartleb, R., 2000, Tectonic Geomorphology of the Eastern Mission Ridge Fault System, Santa Barbara and Ventura Counties, California [MA: University of California, Santa Barbara, 108 p.

Hoover and Associates, 1989, Geologic Map of Carpinteria Bluffs Property.

Hubbard, J., Shaw, J. H., Dolan, J., Pratt, T. L., McAuliffe, L., and Rockwell, T. K., 2014, Structure and Seismic Hazard of the Ventura Avenue Anticline and Ventura Fault, California: Prospect for Large, Multisegment Ruptures in the Western Transverse Ranges: Bulletin of the Seismological Society of America, v. 104, no. 3, p. 1070-1087.

Huftile, G. J., and Yeats, R. S., 1995, Convergence rates across a displacement transfer zone in the western Transverse Ranges, Ventura basin, California Journal of Geophysical Research, v. 100, no. B2, p. 2043-2067.

Huntley, D. J., Godfrey-Smith, D. I., and Thewalt, M. L. W., 1985, Optical dating of sediments: Nature, v. 313, no. 5998, p. 105-107.

Jackson, J., Norris, R., and Youngson, J., 1996, The structural evolution of active fault and fold systems in central Otago, New Zealand: Evidence revealed by drainage patterns: Journal of Structural Geology, v. 18, p. 217-234.

Jackson, J., Ritz, J.-F., Siame, L., Raisbeck, G., Yiou, F., Norris, R., Youngson, J., and Bennett, E., 2002, Fault growth and landscape development rates in Otago, New Zealand, using in situ cosmogenic 10Be: Earth and Planetary Science Letters, v. 195, no. 3–4, p. 185-193.

Jackson, P. A., and Yeats, R. S., 1982, Structural evolution of Carpinteria Basin, western Transverse Ranges, California: AAPG Bulletin, v. 66, no. 7, p. 805-829.

Johnson, S. Y., Dartnell, P., Cochrane, G. R., Golden, N. E., Phillips, E. L., Ritchie, A. C., Kvitek, R. G., Greene, H. G., Endris, C. A., Seitz, G. G., Sliter, R. W., Erdey, M. D., Wong, F. L., Gutierrez, C. I., Krigsman, L. M., Draut, A. E., and Hart, P. E., 2013, California State Waters Map Series—Offshore of Carpinteria, California: U.S.

Geological Survey Scientific Investigations Map 3261, 42 p., 10 sheets, scale 1:24,000.

Kaufman, A., Broecker, W. S., Ku, T. L., and Thurber, D. L., 1971, The status of U-series methods of mollusk dating: Geochimica et Cosmochimica Acta, v. 35, no. 11, p. 1155-1183.

Keller, E. A., Bean, G., and Best, D., 2015, Fluvial geomorphology of a boulder-bed, debris-flow — Dominated channel in an active tectonic environment: Geomorphology, v. 243, p. 14-26.

Keller, E. A., DeVecchio, D. E., and Shroder, J. F., 2013, 5.7 Tectonic Geomorphology of Active Folding and Development of Transverse Drainages, Treatise on Geomorphology: San Diego, Academic Press, p. 129-147.

Keller, E. A., Gurrola, L., and Tierney, T. E., 1999, Geomorphic criteria to determine direction of lateral propagation of reverse faulting and folding: Geology, v. 27, no. 6, p. 515-518.

Keller, E. A., and Gurrola, L. D., 2000, Earthquake Hazard of the Santa Barbara Fold Belt, California: Final report to the US Geological Survey.

Keller, E. A., and Pinter, N., 2002, Active tectonics: earthquakes, uplift, and landscape, Prentice Hall.

Keller, E. A., Zepeda, R. L., Rockwell, T. K., Ku, T. L., and Dinklage, W. S., 1998, Active tectonics at Wheeler Ridge, southern San Joaquin Valley, California: Geological Society of America Bulletin, v. 110, no. 3, p. 298-310.

Lajoie, K. R., Kern, J. P., Wehmiller, J. F., Kennedy, G. L., Mathieson, S. A., Sarna-Wojcicki, A. M., Yerkes, R. F., and McCrory, P. A., 1979, Quaternary marine shorelines and crustal deformation, San Diego to Santa Barbara, California, *in* Abbott, P. L., ed., Geologic Excursions in the Southern California Area: San Diego State University, San Diego, California, p. 3-15.

Lajoie, K. R., Ponti, D. J., Powell, C. L., Mathieson, S. A., and Sarna-Wojcicki, A. M., 1991, Emergent marine strandlines and associated sediments, coastal California: A record of Quaternary sea-level fluctuations, vertical tectonic movements, climatic changes, and coastal processes, *in* Morrison, R. B., ed., Quaternary Nonglacial Geology: Coterminous U.S., Volume K-2, Geological Society of America, p. 190-214.

Lajoie, K. R., Sarna-Wojcicki, A. M., and Yerkes, R. F., 1982, Quaternary chronology and rates of crustal deformation in the Ventura area, California, *in* Cooper, J. D., ed., Neotectonics in Southern California, Guidebook for fieldtrips, Anaheim, Ca, p. 43-51.

Loget, N., and Van Den Driessche, J., 2009, Wave train model for knickpoint migration: Geomorphology, v. 106, no. 3–4, p. 376-382.

Luyendyk, B. P., 1991, A model for Neogene crustal rotations, transtension, and transpression in southern California: Geological Society of America Bulletin, v. 103, no. 11, p. 1528-1536.

Manighetti, I., King, G. C. P., Gaudemer, Y., Scholz, C. H., and Doubre, C., 2001, Slip accumulation and lateral propagation of active normal faults in Afar: Journal of Geophysical Research: Solid Earth, v. 106, no. B7, p. 13667-13696.

McAuliffe, L. J., Dolan, J. F., Rhodes, E. J., Hubbard, J., Shaw, J. H., and Pratt, T. L., 2015, Paleoseismologic evidence for large-magnitude (Mw 7.5–8.0) earthquakes on the Ventura blind thrust fault: Implications for multifault ruptures in the Transverse Ranges of southern California: Geosphere, v. 11, no. 5, p. 1629-1650.

Medwedeff, D. A., 1992, Geometry and kinematics of an active, laterally propagating wedge thrust, Wheeler Ridge, California, *in* Mitra, S., and Fisher, G. W., eds., Structural Geology of Fold and Thrust Belts: Baltimore, Johns Hopkins University Press, p. 3-28.

Melosh, B., and Keller, E., 2013, Effects of active folding and reverse faulting on stream channel evolution, Santa Barbara Fold Belt, California: Geomorphology, v. 186, p. 119-135.

Metcalf, J. G., 1990, Engineering Geology Report for Carpinteria Bluffs Project, University of California, Santa Barbara.

Minor, S. A., and Brandt, T. R., 2015, Geologic Map of the Southern White Ledge Peak and Matilija Quadrangles, Santa Barbara and Ventura Counties, California, USGS Scientific Investigations Map 3321, scale 1:24,000.

Minor, S. A., Kellogg, K. S., Stanley, R. G., Gurrola, L. D., Keller, E. A., and Brandt, T. R., 2009, Geologic Map of the Santa Barbara Coastal Plain Area, Santa Barbara County, California, scale 1:25,000.

Mueller, K., and Talling, P., 1997, Geomorphic evidence for tear faults accommodating lateral propagation of an active fault-bend fold, Wheeler Ridge, California: Journal of Structural Geology, v. 19, no. 3–4, p. 397-411.

Muhs, D. R., Simmons, K. R., Schumann, R. R., Groves, L. T., Mitrovica, J. X., and Laurel, D., 2012, Sea-level history during the Last Interglacial complex on San Nicolas Island, California: implications for glacial isostatic adjustment processes, paleozoogeography and tectonics: Quaternary Science Reviews, v. 37, p. 1-25.

Murray, A. S., and Wintle, A. G., 2000, Luminescence dating of quartz using an improved single-aliquot regenerative-dose protocol: Radiation Measurements, v. 32, no. 1, p. 57-73.

-, 2003, The single aliquot regenerative dose protocol: potential for improvements in reliability: Radiation Measurements, v. 37, no. 4–5, p. 377-381.

Nelson, M. S., Gray, H. J., Johnson, J. A., Rittenour, T. M., Feathers, J. K., and Mahan, S. A., 2015, User guide for luminescence sampling in archaeological and geological contexts: Advances in Archaeological Practice: A Journal of the Society for American Archaeology, v. 3, no. 2, p. 166-177.

Perron, J. T., and Royden, L., 2013, An integral approach to bedrock river profile analysis: Earth Surface Processes and Landforms, v. 38, no. 6, p. 570-576.

Prince, P. S., Spotila, J. A., and Henika, W. S., 2011, Stream capture as driver of transient landscape evolution in a tectonically quiescent setting: Geology, v. 39, no. 9, p. 823-826.

Putnam, W. C., 1942, Geomorphology of the Ventura region, California: Geological Society of America Bulletin, v. 53, no. 5, p. 691-754.

Rittenour, T., 2015, OSL Sampling Do's and Dont's Guide: USU OSL Laboratory.

Rockwell, T. K., Large co-seismic uplift of coastal terraces across the Ventura Avenue anticline: Implications for the size of earthquakes and the potential for tsunami generation, Plenary talk, *in* Proceedings Southern California Earthquake Center Annual Meeting 2011.

Rockwell, T. K., Keller, E. A., and Dembroff, G. R., 1988, Quaternary rate of folding of the Ventura Avenue anticline, western Transverse Ranges, southern California: Geological Society of America Bulletin, v. 100, no. 6, p. 850-858.

Rockwell, T. K., Nolan, J., Johnson, D. L., and Patterson, R., 1992, Ages and deformation of marine terraces between Point Conception and Gaviota, western Transverse Ranges, California: in Quaternary Coasts of the United States: Marine and Lacustrine Systems: Society of Economic Paleotologists and Mineralogists Special Publication No. 48, p. 333-341.

Schumm, S. A., 1986, Alluvial river response to active tectonics: Active tectonics, p. 80-94.

Schwanghart, W., and Scherler, D., 2014, Short Communication: TopoToolbox 2 – MATLAB-based software for topographic analysis and modeling in Earth surface sciences: Earth Surf. Dynam., v. 2, no. 1, p. 1-7.

Siddall, M., Rohling, E. J., Thompson, W. G., and Waelbroeck, C. C. R., 2008, Marine isotope stage 3 sea level fluctuations: Data synthesis and new outlook: Reviews of Geophysics, v. 46, no. 4.

Simms, A., Reynolds, L. C., Bentz, M., Roman, A., Rockwell, T., and Peters, R., 2016, Tectonic Subsidence of California Estuaries Increases Forecasts of Relative Sea-Level Rise: Estuaries and Coasts, p. 1-11.

Simms, A. R., Rouby, H., and Lambeck, K., 2015, Marine terraces and rates of vertical tectonic motion: The importance of glacio-isostatic adjustment along the Pacific coast of central North America: Geological Society of America Bulletin.

Suppe, J., and Medwedeff, D. A., 1990, Geometry and kinematics of fault-propagation folding: Eclogae Geologicae Helvetiae, v. 83, no. 3, p. 409-454.

Trecker, M. A., 1999, Oxygen Isotope Stratigraphy as a Means of Correlating Deformed Marine Terraces [Master of Arts in Geology: University of California, Santa Barbara, 74 p.

Ucarkus, G., Kent, G., and Rockwell, T. K., 2014, Active deformation offshore the Western Transverse Ranges, Abstract T52A-05 presented at 2014 Fall Meeting, AGU, San Francisco, Calif., 15-19 Dec.

Webber, A. C., 1999, Tectonic geomorphology and earthquake hazard analysis of the Rincon Creek anticline and Rincon Creek fault, Carpinteria, Santa Barbara County, California, University of California, Santa Barbara.

Wehmiller, J. F., Lajoie, K. R., Kvenvolden, K. A., Peterson, E., Belknap, D. F., Kennedy, G. L., Addicott, W. O., Vedde, J. G., and Wright, R. W., 1977, Correlation and chronology of Pacific Coast marine terrace deposits of continental United States by fossil amino acid stereochemistry technique, evaluation, relative ages, kinetic model ages, and geologic implications: U.S. Geological Survey Open-file Report 77-680.

Wehmiller, J. F., Lajoie, K. R., Sarna-Wojcicki, A. M., Yerkes, R. F., Kennedy, G. L., Stephens, T. A., and Koh., R. F., 1978, Amino-acid racemization dating of Quaternary mollusks, Pacific Coast, United States, *in* Zartman, R. E., ed., Short papers of the Fourth International Conference, Geochronology, Cosmochronology, Isotope Geology: U. S. Geological Survey Open File Report 78-701, p. 445-448.

Whipple, K., Wobus, C., Crosby, B., Kirby, E., and Sheehan, D., 2007, New tools for quantitative geomorphology: Extraction and interpretation of stream profiles from digital topographic data, GSA Annual Meeting: Boulder, CO.

Whipple, K. X., and Tucker, G. E., 1999, Dynamics of the stream-power river incision model: Implications for height limits of mountain ranges, landscape response timescales, and research needs: Journal of Geophysical Research: Solid Earth, v. 104, no. B8, p. 17661-17674.

Wintle, A. G., and Murray, A. S., 2006, A review of quartz optically stimulated luminescence characteristics and their relevance in single-aliquot regeneration dating protocols: Radiation Measurements, v. 41, no. 4, p. 369-391.

Wobus, C., Whipple, K. X., Kirby, E., Snyder, N., Johnson, J., Spyropolou, K., Crosby, B., and Sheehan, D., 2006, Tectonics from topography: Procedures, promise, and pitfalls: Geological Society of America Special Papers, v. 398, p. 55-74.

Wyss, M., 1979, Estimating maximum expectable magnitude of earthquakes from fault dimensions: Geology, v. 7, no. 7, p. 336-340.

Yeats, R. S., and Rockwell, T. R., 1991, Quaternary Geology of the Ventura and Los Angeles basins, California, *in* Morrison, R. B., ed., Quaternary Nonglacial Geology: Coterminous U.S., Volume K-2, Geological Society of America, p. 185-189.

APPENDIX

Stream Steepness Regressions

Notes:

      The following figures display the results from stream steepness regressions following Whipple et al. (2007). The top plot is a smoothed longitudinal profile with two predicted profiles. The dark blue profile is predicted using the regressed channel concavity and the light blue profile is predicted using the reference concavity of 0.4. The smoothed channel profile is shown in pink and the green profile represents the raw profile elevations. Raw elevations are only visible where they differ from the smoothed elevations. A smoothing window of 60 m was used. The middle plot shows how drainage area changes along the length of the channel. In the lower plot, red squares represent log-bin averages of slope-area data. The regressed k_{sn} value and concavity value for each stream segment are displayed. The same predicted profiles from the top plot are shown in the bottom plot in log-log form.
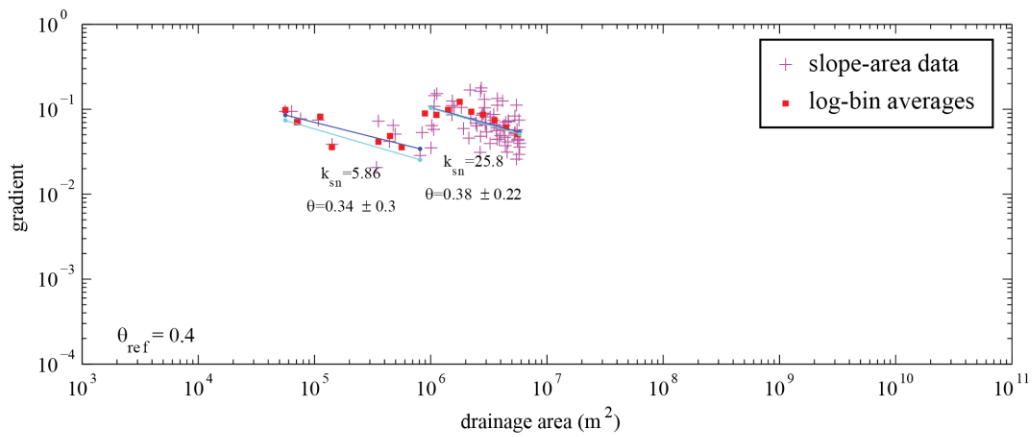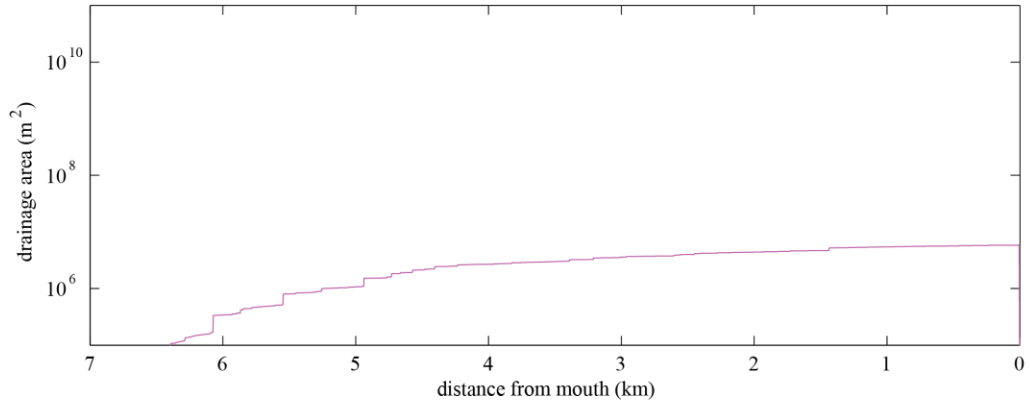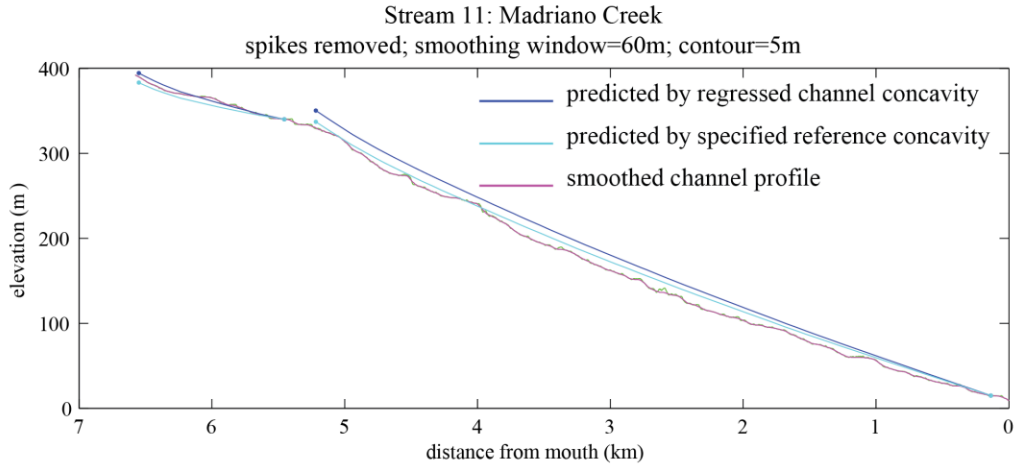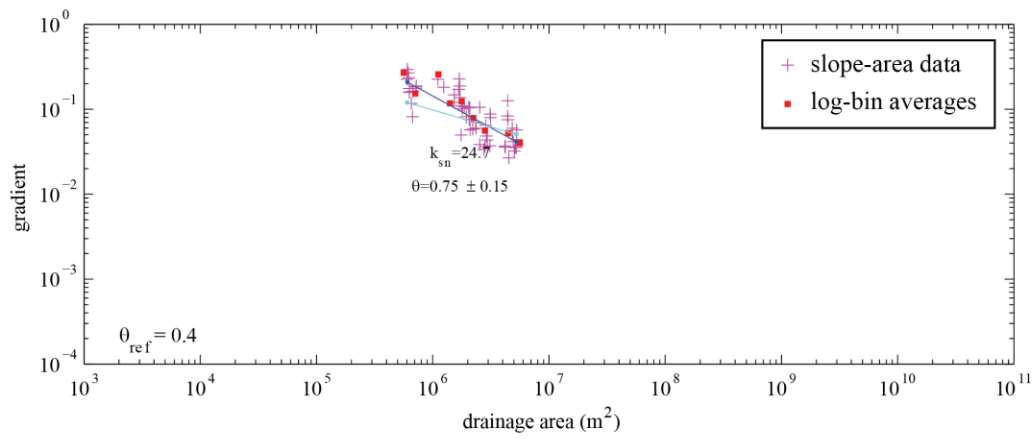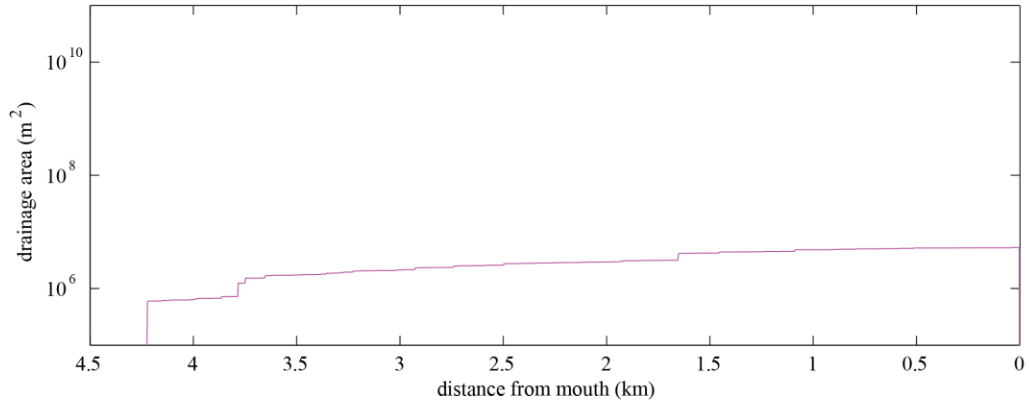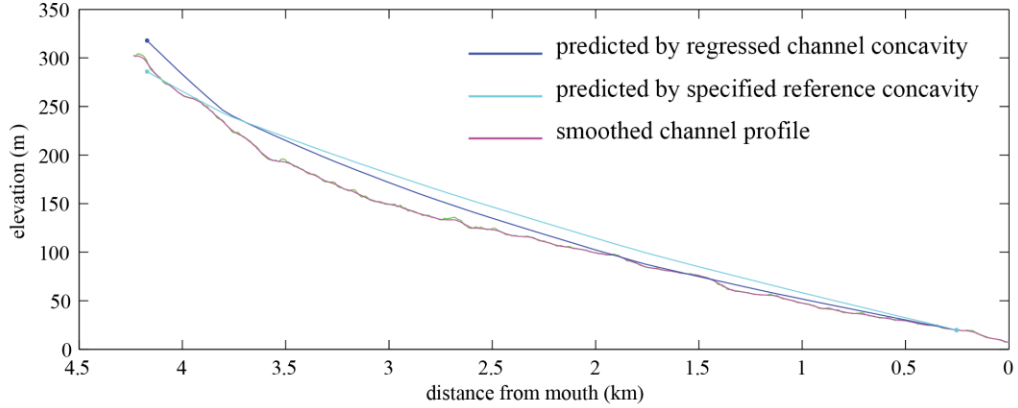
Stream 1: Toro Creek (west)
spikes removed; smoothing window=60m; contour=5m

Legend (top panel):
- predicted by regressed channel concavity
- predicted by specified reference concavity
- smoothed channel profile

Axis labels (top panel): elevation (m); distance from mouth (km)

Axis labels (middle panel): drainage area (m^2); distance from mouth (km)

Legend (bottom panel):
- slope-area data
- log-bin averages

Bottom panel annotations:
k_{sn}=30.8
θ=0.54 $\pm$ 0.12
θ_{ref}= 0.4

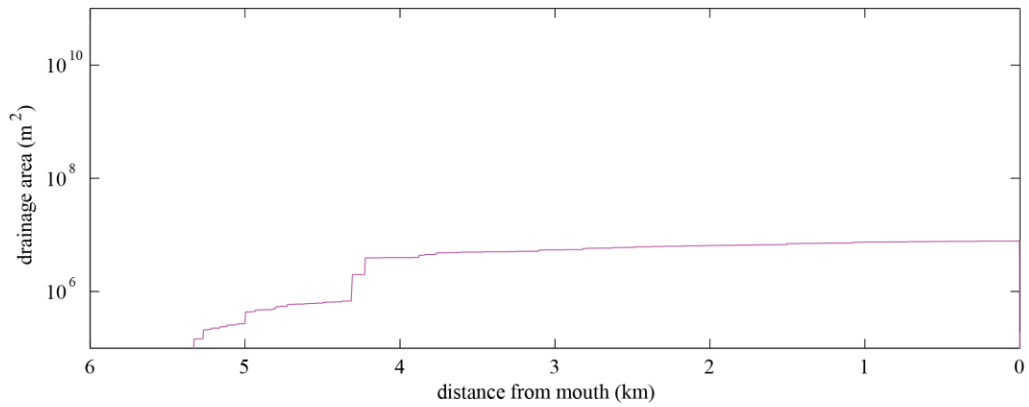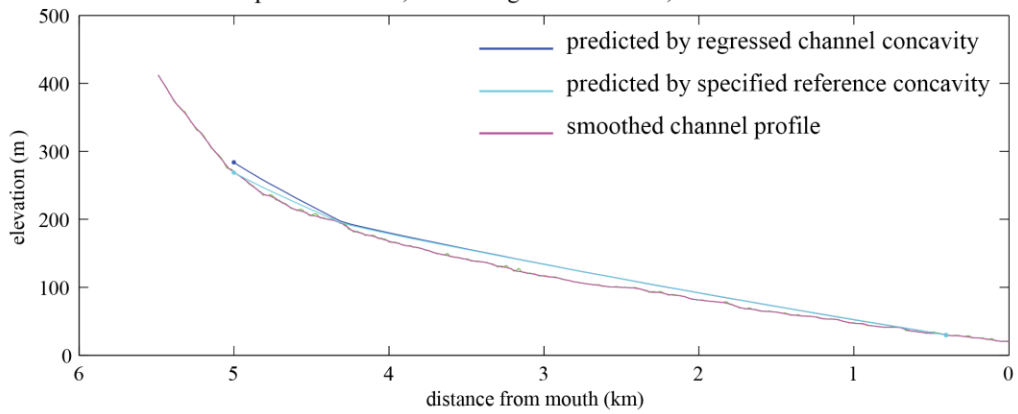Axis labels (bottom panel): gradient; drainage area (m^2)

79

Stream 2: Toro Creek (east)
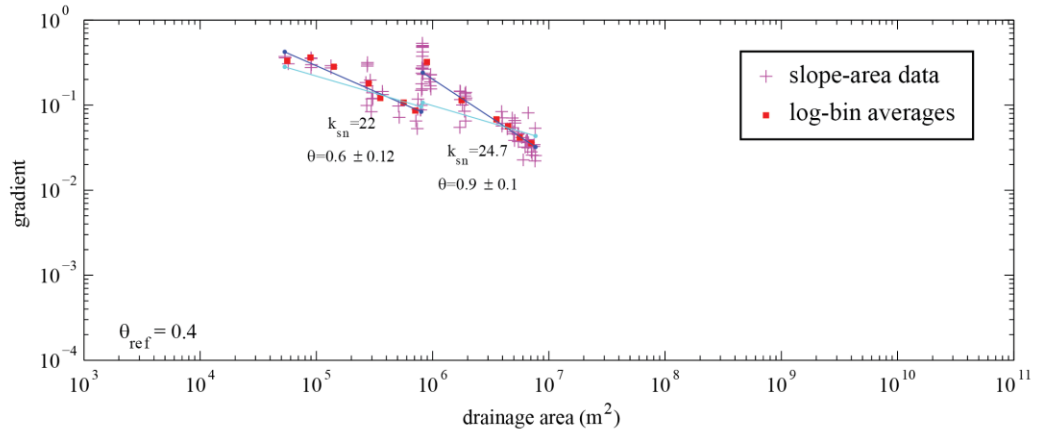spikes removed; smoothing window=60m; contour=5m

Stream 3: Arroyo Paredon
spikes removed; smoothing window=60m; contour=5m

Top panel: elevation (m) vs distance from mouth (km)
Legend:
- predicted by regressed channel concavity
- predicted by specified reference concavity
- smoothed channel profile

Middle panel: drainage area (m^2) vs distance from mouth (km)

Bottom panel: gradient vs drainage area (m^2)
Legend:
- slope-area data
- log-bin averages

k_{sn}=37.3

θ=0.6 $\pm$ 0.068

θ_{ref} = 0.4
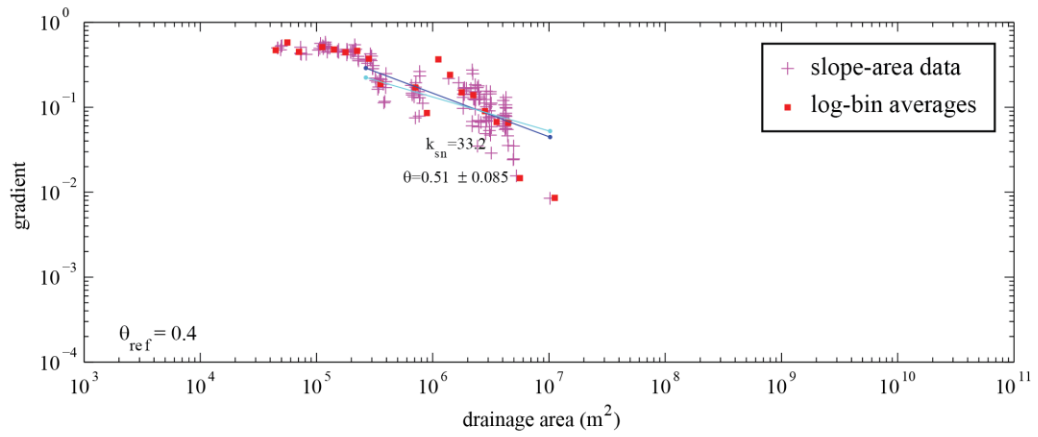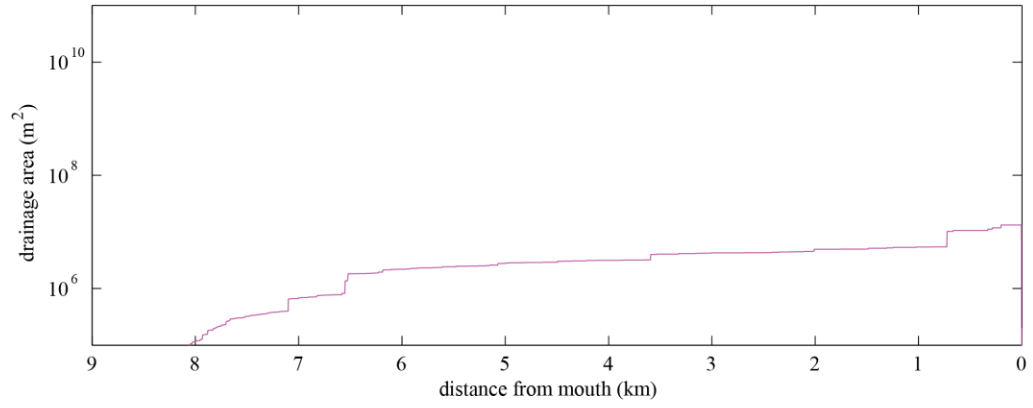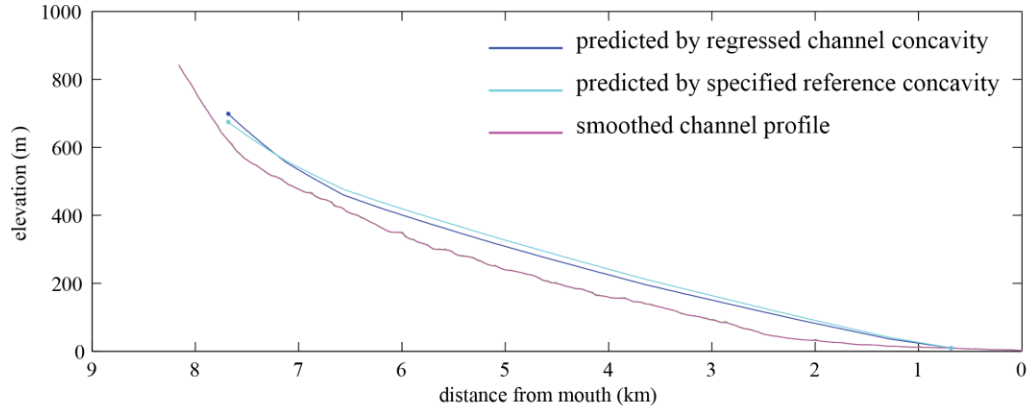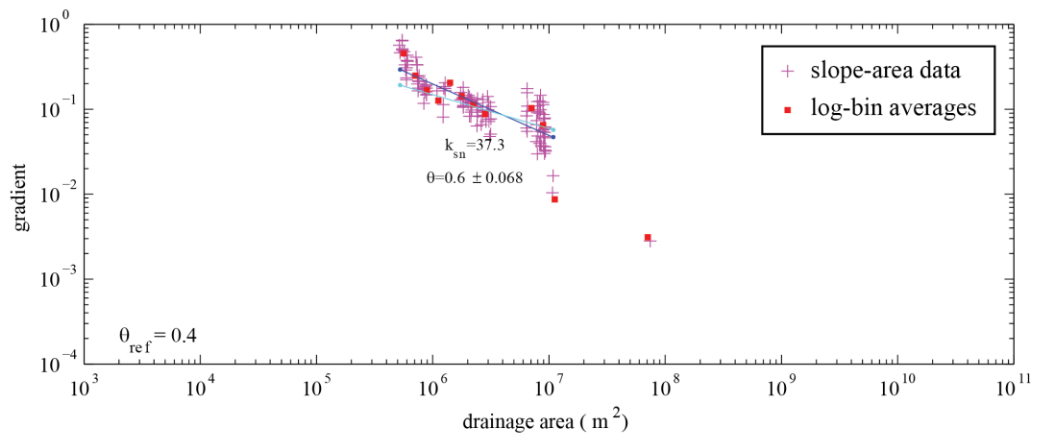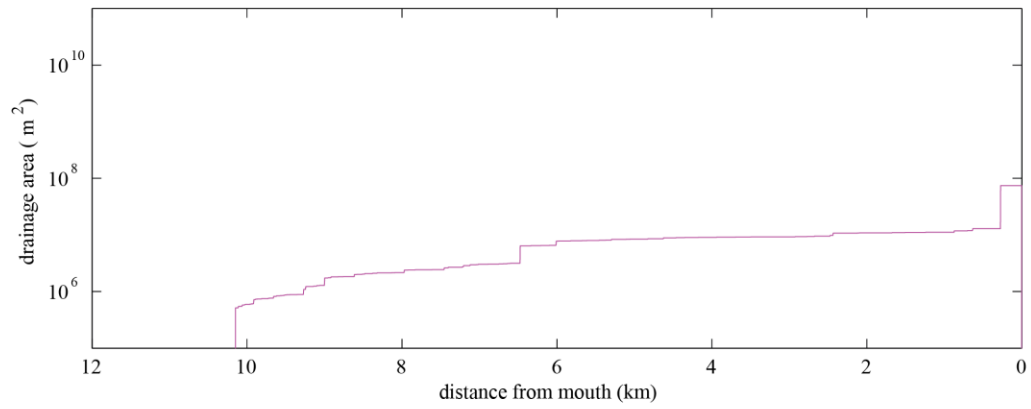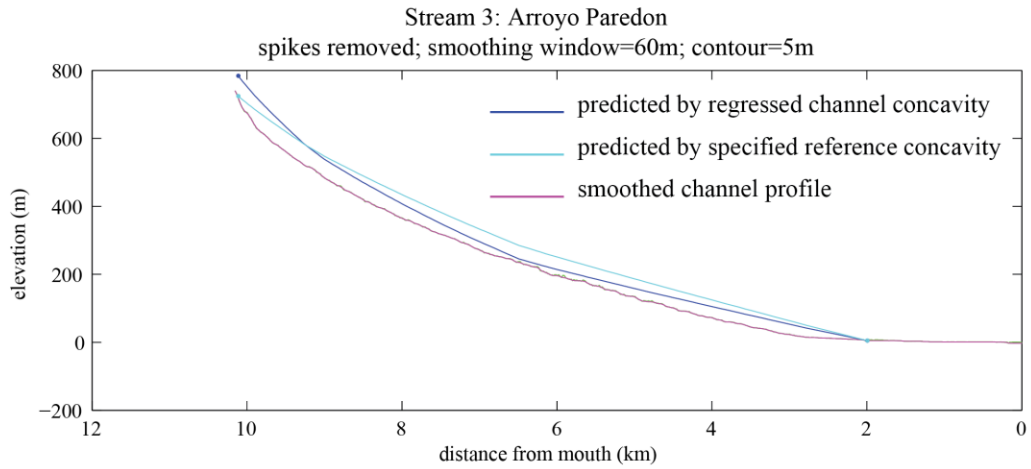
Stream 4: Santa Monica Creek
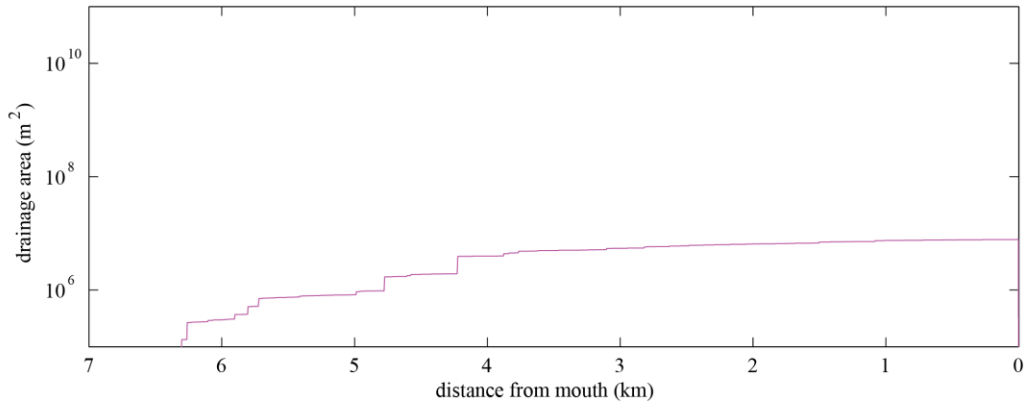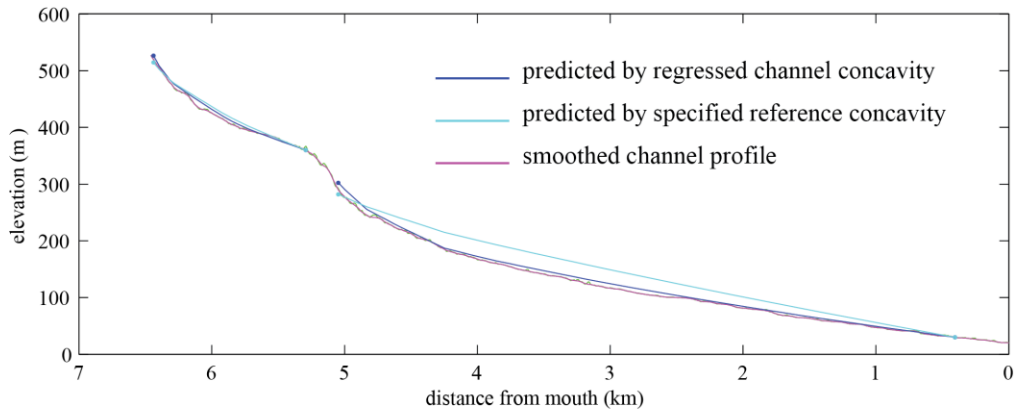spikes removed; smoothing window=60m; contour=5m

predicted by regressed channel concavity
predicted by specified reference concavity
smoothed channel profile

slope-area data
log-bin averages

k_{sn}=45.1
θ=0.53 ± 0.045

θ_{ref} = 0.4

Stream 5: Carpinteria Creek
spikes removed; smoothing window=60m; contour=5m

predicted by regressed channel concavity
predicted by specified reference concavity
smoothed channel profile

k_{sn}=34.3
θ=0.64 ± 0.051

θ_{ref}= 0.4

slope-area data
log-bin averages

Stream 6: Eldorado Creek
spikes removed; smoothing window=60m; contour=5m

Legend for top plot:
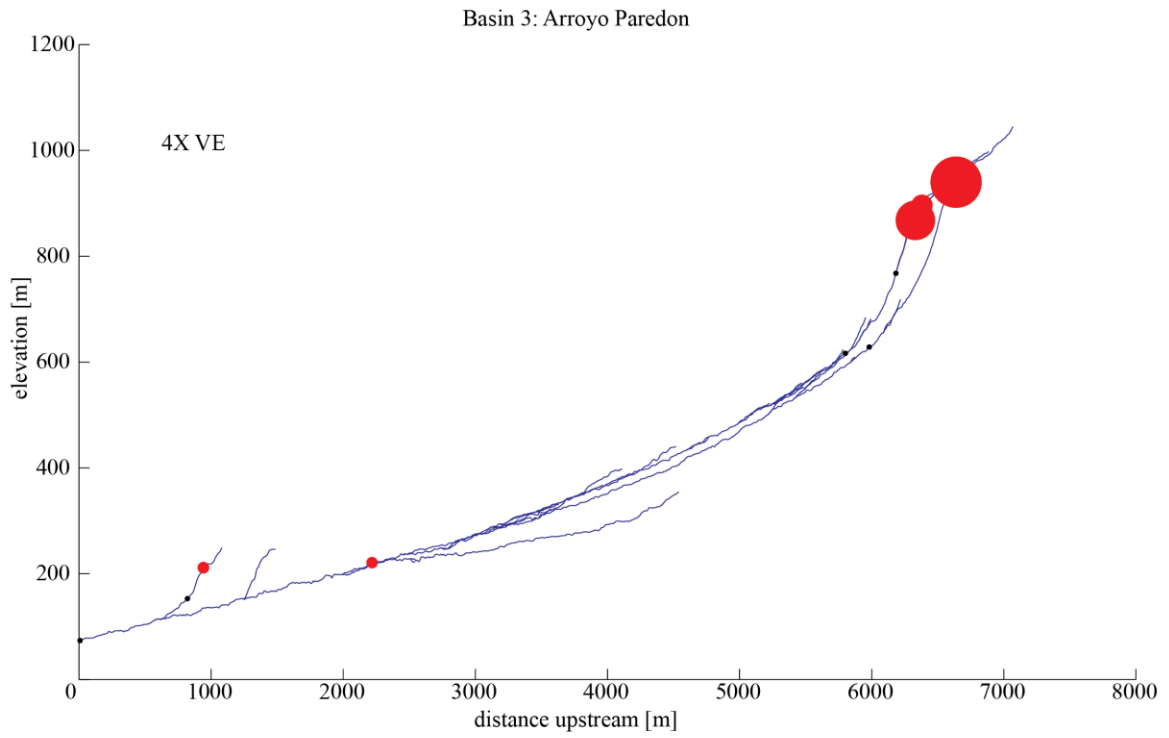- predicted by regressed channel concavity
- predicted by specified reference concavity
- smoothed channel profile

Legend for bottom plot:
- slope-area data
- log-bin averages

$k_{sn}=33.8$

$\theta=0.57 \pm 0.088$

$\theta_{ref}= 0.4$

Stream 7: Steer Creek
spikes removed; smoothing window=60m; contour=5m

elevation (m)

- predicted by regressed channel concavity
- predicted by specified reference concavity
- smoothed channel profile

distance from mouth (km)

drainage area (m^2)

distance from mouth (km)

gradient

- + slope-area data
- ■ log-bin averages

k_{sn} =36.5
θ=0.76 ± 0.13

θ_{ref} = 0.4

drainage area (m^2)

Stream 8: Rincon Creek
spikes removed; smoothing window=60m; contour=5m

Legend (top panel):
- predicted by regressed channel concavity
- predicted by specified reference concavity
- smoothed channel profile

elevation (m) vs distance from mouth (km)

drainage area (m^2) vs distance from mouth (km)

gradient vs drainage area (m^2)

Legend (bottom panel):
- slope-area data
- log-bin averages

k_{sn} =44.3

θ=0.52 $\pm$ 0.064

θ_{ref} = 0.4

Stream 9: Los Sauces Creek (west)
spikes removed; smoothing window=60m; contour=5m

Stream 10: Los Sauces Creek (east)
spikes removed; smoothing window=60m; contour=5m

Stream 11: Madriano Creek
spikes removed; smoothing window=60m; contour=5m

Stream 12: Javon Creek
spikes removed; smoothing window=60m; contour=5m

Stream 13: San Juan (west)
spikes removed; smoothing window=60m; contour=5m

Legend:
- predicted by regressed channel concavity
- predicted by specified reference concavity
- smoothed channel profile

- slope-area data
- log-bin averages

$k_{sn}=21.5$

$\theta=0.46 \pm 0.089$

$\theta_{ref}= 0.4$
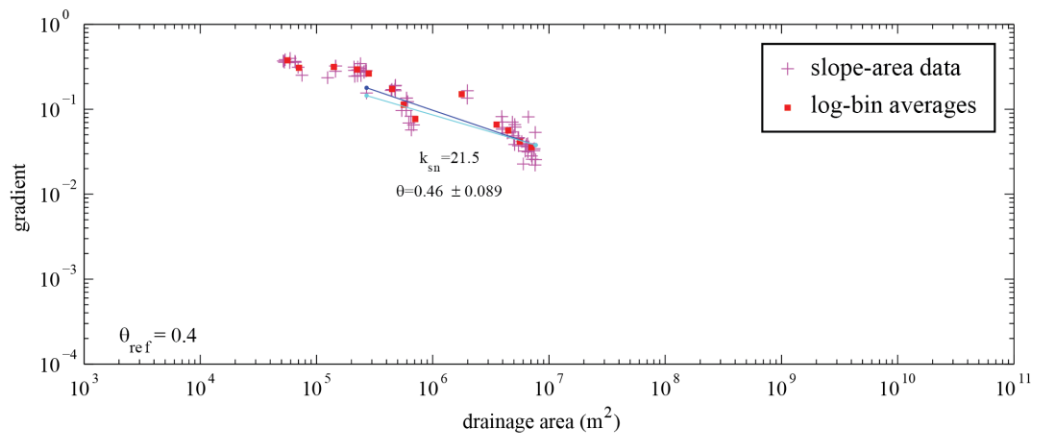
Stream 14: San Juan (east)
spikes removed; smoothing window=60m; contour=5m

Longitudinal Stream Profiles with Knickpoints

Notes:

Longitudinal profiles with knickpoint lips and bases were generated with a custom algorithm by Alexander Neely. Knickpoints are presented here by stream basin. The symbol size of the knickpoint lip reflects the magnitude of the knickpoint. Knickpoint lips are shown in red and knickpoint bases are shown in black. Tributaries are included in the profiles. Profiles are four times vertically exaggerated. Notice the relative abundance of knickpoints in Rincon Creek compared to the other streams.

Stream Network Longitudinal Profiles with Knickpoints

Basin 1: Toro Creek West

Basin 2: Toro Creek East

Basin 3: Arroyo Paredon

Basin 4: Santa Monica Creek

Basin 5: Carpinteria Creek

4X VE

distance upstream [m]

elevation [m]

Basin 6: Eldorado/Steer Creek

4X VE

distance upstream [m]

elevation [m]

Basin 7: Rincon Creek

Basin 8: Los Sauces Creek

Basin 9: Madriano Creek

Basin 10: Javon Creek

Basin 11: San Juan
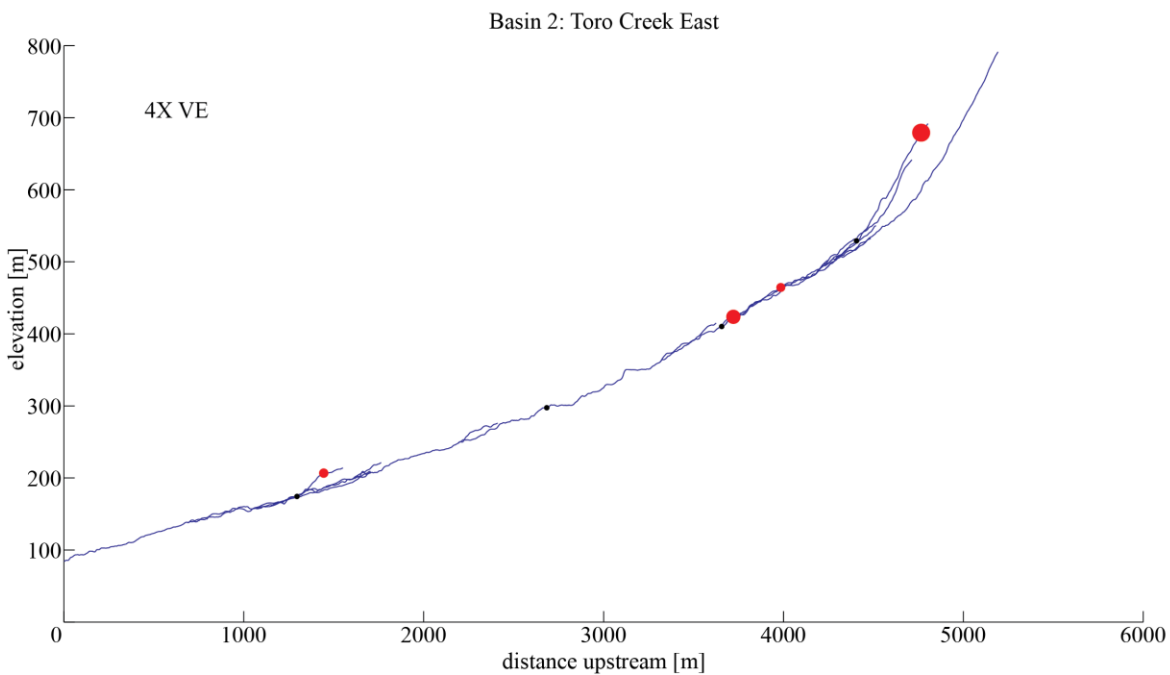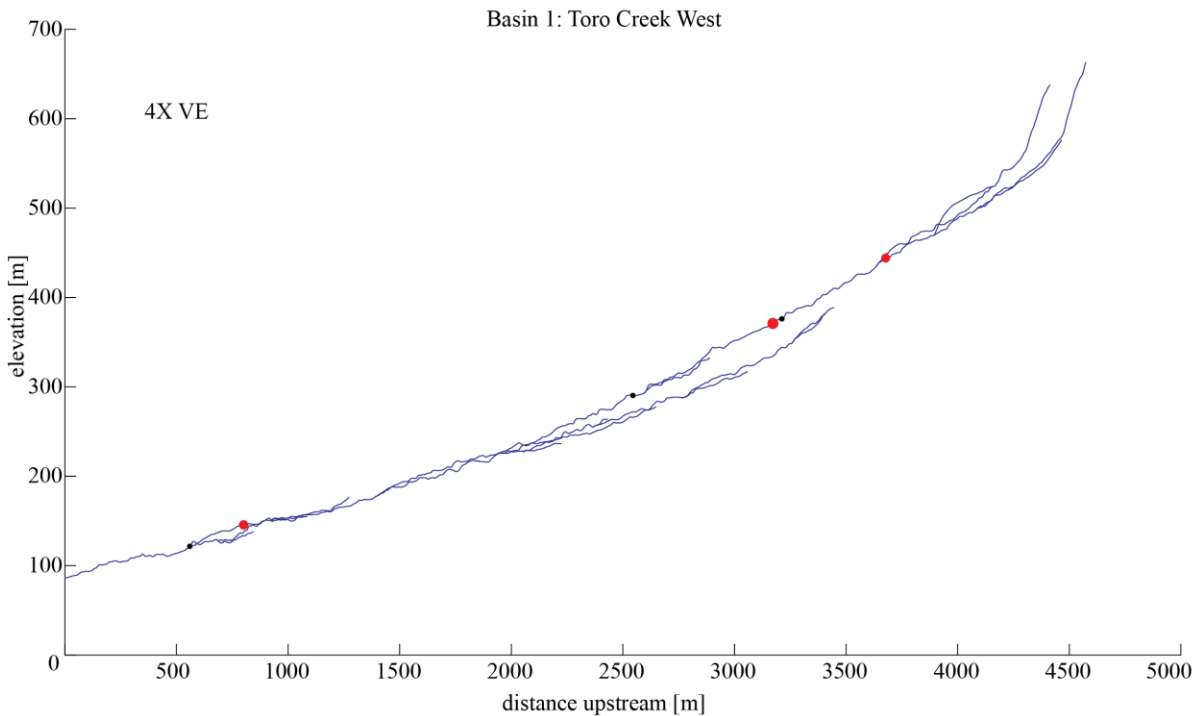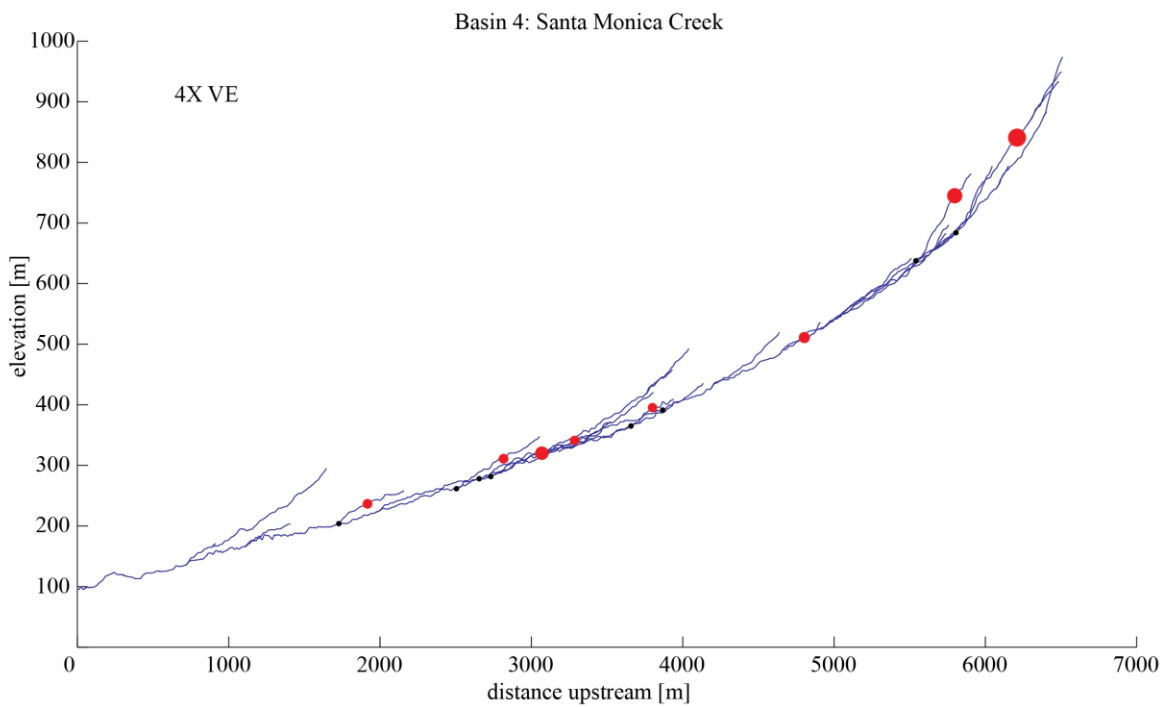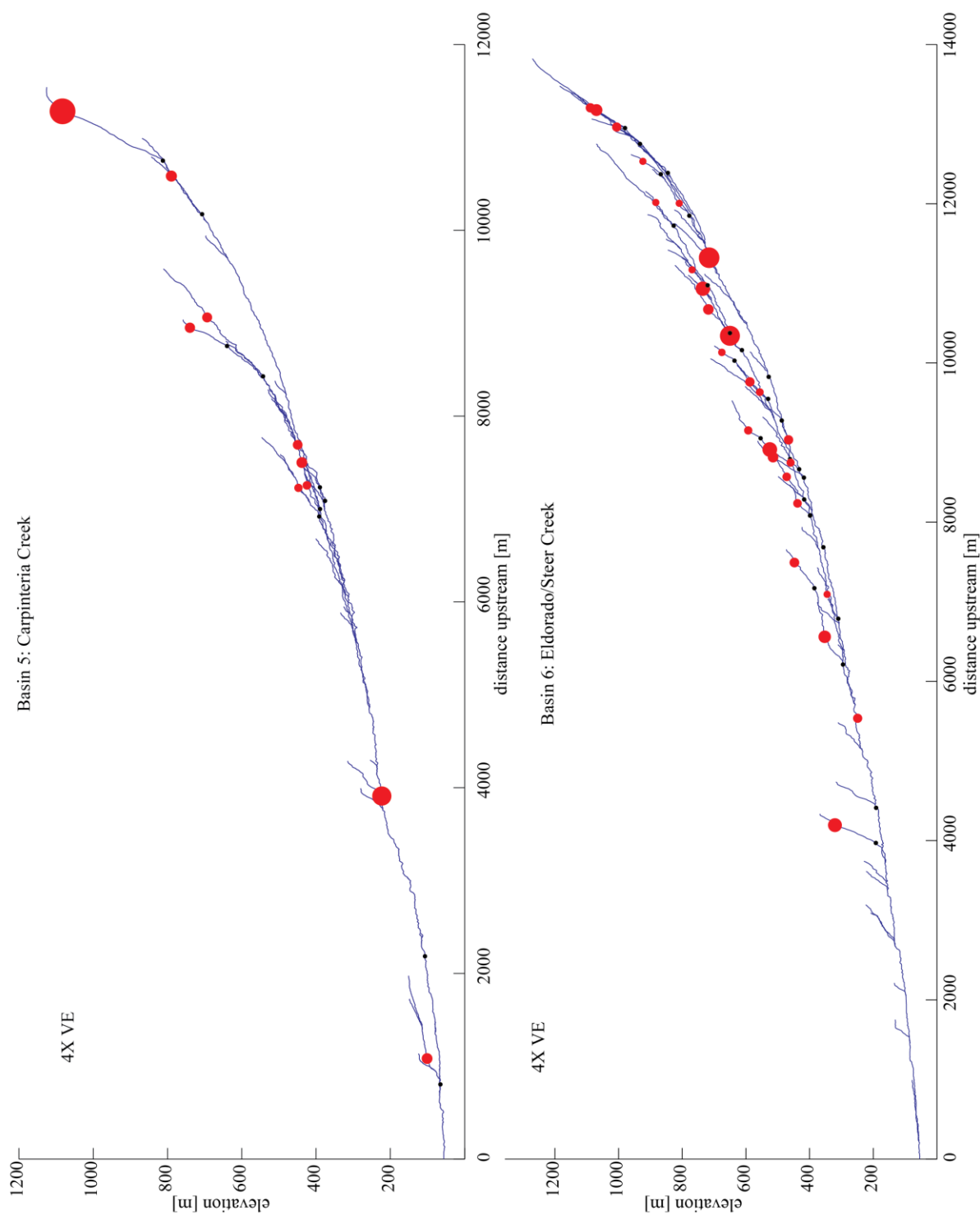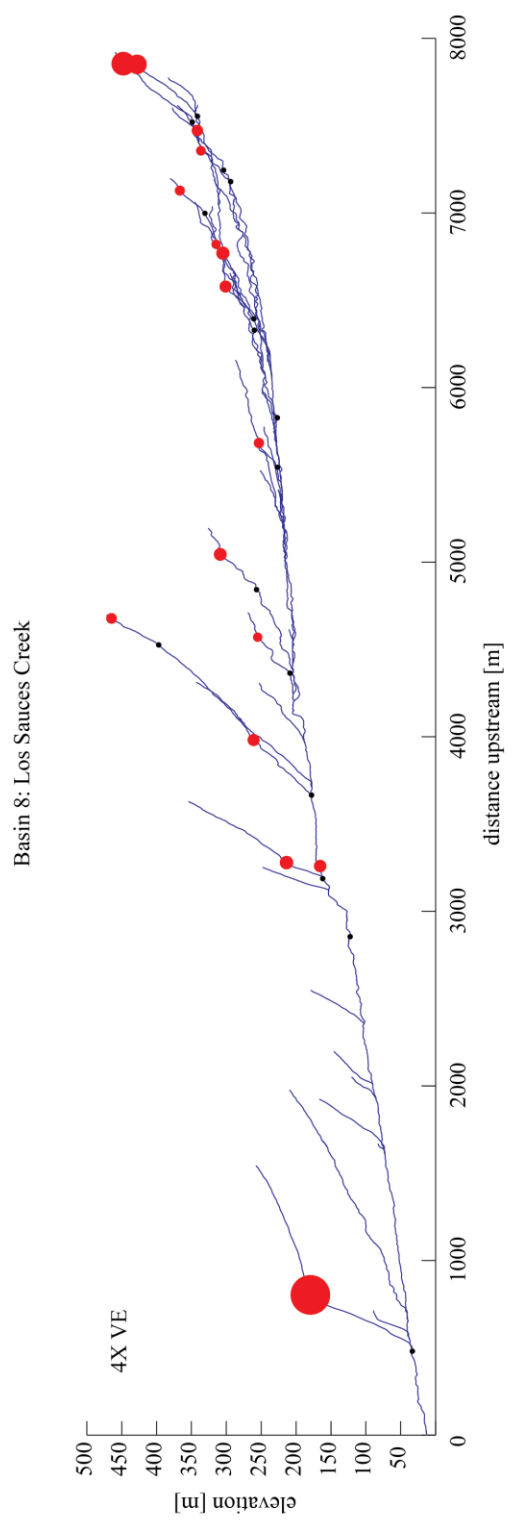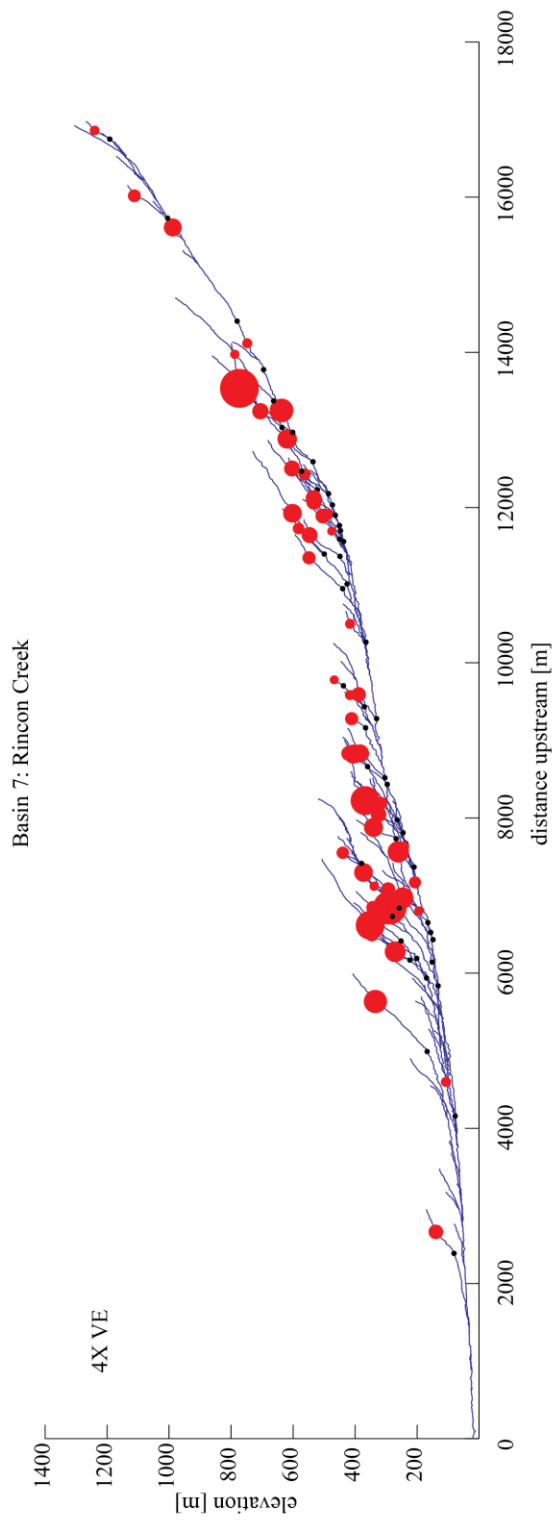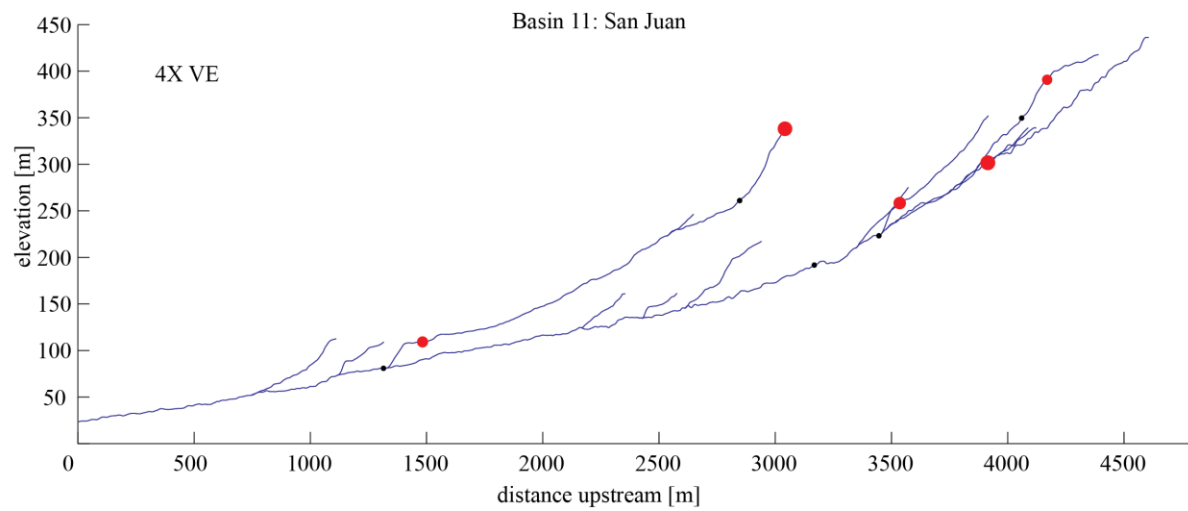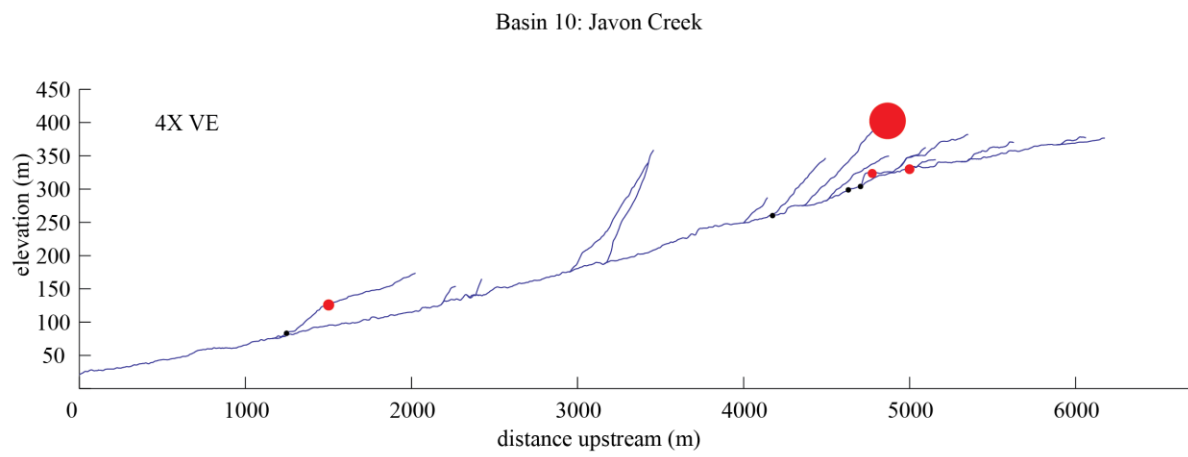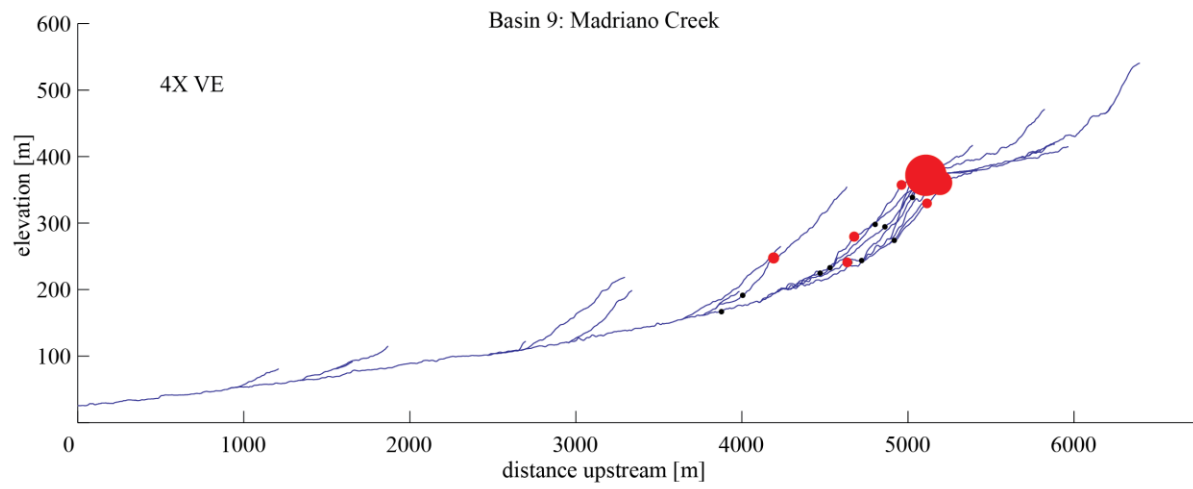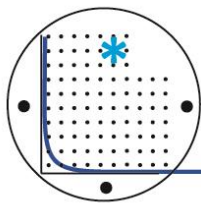
Project: **Rincon Point, CA**   Project #: **215**
Scientists: **Shelby Fredrickson, UCSB**
Report by: **Tammy Rittenour**   Report date: **June 2, 2016**

Final Luminescence Age Report

Table 1. Optically Stimulated Luminescence Age Information

Sample num.	USU num.	Depth (m)	Num. of aliquots[1]	Dose rate (Gy/ka)	D_E[2] ± 2σ (Gy)	OD[3] (%)	OSL age ± 2σ (ka)
CarpB_OSL_1	USU-2021	4.0	14 (29)	3.48 ± 0.15	96.77 ± 23.71	38.4 ± 9.8	**27.79 ± 7.36**
CarpB_OSL_2	USU-2022	2.75	19 (42)	3.14 ± 0.14	79.32 ± 20.82	51.3 ± 10.1	**25.27 ± 7.09**
CarpB_OSL_3	USU-2023	4.5	18 (32)	3.52 ± 0.15	110.17 ± 18.19	30.6 ± 6.4	**31.31 ± 6.06**
CarpB_OSL_4	USU-2024	4.5	17 (35)	3.53 ± 0.15	121.19 ± 15.60	22.8 ± 5.2	**34.31 ± 5.61**
RincP_OSL_1	USU-2025	14.0	24 (35)	2.91 ± 0.13	112.07 ± 12.43	21.5 ± 4.6	**38.58 ± 5.72**
RincP_OSL_2	USU-2026	16.0	22 (36)	3.00 ± 0.13	119.57 ± 13.96	21.0 ± 5.1	**39.80 ± 6.07**
CarpB_OSL_5	USU-2027	4.5	17 (31)	3.59 ± 0.15	84.42 ± 16.79	34.9 ± 8.0	**23.54 ± 5.25**

[1] Age analysis using the single-aliquot regenerative-dose procedure of Murray and Wintle (2000) on 1-2mm small-aliquots of quartz sand. Number of aliquots used in age calculation and number of aliquots analyzed in parentheses.

[2] Equivalent dose (D_E) calculated using the Central Age Model (CAM) of Galbraith and Roberts (2012).

[3] Overdispersion (OD) represents variance in D_E data beyond measurement uncertainties, OD >20% may indicate significant scatter due to depositional or post-depositional processes.

Table 2. Dose Rate Information

Sample num.	USU num.	In-situ H_2O (%)[1]	Grain size (μm)	K (%)[2]	Rb (ppm)[2]	Th (ppm)[2]	U (ppm)[2]	Cosmic (Gy/ka)
CarpB_OSL_1	USU-2021	0.1	150-250	3.09±0.08	108.5±4.3	3.8±0.3	1.0±0.1	0.13±0.01
CarpB_OSL_2	USU-2022[3]	0	150-250	2.57±0.06	89.7±3.6	4.2±0.4	1.4±0.1	0.15±0.01
CarpB_OSL_3	USU-2023	3.8	90-180	3.09±0.15	114.5±4.6	3.7±0.3	0.9±0.1	0.12±0.01
CarpB_OSL_4	USU-2024	1.7	90-180	3.05±0.08	111.0±4.4	3.8±0.3	1.1±0.1	0.12±0.01
RincP_OSL_1	USU-2025	1.9	150-250	2.26±0.06	83.8±3.4	6.3±0.6	1.5±0.1	0.05±0.0
RincP_OSL_2	USU-2026	1.1	90-180	2.21±0.06	83.5±3.3	7.0±0.6	1.7±0.1	0.04±0.0
CarpB_OSL_5	USU-2027	1.4	150-250	3.14±0.08	112.0±4.5	4.1±0.4	1.2±0.1	0.12±0.01

[1] Assumed 5±2% for moisture content over burial history.

[2] Radioelemental concentrations determined by ALS Chemex using ICP-MS and ICP-AES techniques; dose rate is derived from concentrations by conversion factors from Guérin et al. (2011).
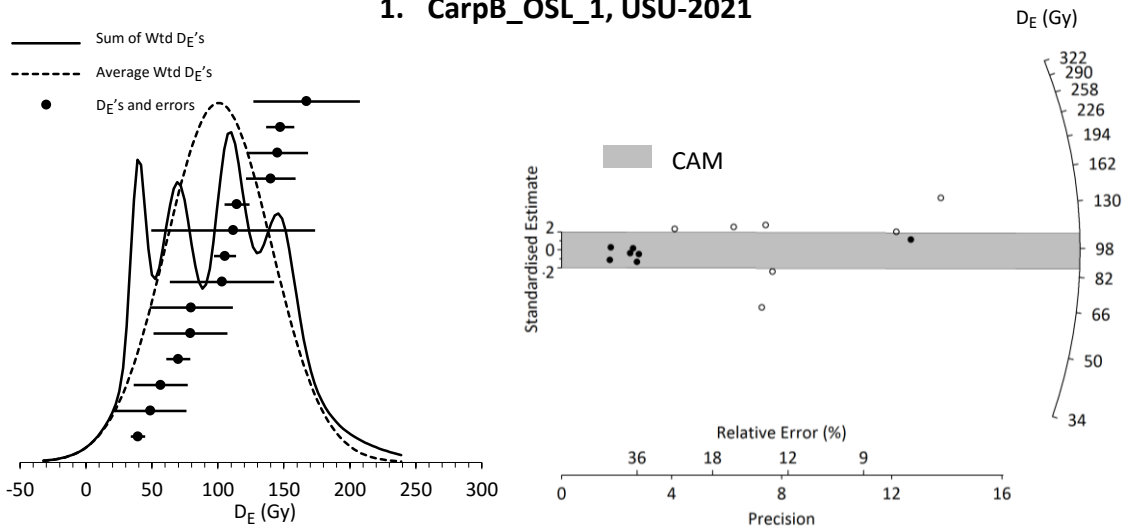
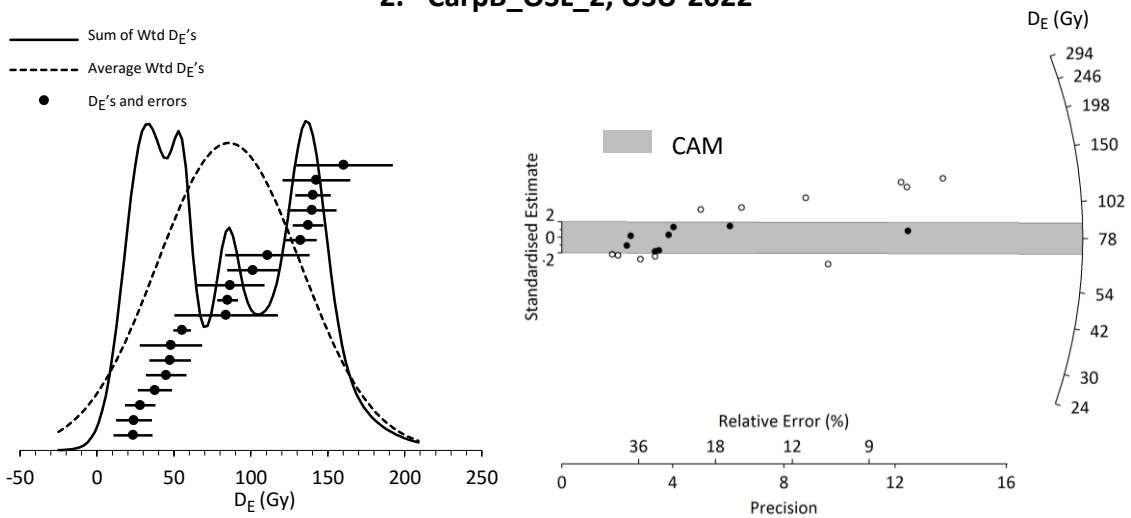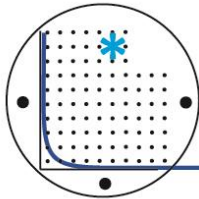[3] Chemistry is the average of 3 subsamples.
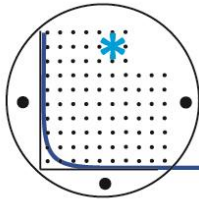
Equivalent dose (D$_E$) Distributions: Probability density functions and radial plots
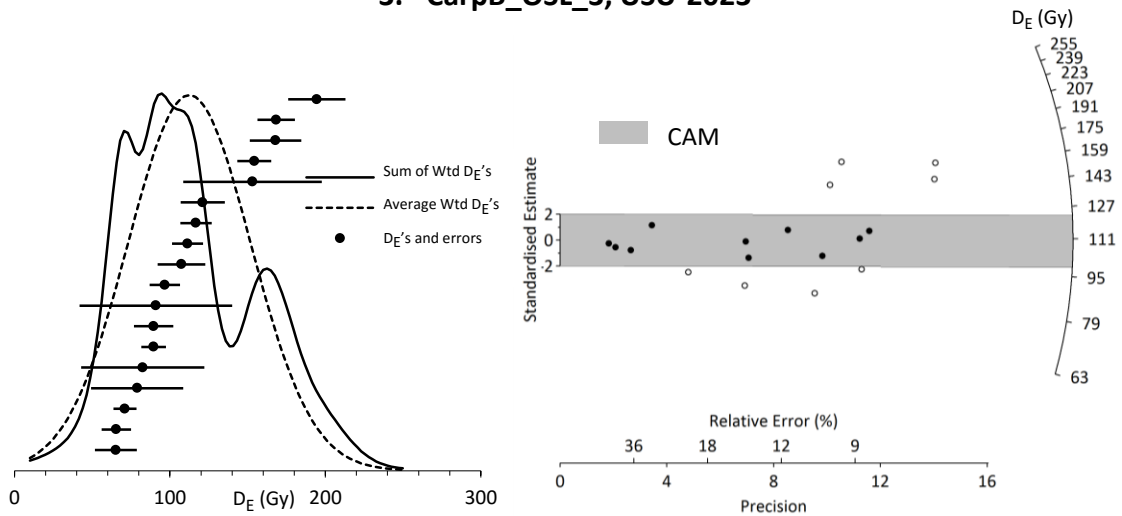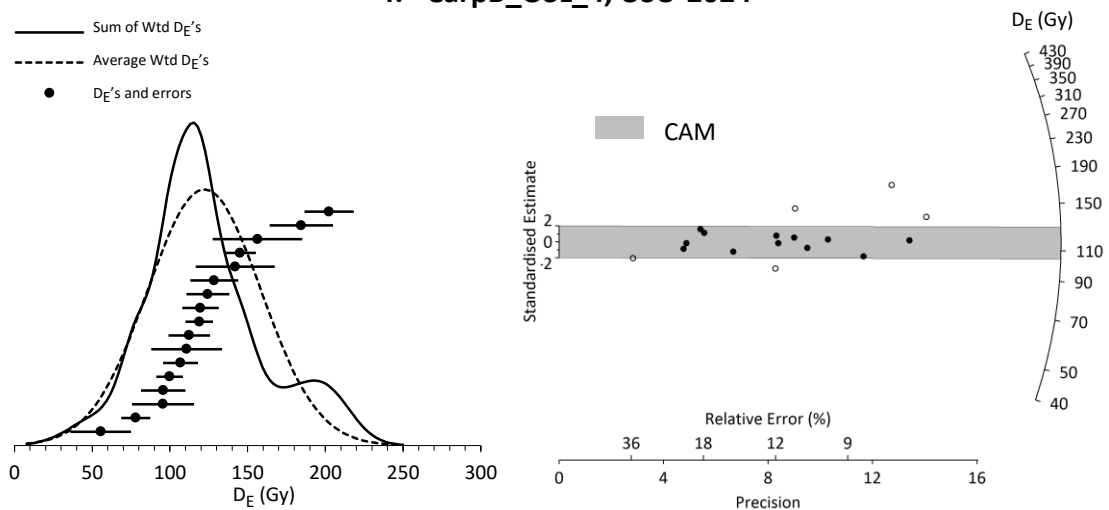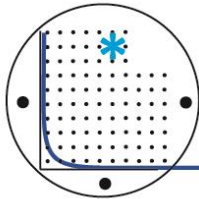
1. CarpB_OSL_1, USU-2021
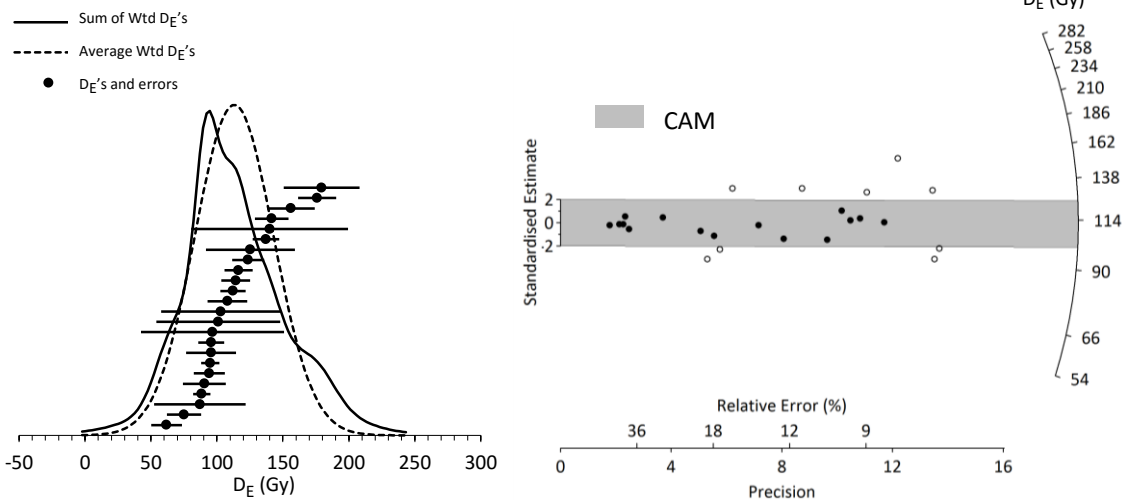

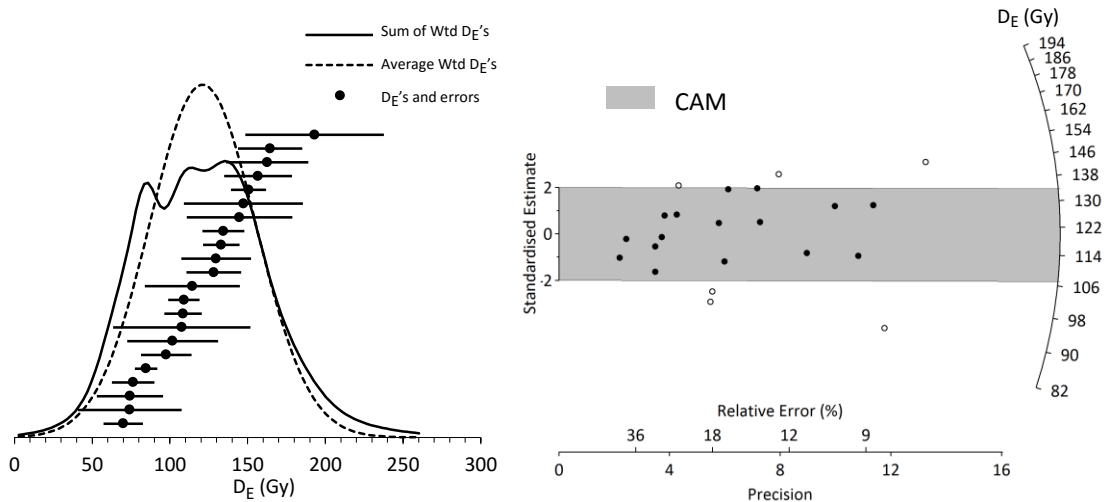### 2. CarpB_OSL_2, USU-2022

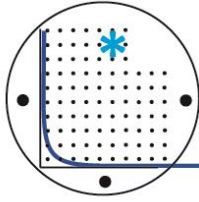### 3. CarpB_OSL_3, USU-2023

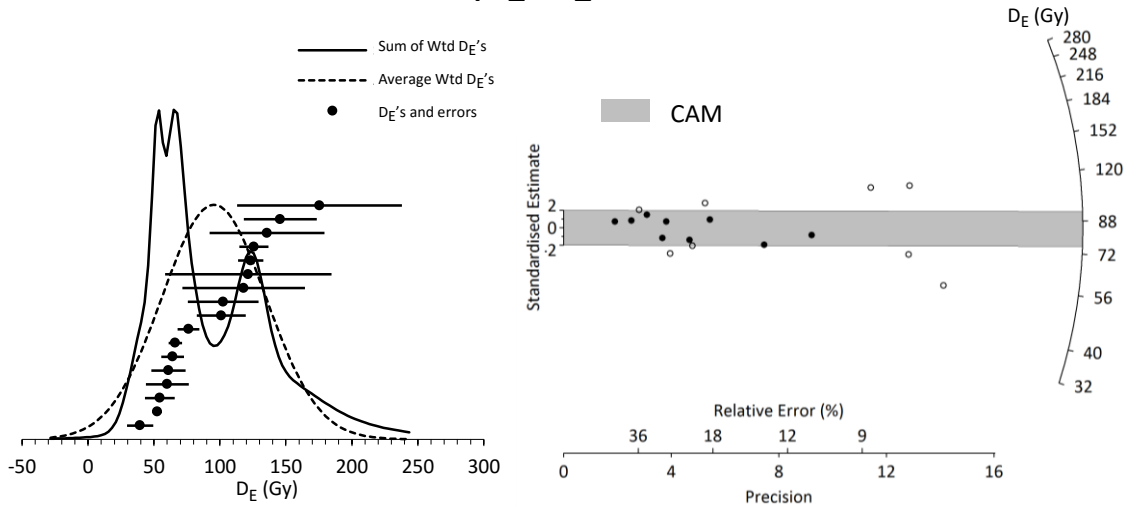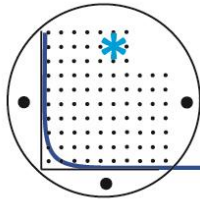### 4. CarpB_OSL_4, USU-2024

5. RincP_OSL _1, USU-2025

6. RincP_OSL _2, USU-2026

7. CarpB_OSL_5, USU-2027

Procedures for sample processing and small-aliquot OSL age analysis:

All samples were opened and processed under dim amber safelight conditions within the lab. Sample processing for quartz optically stimulated luminescence (OSL) dating followed standard procedures involving sieving, HCl and bleach treatments, heavy mineral separation at 2.72 g/cm³, and acid treatments with HCl and HF to isolate the quartz component of a narrow grain-size range, usually 90-150 μm*. The purity of the quartz samples was checked by measurement with infra-red stimulation to detect the presence of feldspar.

The USU Luminescence Lab follows the latest single-aliquot regenerative-dose (SAR) procedures for OSL dating of quartz sand (Murray and Wintle, 2000, 2003; Wintle and Murray, 2006). The SAR protocol includes tests for sensitivity correction and brackets the equivalent dose (D_E) the sample received during burial by irradiating the sample at five different doses (below, at, and above the D_E, plus a zero dose and a repeated dose to check for recuperation of the signal and sensitivity correction). The resultant data are fit with a saturating exponential curve from which the D_E is calculated on the mean, Central Age Model (CAM) or the Minimum Age Model (MAM) of Galbraith and Roberts (2012), depending on the distribution of D_E results and evidence for partial bleaching*. In cases where the samples have significant positive skew, ages are calculated based on a MAM. The OSL age is reported at 2σ standard error and is calculated by dividing the D_E (in grays, gy) by the environmental dose rate (gy/ka) that the sample has been exposed to during burial.

Dose-rate calculations were determined by chemical analysis of the U, Th, K and Rb content using ICP-MS and ICP-AES techniques by ALS Chemex, Elko NV and conversion factors from Guérin et al. (2011). The contribution of cosmic radiation to the dose rate was calculated using sample depth, elevation, and latitude/longitude following Prescott and Hutton (1994). Dose rates are calculated based on water content, sediment chemistry, and cosmic contribution (Aitken and Xie, 1990; Aitken, 1998).

Under the collaborative agreement to analyze samples at the USU Luminescence Lab, please consider including Dr. Rittenour as a co-author on resultant publications. Contact me for additional information and help with describing the OSL technique when you plan your publication.
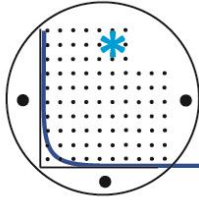Dr Tammy Rittenour

Director
USU Luminescence Lab
1770 N Research parkway, suite 123
North Logan, UT 84341

Associate Professor
Department of Geology, Utah State University
4505 Old Main Hill
Logan, UT 84322-4505

tammy.rittenour@usu.edu

http://www.usu.edu/geo/luminlab/

* These parameters are sample dependent, see first page of report for specific sample information

References cited:

Aitken, M.J. 1998: An Introduction to Optical Dating: The dating of Quaternary sediments by the use of photon-stimulated luminescence. New York, Oxford University Press, 267 p.

Aitken, M.J., Xie, J., 1990. Moisture correction for annual gamma dose. Ancient TL 8 (2), 6-9.

Auclair, M., Lamothe, M., Huot, S., 2003. Measurement of anomalous fading for feldspar IRSL using SAR. Radiation Galbraith, R.F., and Roberts, R.G., 2012. Statistical aspects of equivalent dose and error calculation and display in OSL dating: An Overview and some recommendations. Quaternary Geochronology 11, 1-27.

Guérin, G., Mercier, N., Adamiec, G., 2011. Dose-rate conversion factors: update: Ancient TL 29, 5-8.

Prescott, J. R., Hutton, J.T., 1994. Cosmic ray contributions to dose rates for luminescence and ESR dating: Radiation Measurements 23, 497-500.

Murray, A.S., Wintle, A.G., 2000. Luminescence dating of quartz using an improved single aliquot regenerative-dose protocol. Radiation Measurements 32, 57-73.

Murray, A.S., Wintle, A.G., 2003. The single aliquot regenerative dose protocol: potential for improvements in reliability. Radiation Measurements 37, 377-381.

Wintle, A.G. Murray, A.S., 2006. A review of quartz optically stimulated luminescence characteristics and their relevance in single-aliquot regenerative protocols: Radiation Measurements, v. 41, p. 369-391.